Addis Ababa University

Addis Ababa Institute of Technology (AAIT)

School of Civil and Environmental Engineering

Geodesy and Geomatics Program

(Geomatics stream)

Assessment of Groundwater Recharge Change Using WetSpass Model in the Birr Watershed, Abay Basin, Ethiopia.

Yiheys Degu

ID No. GSR/8621/11

Advisor

Andenet Ashagrie (PhD)

A Thesis Submitted to School of Civil and Environmental Engineering Graduate Studies of Addis Ababa Institute of Technology in Partial Fulfillment of the Requirement for the Degree of Masters of Science in Geodesy and Geomatics (specialization in Geomatics).

Addis Ababa, Ethiopia

June, 2023

Addis Ababa University
Addis Ababa Institute of Technology (AAIT)
School of Civil and Environmental Engineering
Geodesy and Geomatics Program
(Geomatics stream)

Assessment of Groundwater Recharge Change Using WetSpass Model in the Birr Watershed, Abay Basin, Ethiopia, Ethiopia.

Yiheys Degu
ID No. GSR/8621/11

Advisor
Andenet Ashagrie (PhD)

A Thesis Submitted to School of Civil and Environmental Engineering Graduate Studies of Addis Ababa Institute of Technology in Partial Fulfillment of the Requirement for the Degree of Masters of Science in Geodesy and Geomatics (specialization in Geomatics).

Addis Ababa, Ethiopia
June, 2023

APPROVAL SHEET

Addis Ababa University

Institute of Technology (AAIT)

School of Civil and Environmental Engineering

Geodesy and Geomatics

This is to certify that the thesis prepared by **Yiheys Degu**, entitled: Assessment of Groundwater Recharge Change Using WetSpass Model in the Birr Watershed, Abay Basin, Ethiopia, which is submitted to School of Civil and Environmental Engineering Graduate Studies of Addis Ababa Institute of Technology in Partial Fulfillment of the Requirement for the Degree of Masters of Science in Geodesy and Geomatics (specialization in Geomatics) compiled with the regulations of the university and meets the accepted standards of the university regarding quality and originality.

Yiheys Degu

Andenet Ashagrie		July 07, 2023
Advisor	**Signature**	**Date**
Hamere Yohannes		07/12/2023
Internal Examiner	**Signature**	**Date**
Dr. Surya		12-07-2023
External Examiner	**Signature**	**Date**
Abrham Gebre (Dr.) Dean, School of Civil & Environmental Engineering		
Chair Person	**Signature**	**Date**

Director of Postgraduate Program
Addis Ababa University
Addis Ababa Institute of Technology

III

Acknowledgements

Above all, I thank Jesus Christ for his guidance and grace upon me and my family in all my life.

Next, I would like to express my gratitude to my advisor Dr. Andenet Ashagrie, for his constructive comments, guidance, suggestion, and corrections in my thesis writing.

I would like to express my deepest gratitude to my beloved wife Senait Abebe, and her sister Tirngo Abebe for their advice and support during my study by taking care of my children and carrying out most of the household responsibilities.

I would also thank Ethiopian Meteorological Agency, Geological Survey of Ethiopia, Ministry of Agriculture, and Amhara Water Works Enterprise for their kindness in providing valuable data and necessary information to carry out this research.

It is also my pleasure to tank my friends Nigus Adane, Wondifraw Nigusie and my staff members for their constant encouragement and support throughout this work.

Table of Contents

List of Tables

List of Figures

List of Acronyms

AET	Actual Evapotranspiration
CHIRPS	Climate Hazard Group Infrared Precipitation with Station Data
FAO	Food And Agriculture Organization
GDP	Gross Domestic Product
GSE	Geological Survey of Ethiopia
IPCC	Intergovernmental Panel on Climate Change
LULC	Land Use Land Cover
MWR	Ministry Of Water Resource
NASEM	The National Academics of Science Engineering and Medicine
NMA	National Meteorological Agency
PET	Potential Evapotranspiration
RRC	Relief And Rehabilitation Commission
UNDP	United Nation Development Program
UNFCC	United Nations Framework Convention on Climate Change
WetSpass	Water And Energy Transfer Between Soil, Plants and Atmosphere Under Quasi-Steady State

Abstract

Understanding the long-term spatial extent of environmental and LULC changes in different time epochs helps to evaluate the impact of climate and LULC changes on water resources. Therefore, estimating the spatial and temporal extent of groundwater recharge in response to climate and LULC changes are crucial for the proper management of the water resources in the watershed. This study quantifies the effects of climate and LULC change on groundwater recharge for the Birr watershed from 1990-2020 periods using WetSpass model. The LULC maps of the study area were classified from multi-temporal Landsat imageries of Landsat 5(TM), Landsat 7(ETM+), and Landsat 8(OLI) using supervised maximum likelihood classification algorithm. The accuracy of classified images was checked by overall accuracy and kappa coefficient. In the study area, agriculture, built-up, and bare land increases through time while grassland, forest, wetland, and shrubland decreases during the last three decades due population growth and rapid expansion of farmland. The monthly reanalysis of climatological satellite products of precipitation, temperature, and windspeed maps was prepared from the decadal average of 1990-1999, 2000-2009, and 2010-2020 for the model simulation. The trend of the climate change in the watershed were analyzed and tested by Mann Kendall test R programming software. The temperature in the watershed has increasing trend over the last 30 year and increase by 0.033^{o}c per year. Whereas, rainfall and wind speed have no significant trend in 95% confidence level. Moreover, a 12m resolution ALOSDEM was used to delineate the watershed and to develop slop and elevation input maps. The slope and elevation maps were finally resampled to 30m resolution. The study result shows that the annual groundwater recharge in the watershed decreases on average from 162.3mm to 128.6mm in from the first phase to the second phase and declines to 121.2mm in the third phase. it is important to take LULC conservation mechanisms and environmental rehabilitation measures in the study area. The study gives a piece of baseline information about impact of climate and LULC on the groundwater recharge of the study area for policymakers and the society of the watershed.

***Keywords**:* - WetSpass model; Groundwater recharge; Birr watershed

Chapter One

Introduction

1.1 Background of the Study

Groundwater is a precious, limited (Dereje & Nedaw, 2018), and the most widely distributed resource of the planet Earth. It is the primary source of potable water which constitutes the majority of freshwater in the world (Kurwadkar et al., 2020; Shiri et al., 2021). However, until recently the groundwater sector has been given limited attention (Awulachew et al., 2007 ; Margat & Gun, 2013). The groundwater resource quality and quantity decreased over time due to climate variability (Kalhor et al., 2019; Singh, 2018b; Singh, 2018a) land cover change (Sugawara & Nikaido, 2014), and anthropogenic activity (Poeter et al., 2020a). The population growth, climate change, expansion of industries, agriculture and urbanization worsen the pollution and depletion of the resource (Kurwadkar et al., 2020; Poeter et al., 2020).

Groundwater recharge refers to the downward movement of water into the saturated zone, reaching the water table surface, and the associated flow of water away from the water table (Poeter et al., 2020; Obiefuna & Orazulike, 2011). It stands for the process of water flowing from precipitation, septic tanks, lakes, sewers, ponds, etc. that percolates into the soil and reaches the water table either naturally or artificially to replenish the aquifer (Bedaso et al., 2019). It has a strong connection with the atmosphere, the land surface, and subsurface water balance components. As a result, it is sensitive to climatic and anthropogenic factors (Jyrkama & Sykes, 2007; Herrera-Pantoja & Hiscock, 2008). Groundwater is directly dependent on the recharge and it is the crucial element in the analysis of groundwater resource (Qablawi, 2016). Thus, quantifying the recharge and understanding its process has paramount importance for the proper management of groundwater resources (Obuobie, 2008). However, quantify the spatial distribution of groundwater recharge is the most difficult measurement (Alley et al., 2002; Batelaan & De Smedt, 2007 ; Addisie, 2022). This is because the recharge is dynamic, and it varies with space and time (Karunakalage et al., 2023). Therefore, estimate recharge using physical models like WetSpass (water and energy transfer in plants, soil, and the atmosphere under a quasi-steady state) helps to understand its spatial distribution in a watershed.

Groundwater recharge is influenced by several factors (Armanuos & Negm, 2016), such as topography, climate, soil texture, and LULC (land use land cover) type (Dragoni & Sukhija, 2008). Recharge in a watershed is a function of many varied factors such as amount, distribution, and frequency of rainfall across the watershed, land cover, the area of bare soil, vegetation type, soil type, soil properties, and the like. As a result, the recharge is highly variable (Alley et al., 2002) according to the locations characteristics. As precipitation gets varied due to variations in temperature and evapotranspiration, there is a variation in

groundwater recharge. Therefore, understanding groundwater recharge has a significant role in the efficient and sustainable management of groundwater resources (Addisie, 2022). Climate and LULC changes are the major factors that affect global ecology. Climate change can significantly alter the water quality by changing the temperature, runoff rates, and its timing, flows, and capability of watersheds to absorb wastes and pollutants (Jacobs et al., 2000). On the other hand, industrial and agricultural activities coupled with the rapid expansion of population growth contribute to the processes of global warming and thus alter world climate patterns. Likewise, LULC changes influence the flux of mass and energy of the biodiversity (Virginia, 1997) that affects hydrological processes, resulting in alterations of surface and subsurface flows (Chen et al., 2012; Niraula et al., 2015). In Ethiopia (Awulachew et al., 2007) and (Ministry of Water Resource, 2002) stats that the country has groundwater potential, ranging from 2.6 to 2.65 billion m^3. However, this water potential is currently threatened by LULC dynamics, and climate change and about 122 billion m^3 of water is released through runoff per year and of this 52.6 billion m^3 is in Abbay basin.

Several techniques are available to evaluate and quantify groundwater recharge. These include numerical models, hydrological budgets, water table fluctuations, tracer techniques and other multiple methods (Singh et al., 2019). Each method has its own limitations and advantages, selecting the right method depends on the availability of data and the study area characteristics. Nowadays, the WetSpass model has been widely used to evaluate groundwater recharge. Most groundwater models are often in quasi-steady state that needs long-term average recharge input data (Batelaan & De Smedt, 2001). This study aims to assess the spatial distribution of groundwater recharge in the Birr watershed by using the WetSpass model.

1.2 Statement of the Problem

Groundwater is the fundamental source of water supply for most economic activities. Currently, it is used in all parts of the world, including the study area, to meet the rapidly increasing agricultural, industrial, and domestic water supply requirements. However, society uses it with limited knowledge of its potential and without understanding how the resource is affected by human's day-to-day activities, climate change and land use land cover dynamics. Climate change has a significant impact on water resources (Piao et al., 2010). In this century, the global climate is changing rapidly due to the anthropogenic production of greenhouse gases, air pollutants and land use changes. The Fifth Assessment Report (IPCC, 2014) shows by the Representative Concentration Pathways (RCP8.5), the global mean surface temperature is expected to increase on average by 2 °C and 3.7 °C in the mid and late 21st centuries, respectively. Scholars note that the developing world (Africa) has been extremely hated economically due to climate change. For instance, by 2060 the mean temperature rises by

2.2°C, and the economic cost increases by 3.4 percent of Africa's GDP (Clements, 2009). The continent's surface temperature will increase by 1.5 times the global average increase (Dessalegn & Akalu, 2015). Moreover, Africa is the most vulnerable region to climate change due to their low economy, limited access to capital, technology, and institutional capacity (UNFCC, 2007). The content has faced several challenges, including population pressure, LULC change, erosion, famine, flooding, and other possible ecological consequences of LULC changes and climate variability. Generally, environmental change affects the quality and quantity of regional groundwater resources (Jacobs et al., 2000). It can significantly affect the local climate by changing the surface roughness, radiation, cloudiness, and surface temperatures, which so affects the groundwater recharge rate, the water balance, and surface energy of the region (IPCC, 2007).

The topographical and biophysical characteristics of Ethiopia are sensitive to LULC changes and climate variability. The Nile Basin regions are more sensitive to climate variations (Conway, 2005). As a result, scholar's recommend that there should be greater attention and a sustained study on the impact of natural climate variation and LULC changes in hydrology of the Blue Nile basin Melesse et al., (2009). In Ethiopia, the frequency and the spatial distribution of drought increases from time to time (Walravens et al., 2009) and the country is suffering from a shortage of food due to erratic precipitation and unsustainable use of water resources. The low economic, institutional and adaptive capacity of the country make such climatic impacts serious in country. LULC change, and climate variability are among the crucial environmental challenges that the community should address. In the Birr watershed, the biophysical characteristics the catchment, the economic lifestyle of the society and the rapid population growth aggravates the LULC change and climate variability. The society led their lives by agriculture which can easily be affected by climate change. Consequently, climate change and land cover dynamics intensify the quality and quantity of water resources. Therefore, understanding the impact of LULC dynamics and climate change, and their spatial extent on groundwater resources, especially on groundwater recharge, runoff, and evapotranspiration, is critical for pre-planning, efficient and proper management of groundwater resources, landscape management, environmental conservation, and agricultural production improvement. This study aims to evaluate the scale, temporal and spatial distribution of groundwater recharge and assess the impact of climate variability and LULC change in the recharge process of the watershed using WetSpass hydrological model integrating GIS and remote sensing techniques.

1.3 Objectives of the Study

1.3.1 General Objective

The main objective of this study is to evaluate groundwater recharge in Birr watershed using WetSpass hydrological model.

1.3.2 Specific Objectives

- To examine and produce the LULC map of the Birr watershed for 1990, 2005 and 2020
- To analyze the 30-year climate trend in the study area
- To quantify the mean annual groundwater recharge of 1990, 2005 and 2020

1.4 Research Questions

- Did the LULC of the study area changed through time?
- How has the climate trend look like in the past 30 years in the study area?
- How much is the mean annual groundwater recharge in the Birr watershed in 1990, 2005 and 2020?

1.5 Significance of the Study

To evaluate the impact of climate variability and LULC dynamics on groundwater, it is important to understand the pattern of LULC change, and the trend of climate variability in the watershed. In this study, to assess the impact of LULC dynamics and climate changes, the annual groundwater recharge, runoff and evapotranspiration of the study area are quantified by WetSpass model. The study is also expected to create awareness for society and policymakers about the correlation and interdependence of climate variability, land cover change, and groundwater resource.

Generally, the study has the following importance:

- ✓ It supplies necessary information about the groundwater recharge of the watershed for the community and policymakers to manage water resources effectively.
- ✓ The study gives professional recommendations about the impacts of LULC dynamics and climate changes on groundwater recharge.
- ✓ It will serve as input for further studies in this area.

1.6 Limitation of the Study

The study uses the same ground depth data for all phases and months due to well organized boreholes data limitations. Additionally, the study uses the groundwater level (GWL) measurements taken at the date of construction. Due to time and financial limitation, it is not possible to measure GWL in the field. There are many boreholes constructed by different governmental and non-governmental organizations at various times, but all the necessary data of boreholes is not documented and registered both at the federal and regional levels.

1.7 Organization of the Thesis

The paper is organized into five chapters. The first chapter is an introduction section, in which problem statement, objective of the study, research questions, and significance of the study are presented. The second Chapter covers the related literature about the concept of water resources, groundwater recharge, groundwater recharge estimation methods and models, LULC change, and climate variability. The third chapter focuses on the method, input data, image preprocessing, classification and accuracy assessment, hydrological model selection, and description of the study area. In the fourth chapter, the results and discussion are described with an illustration of the model. In this section the long-term trend of LULC change and climatological variables are analyzed and discussed. Finally, the fifth chapter elaborates the conclusion and recommendations of the study.

Chapter Two

Literature Review

2.1 Water Resources

Water is the most widely used resource on Earth. It refers to the supply of both groundwater and surface water in each area (NASEM, 2018). It is a naturally circulating resource that is constantly recharged and moves through the atmosphere in its liquid, solid, and vapor phases. it has linkage among most dynamic processes of land (Oki & Kanae, 2006). The water circulation involves many processes, precipitation such as rain or snow, evapotranspiration and evaporation, snowmelt, condensation, sublimation, surface runoff, infiltration, percolation, and groundwater flow of the hydrological cycle (NASEM, 2018).

The total water resources available in the World are estimated to be 1.36 billion Km^3 and about 97.2% of this resource is salt water, and only 2.8% is freshwater (Raghunath, 2006), which is especially important for economic and social activities. It is used for potable water, sanitation, agriculture, industry, urban development, hydropower generation, and the like. Ethiopia is endowed with water resources. It has nine lakes and 12 river basins; of which 9 are wet river basins; 1 Lake Basin; and the remaining 3 are dry river basins (Ministry of Water Resource, 2002). The country has about 111 billion m^3 of total annual water resources, and 75.5 billion m^3 of this is in the Abbay Basin (Hagos, 2005). Currently demand of water is increased worldwide as a result of rapid population growth, urbanization and food and energy policies (UNWWAP, 2015). Due to the lack of rainfall, many people are dependent on groundwater. In Africa inadequacy of rainfall is not the fundamental problem IPCC, (2007), the key issues on the continent appear to be related to the management of the available resources. The issue relates to the adequacy of the enabling environment under which water resources are managed at local, national, and inter-country levels.

2.2 Groundwater

Groundwater can be defined from different perspectives and expressed by several names. It is also called subsurface water, and underground water (Kebede, 2013). Groundwater is shortly the percolated precipitation water in the saturated zone (Poeter et al., 2020b). it is the underground water held in the soil and rocks or beneath the surface of the ground, consisting of surface water that has seeped down. The total groundwater of the world is estimated to be 10.53 million km^3 (Delleur, 1999) which forms 99% of the earth's available freshwater resources (Delleur, 1999; Poeter et al., 2020b). Groundwater is crucial in various sectors. It is used to keep wetland hydrology and other environmental functions. Groundwater has played a key role in storing, filtering, and transforming abilities, and regulates atmospheric, hydrological, and nutrient cycles (Kebede, 2013).

In Ethiopia, the total groundwater storage potential is estimated to be 1 trillion m^3 (Kebede, 2013). However, this result contradicts (Awulachew et al., 2007) estimation, which has about 2.6 to 6.5 billion m3, but this figure was extremely underestimated. Therefore, it needs further investigation on this issue in the country. Groundwater storage potential in Ethiopia is influenced by the higher slope drainage basins, dissection of the aquifers into smaller pockets, and lower storage ability of crystalline rocks. As a result, storage potential is low in Ethiopia as compared to other aquifer regions in Africa (Kebede, 2013).

2.3 Groundwater recharge

Groundwater recharge refers the downward movement of a portion of precipitation to aquifer (Addisie, 2022). It is universally accepted as a movement of water in any direction that reaches an aquifer crossing the water table (Simmers, 1988). Recharge occurs through the water cycle naturally and through anthropogenic processes artificially. Naturally, it can recharge from precipitation, snow melts, and surface water (Addisie, 2022). To quantify recharge from precipitation, it is critical to understand rainfall-runoff relationships. The first step is to figure out the fraction of precipitation available for groundwater recharge, after subtracting what is lost to overland flow (runoff) and evapotranspiration (ET). For sustainable water resources management, understanding, and quantifying rates of groundwater recharge spatially, and temporally are critically important (Simmers, 1988).

Groundwater recharge is one of the most critical issues in groundwater studies, but it is the least understood because measuring recharge directly in the field is difficult and varies widely in space and time (Healy & Scanlon, 2010a; Karunakalage et al., 2023). Thus, before deciding which recharge quantification method to use, it is important to show the probable flow mechanisms and features influencing the recharge. These include data availability, the topography, geological structure, and spatial and temporal characteristics of the study area (Ali & Mubarak, 2017; Islam et al., 2016). Recharge mechanisms can be categorized as direct (focused) recharge: entry of water to the groundwater by direct vertical percolation from precipitation, indirect (diffuse) recharge: recharge to the water table through infiltration following runoff the beds of surface watercourses, such as beneath rivers and lakes and localized recharge: an intermediate groundwater recharge (Misstear, 2000; Simmers, 1988). These mechanisms usually do not occur separately, and this makes the recharge assessment complex. On the other hand, the recharge and discharge conditions of a given area are influenced by several factors such as; precipitation (volume, intensity, duration), topography, vegetation (cropping pattern, rooting depth) and evapotranspiration, soil and subsoil types, flow mechanisms in the unsaturated zone, bedrock geology, available groundwater storage, presence of infant rivers and the presence of karst features, etc. (Misstear, 2000).

2.4 Groundwater Recharge Estimation

Estimation of groundwater recharge is a prerequisite for efficient and sustainable management of groundwater resources. Studying the rate, spatial location, and timing of recharge has a significant role in water resource management. But groundwater recharge evaluation is difficult (Batelaan & De Smedt, 2007; Alley et al., 2002). Especially, in arid and semi-arid regions the recharge is low as compared to average annual rainfall or evapotranspiration, and these make it difficult to estimate precisely (Scanlon et al., 2002).

On this day, a variety of methods and techniques are applied to quantify groundwater recharge (Singh et al., 2019). Scanlon et al., (2002) divided these techniques based on a hydrologic zone into surface water, unsaturated, and saturated zone techniques and further classified into physical techniques, tracers (chemical), and numerical modeling within each of the hydrologic zones. Sophocleous, (2004) also grouped the techniques based on analysis of inflow, outflow, or aquifer response; unsaturated or saturated zones, numerical modeling of groundwater flow, soil-water flow, direct or indirect; physical, chemical, or isotopic; soil and groundwater flows, or modeling of the hydrologic balance at plot, field, or watershed scales. During recharge estimation, several factors should be considered to obtain the required recharge accuracy. These may include the data accuracy, goal of the study, reliability, space and time, scale, the range of the expected recharge estimates, the time duration of the study, and the financial capacity that should be considered for precise groundwater recharge estimation (Scanlon et al., 2002).

2.5 Groundwater Recharge Models

Models can supply crucial penetration for the functioning of hydrologic systems by elaborating factors that influence recharge. There are many hydrological models used today to estimate groundwater recharge and most of them are deterministic mathematical models. These models are based on the preservation of mass, momentum, and energy and describe cause and effect relations (Delleur, 1999) which means these hydrological simulation models including groundwater flow models, and watershed models that are applied by some form of water-budget equation (Healy & Scanlon, 2010b). Models can be categorized as conceptual, distributed, undistributed or stochastic, etc. Based on their physical parameterization and model structure, groundwater recharge studies in humid areas must take four essential steps: calculation of long-term averages and variabilities of precipitation and evapotranspiration, analysis of existing run-off data to complete, specify and quantify the meteorological water balance, define the scale for which these results on groundwater recharge are representative, and developing a suitable conceptual model of discharge and run-off mechanisms in a concern,

contribute to the development of management and protection strategies through mathematical modeling (Seiler & Gat, 2007).

2.6 WetSpass Model and its Application

In this study the WetSpass hydrological model is used to estimate the groundwater recharge of the Birr watershed. The model is primarily developed for temperate regions (Batelaan & De Smedt, 2001; Batelaan & De Smedt, 2007) and currently, it is used worldwide. WetSpass is an acronym for water and energy transfer between soil, plants, and the atmosphere under quasi-steady state conditions (Batelaan & De Smedt, 2001). It is a physically based model for the estimation of long-term average spatial patterns of groundwater recharge, surface runoff, and evapotranspiration. This model is a regional groundwater model used to simulate infiltration discharge relations based on long-term average recharge input data.

The WetSpass model is based on the water balance equations of vegetation surfaces, bare land, open water, and an impervious surface; it is used for groundwater recharge estimation at the watershed level (Aish et al., 2010). WetSpass can estimate groundwater recharge on seasonal and annual scales. The model was successfully applied in Belgium (Batelaan & De Smedt, 2001) and in other areas of the world that have different environmental characteristics. For instance, it was used in Gaza Strip, Palestine (Aish et al, 2010), Nile Delta aquifer, Egypt (Armanuos & Negm, 2016), and in Ethiopia Birki watershed (Meresa & Taye, 2019), and Geba catchment, (Gebreyohannes et al., 2013). They confirmed that the model can estimate groundwater recharge successfully. Warku et al., (2022) was used this model to evaluate LULC change and climate variability impacts on hydrological components such as groundwater recharge, surface runoff, and evapotranspiration in Ethiopia.

2.7 Climate variability

The climate is defined as the “average weather.” It indicates the longer period patterns of atmospheric quantities such as temperature, precipitation, and wind. These relevant atmospheric components are continuously changing due to internal and external factors. Climate Variability is referred to as the change in the mean state and other aspects of the climate on all temporal and spatial scales, which is beyond the individual weather events. IPCC, (2014) noted that according to its Fifth Assessment Report (AR5), the average global surface temperature has increased during the twenty-first century under all its scenarios. The report has four scenarios called Representative Concentration Pathways (RCPs). For example, the intermediate scenario RCP6.0 shows that the average global surface temperature has increased by 1.3°C and 2.2 °C between 2046–2065 and 2081–2100, respectively. An increase in the average temperature of the earth's atmosphere, especially a sustained increase sufficient to cause climatic change. This suggests that rising global temperatures affect various climatic and

meteorological factors, including wind, precipitation, humidity, evaporation, temperature, and evapotranspiration.

Africa is a continent currently under climate change stresses and is highly vulnerable to climate change impacts. Even though developed countries are the most cause of the anthropogenic production of greenhouse gases, the poorest developing countries are more severely affected by climate change impacts. This is because developing countries have a high number of poor people, physical impacts are higher in these regions, their economy is depending on agriculture, which is easily affected by climate variability and developing countries are the extremely limited economy and technological ability to adopt climate change impacts (Mertz et al., 2009; UNFCC, 2007). Due to the uneven distribution of solar heating, the individual responses of the atmosphere, oceans, land surface, and the physical characteristics of the regions, the climate varies from region to region.

Africa is the most impacted continent by climate change (Niang et al., 2014). In some parts of the continent, especially in eastern Africa (Nicholson, 2016; Funk et al., 2015) the problem becomes more intense and frequent (Gizaw et al., 2017). According to the IPCC Regional Climate Projections report of 2007, the median temperature increase in Africa by the years 2080 to 2099 surface temperature lies between 3°C and 4°C in all regions and all seasons, which is 1.5 times the global mean increase. Thus, warming in Africa is more severe than other in regions (Dessalegn & Akalu, 2015). Horn African Countries are among the most vulnerable countries to climate variability. However, because of their economic capacity, these countries are the least prepared for adverse global environmental challenges in the world (Aklilu & Alebachew, 2012).

In Ethiopia famine has repeatedly occurred because of extreme events of climate change and becomes a cause for widespread disruption of the socio-economic well-being of the society. The country is characterized by a wide variety of landscapes, with marked contrasts in relief and altitudes. It has elevations ranging from 125 m (about 410.1 ft) below sea level in the Danakil depression, to 4,620m (about half the height of Mount Everest) above mean sea level at Ras Dashen Mountain, a world heritage site (Asefa et al., 2020). In addition to its geographic position, it is close to the equator and the Indian Ocean, which results in large spatial variations in temperature and precipitation.

2.8 Impact of Climate Variability on Groundwater Recharge

Climate change intensifies the global hydrological cycle (Huntington, 2006). Hydrologic cycle components are sensitive to climate change; thus, any climate change has a significant impact on water resources (Zhang et al., 2018). For example, temperature and precipitation changes can affect runoff, evapotranspiration, groundwater recharge, and discharge process. Such

phenomena have their own consequences on water resources which indirectly affect agricultural production, industry, and urban development. UNFCC, (2007) states that by 2030 greenhouse gas emissions will rise by 25 – 90 percent which causes the Earth to warm by 3°C. Additionally, the report shows that by 2020, about 250 million people in African countries could be endangered by the elevated risk of water stress.

Because of the weather and geographical settings of the country, Ethiopia is more vulnerable to climate change and the country is more sensitive to hydrological variations (World Bank, 2008; Abdo et al., 2009). Ethiopian economy relays on agriculture depends on both surface and groundwater resources. However, much of the country is grouped under arid and semi-arid climate zones which are sensitive to drought and desertification (Abdo et al., 2009). The effect of climate change varies spatially within a watershed. This is because of the differences in regional climate conditions, topographic characteristics, and sensitivity to response to human-induced environmental changes in the watershed (Arnell, 2003). IPCC noted that climate variability can deteriorate groundwater availability, and decrease its quality, and water supplies. Therefore, further study is essential to quantify the climatic impacts (Niang et al., 2014).

2.9 Land Use Land Cover Change

Land use land cover change is the modification of the terrestrial Earth's surface through human activity. Land use is the way human beings use their land for a particular purpose (Alemayehu et al., 2009 ; Virginia, 1997). For instance, using the land for agricultural, commercial, or industrial purposes. While land cover shows the physical and biophysical features that cover the land, it may be vegetation, water body, bare soil, etc. However, land cover is the ecological state or the status of the vegetation in each area (Virginia, 1997). Land use changes are the frequent causes of land-cover modification (Turner et al, 1993).

LULC change are widespread, hastening, and complex processes which can be aggravated by human activities (Leh et al., 2013) that result in changes affecting human beings (Agarwal et al., 2002). It is occurring due to the conversion and intensification of resources by human action (Virginia, 1997). For centuries, human beings have been altering the surface of the earth to obtain food and fiber (Lambin et al., 2003). For instance, during the past 3 centuries, 2 million km^2 of forest and woodland and 5.6 million km^2 of grazing land have been globally changed to other land uses (Ramankutty & Foley, 1999). In the same period (Turner et al, 1993) also show that there has been a net loss of 6 million km^2 of forest area, a net gain of 12 million km2 of cropland, and a net loss of 1.6 million km2 of wetlands. In Ethiopia, the deforestation rate is accounted for around 2% and about 700,000 ha forest has been cleared annually (Yitebitu et al., 2010). Due to the expansion of agriculture, fuelwood collection, and overgrazing

biophysical resources such as water, soil, vegetation greatly altered. This type of conversion has large impacts on the biological, geological, and chemical processes and on water and energy balance. However, land-cover modification is a more elusive change that affects the land-cover characteristics without changing its overall classification (Lambin et al., 2003).

2.9.1 Drivers of LULC Change

In developing countries like Ethiopia, the major cause of LULC is rapid population growth (Woldeamlak, 2002). The driving force for LULC changes is the sum of multiple interacting variables. These driving forces vary in space and time and the variables may be fast or slow. The major causes for land use changes are resource scarcity leading to an increase in the pressure of production on resources, changing opportunities created by markets, outside policy intervention, loss of adaptive ability and increased vulnerability, and changes in social organization, in resource access, and in attitudes (Lambin et al., 2003).

Turner et al, (1993) divide the plausible causes of land use and land cover changes into six categories. This includes population growth, technology, level of affluence, political economy, political structure, attitudes, and values. Milkias & Toru, (2018) also identify six LULC change divers in Dire Dawa administration, Ethiopia. These are cutting woody plants for fuel wood and making charcoal, Population growth, Expansion of cultivated land, Drought, Housing (settlement), and Livestock ranching.

Most literature shows that LULC changes and socio-economic activities have a strong correlation with population numbers that enhance resource demand for food and energy such as cultivated land, fuel wood; housing and grazing land. Therefore, population pressure is the major causes of environmental degradation in Ethiopia.

2.9.2 Impact of Land Use Land Cover Change on Groundwater Recharge

In addition to climate variability, LULC change is another factor that affects water resources. LULC changes have a significant impact on biodiversity, hydrological cycles, biogeochemical cycles, soil fertility, land productivity, energy balance, and environmental sustainability (Lupo et al., 2001). LULC has several interactions with hydrological cycles. For example, deforestation contributes to rainfall declination and the creation of more rapid runoff after precipitation (Legesse et al., 2003) which affects the infiltration rate.

Generally, understanding the impact of LULC change on water resources should be based on evaluating the past and the current climate and LULC change patterns. Therefore, understanding the rate, and the spatial and temporal change of LULC is critically important for future land use planning and to take immediate conservation measurements.

Chapter Three

Materials and Methods

3.1 Description of the Study Area

The Birr watershed is found in the Amhara region on the southern fringe of the west Gojjam administrative zone. Geographically, it is located between 37° 01′ E to 37° 41′E longitude and 10° 19’ N to 11° 07′ N latitudes. The watershed covers a total area of 3163 km^2 which extends from Adama Mountain up to the junction of the Temcha River (Figure 3.1). The watershed is about 356 kilometers away from Addis Ababa along Addis Ababa-Debre Markos main asphalt road. The major towns in the watershed include Burie, Finote Selam, Mankusa, Jiga, Genet Abo, Gebeze Mareyam, Yechereka, and Agut. It gets the name Birr watershed from the river Birr. The river originates in the southern part of the Adama Mountain, a continuum of Choke Mountain near Quarit town, and drained to the southwest of the watershed, and finally joined the Temcha River in the Abbay gorge and goes to the Abbay River. The river has several tributaries such as Lah, Arara, Gunagun, Leza, Guyasa, Debolah, Silala, and Geray.

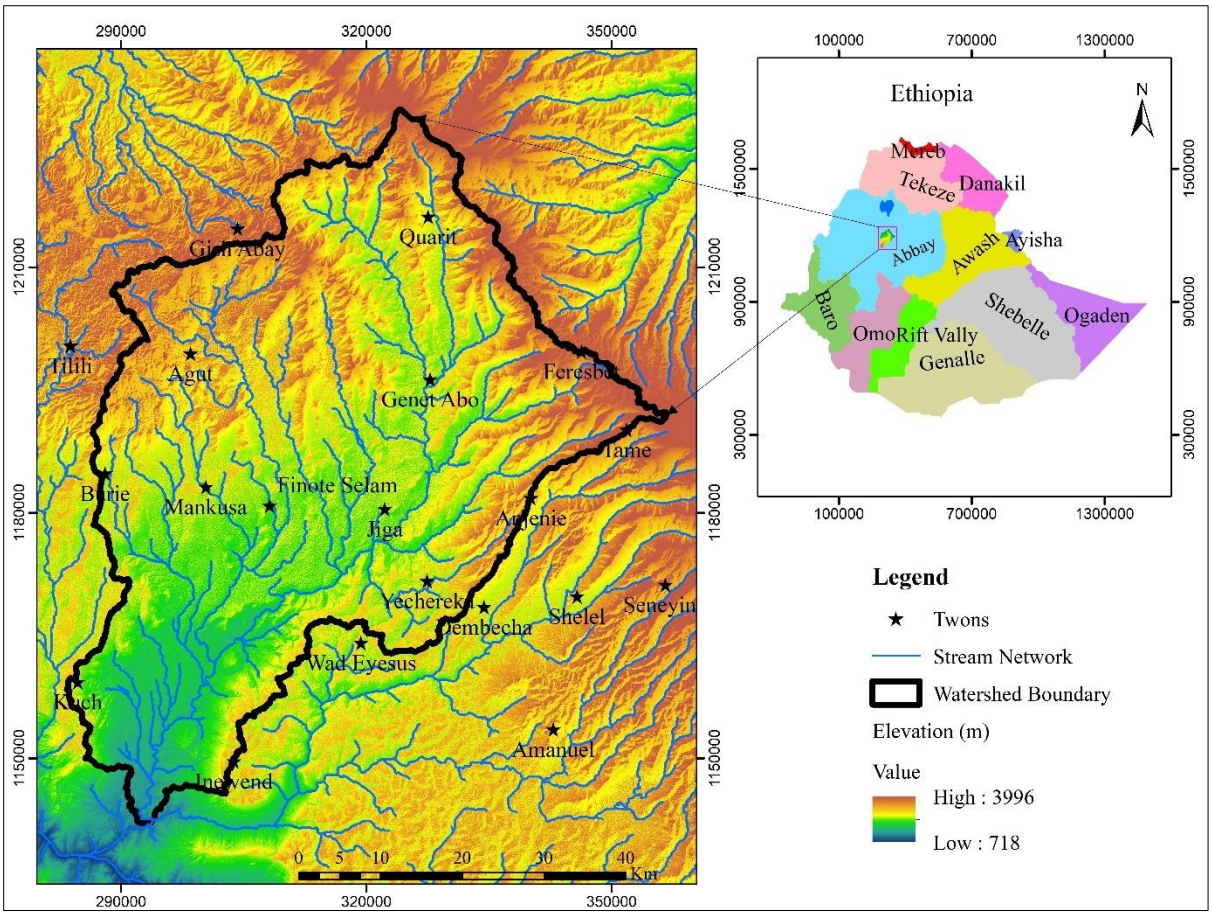

Figure 3. 1 Location map of the study area

3.1.1 Topography

The Birr watershed has diverse topographic characteristics. The north and northeastern part of the watershed is highly mountainous and characterized by undulating topography with a steep slope, the central, south, and southwest or downstream part of the watershed is characterized by gentle slopes. The elevation of the watershed ranges from 972 meter to 3519 meter above mean sea level (Figure 3.2a). The digital elevation map (DEM) of the study area is downloaded from Alaska satellite facility (https://asf.alaska.edu/data-sets/). The advanced land observation satellite (ALOS) radiometric terrains corrected high-resolution DEM is used to delineate the watershed boundary. ALOSPALSAR DEM has12.5m by 12.5m resolution. The elevation and slope map were resampled to 30m*30m for the WetSpass model simulation. According to RRC et al., (1986) slope classification: the slope map of the watershed (Figure 3.2b) shows that 65% of the catchment fall in the slope range (0-8%), which is considered as flat to gently sloping; 31% are between (8-30%) which considered as slope to the moderately steep slope, 3% has a slope of 30-50%, which is classified as steep, and the rest 0.2% is above the slope of 50% which is very steep. Most of the study area is relatively uniform and highly suitable for agricultural activities. Agriculture is the community's main lifestyle, and the watershed has pleasant weather conditions.

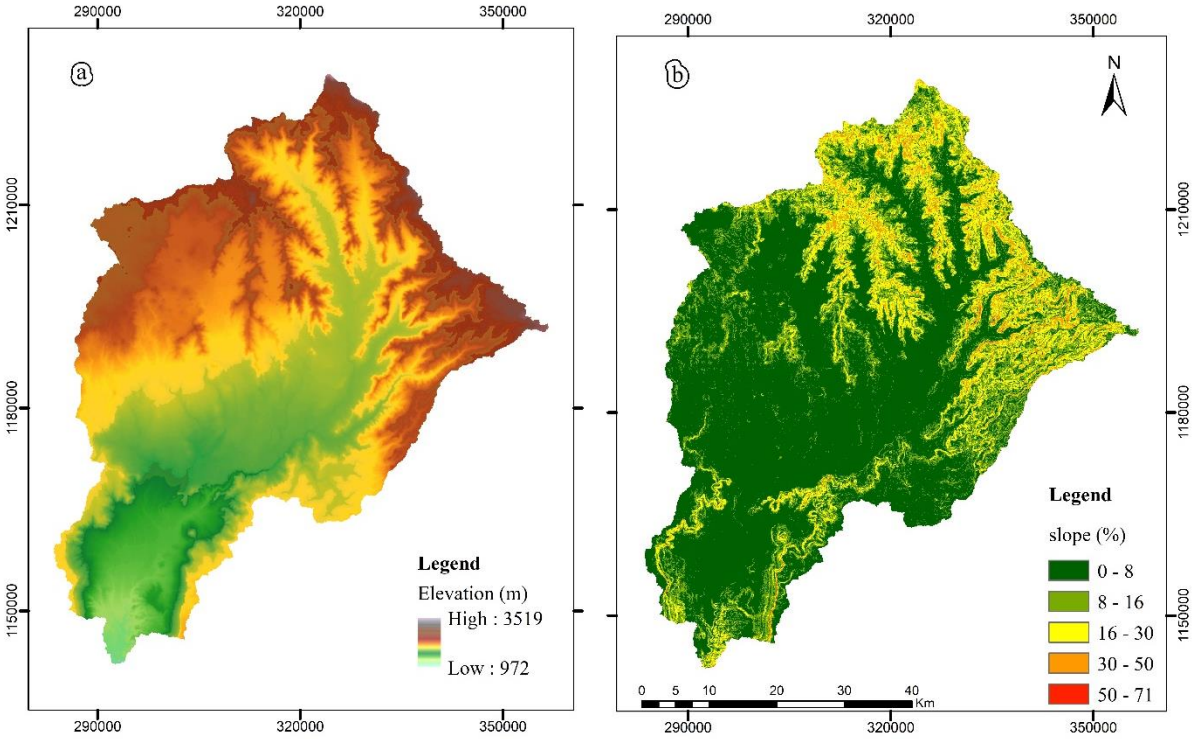

Figure 3. 2 Physiography(a), and Slope(b) map of the study area

3.1.2 Climate

Ethiopia is one of the largest countries situated in the horn of Africa that laying in the tropical zone between the equator and the tropic Cancer. The country has diverse ecology. The climate of the country ranges from hot or semi-desert to mild and humid zone. The rainfall distribution

of the country is affected by the summer monsoon (USAID, 2020), tropical upper easterlies, and local convergence in the red sea (Conway, 2000) and by the complexity of its topography. The country has several climate zones ranging from tropical savanna in the west to warm desert climate in the east. Conway, (2000) categorizes the climate zone of the Upper Blue Nile basin into three, namely, kola zone, which is below 1800m and temperature range between 20-28°C, Woina Dega zone that ranges 1800-2400m with 16-20°C temperature and Dega zone that has above 2400m elevation with an average temperature of 6-16°C.

The Birr watershed has a unimodal rainfall system, and the society produces once a year in the summer season only. But these days the society uses irrigation as an alternative to upgrade their lifestyle by using the groundwater resource. According to the national meteorological service agency climate classification, Birr watershed experience three different climate zones namely the Kola (tropical zone), Woina Dega (subtropical zone) and Dega (cool zone) (Figure 3.3).

The kola region has an elevation below 1500 meters above mean sea level and a temperature above 20°C; found in the south of the watershed around Abbay Gorge. The Woina Dega region covers the highland areas that have 1500-2300-meter elevation above mean sea level and temperature range between 16-20°C; located in the central, western, and southeastern part of the watershed (consists of the plateaus of Bure, Jabi Tena, Genet Abo, Quarit and Yechereka regions). The Dega climate zone of the watershed covers altitudes above 2300 meters above mean sea level and a temperature range of about 10-15 degrees Celsius, located at the north and northeastern part of the watershed.

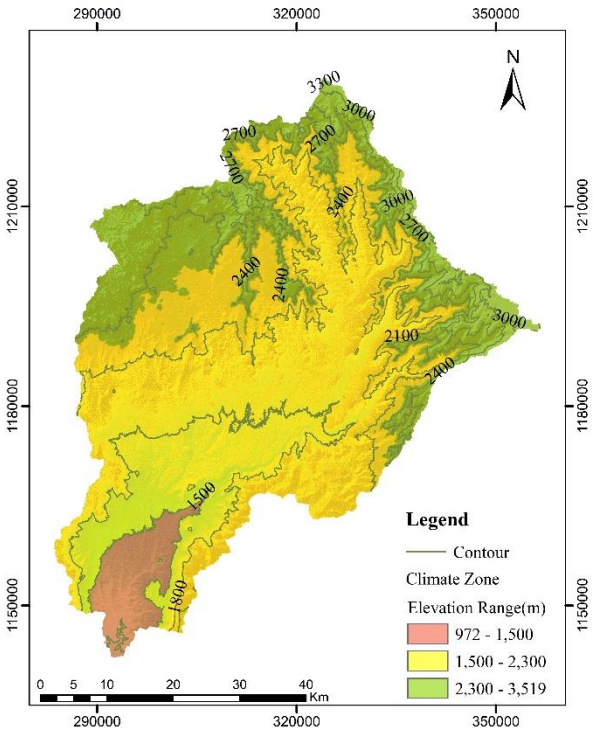

Figure 3. 3 Agro-ecology map of the study area

3.1.3 Geology and Lithology

In Ethiopia, there are four principal physiographic regions, namely the western Plateau, the southeastern plateau, the main Ethiopian rift valley and the afar depression (Coltorti, 2014). According to the ministry of mines and geological survey of Ethiopia, the lithological units of the study area grouped under Precambrian crystalline rocks, Paleozoic-Mesozoic sediments, and Cenozoic volcanic rocks (Tertiary) and Quaternary or recent unconsolidated sediments. The geological map of the Birr watershed (Figure 3.4) is compiled from three 1:250,000 scale map sheets of Ethiopia. The watershed covers 85% (2,695.32km^2) in the Burie map sheet (NC 37-5), 9% (295.34km^2) in the Debre Markos map sheet (NC 37-6) and 6% (172.82km^2) in the Bahir Dar map sheet (NC 37-1). As described in (GSE, 2008; GSE, 2015) the study area's lithologic units include Lower basalt (Tlb), Upper basalt (Tub), the Elluvial (Qel) and Alluvial (Qal) sedments, Migmatitic gneiss (Pmggn), Late- to post-tectonic granite (Pgt2), Agglomerate (Tag), Pyroclasts (Qv1), Thin Scoraceous basalts (Qv2), Yejube (Tv2), and Debre Markos basalt (Tv3) geological units (Figure 3.4) and (Table 3.1).

The Lower basalt (Tlb) is Mesozoic sediment (Msst) rock which covers 15.24% of the study area and usually occurs at the bottom of the Tertiary volcanic rocks. This basalt forms gently to moderately steep topographic features and infrequently short cliffs. It is dark gray to light-brownish gray and yellowish-brown color with medium-grained sandstone and limestone. It has unconformable contact with the overlying upper basalt (Tub). In the study area, this unconformity contact was found in the Wange quarry segment along the main road cut between Angut Michael and Yechereka town. The lower basalt is fine-grained, porphyritic, and characterized by the average composition of 40 % plagioclase, 15 % pyroxene, 15 % amygdaloidal minerals (zeolite, calcite, and chalcedony), 12 % opaque minerals (Fe-oxides) and 3% iddingsite.

Upper basalt (Tub) is mesozoic sediments (Msst) which are usually exposed as a continuous, patchy and fragmental outcrop and usually form the topmost part of the plateau. It is texturally coarse and immature sandstone holding quartz Wacke, lithic greywacke, and feldspathic greywacke rocks with subordinate beds of mature quartz arenite rocks. This lithologic unit covers 10.24% of the study area and is commonly exposed above 2400 m elevation. This basalt is fine to aphanitic, porphyritic with plagioclase, olivine, pyroxene and rarely amphibole phenocrysts in the study area. It is fine to medium grained porphyritic basalt with an average composition of 45 % plagioclase, 25 % pyroxene (augite), 10 % live-in, 10 % opaque, about 7 % secondary minerals including zeolite, calcite, and chalcedony and 3 % iddingsite.

The Elluvial Soil (Qel) and Alluvial Soil (Qal), the quaternary basalt which covers 26.51% of the study area. It is red to reddish brown silty to sandy soil commonly having basalt rock

fragments. Its exposed thickness reaches up to 5 m. The Alluvial soil is recent sediment that covers 22.66% of the watershed and occurs along river and stream valleys and its surroundings. It is commonly black cotton soil and rarely mahogany brown silty soil. The exposed thickness of the alluvial soil along the Birr River valley is about 8 m thick.

Migmatitic gneiss (Pmggn) is high grade metamorphic Precambrian rock found in the southern part of the watershed and covers 1.39% of the watershed. It includes variably interlayered units of mafic gneisses, quartzofeldspathick gneiss and minor Sillimanite and garnet bearing gneiss. The late-to post-tectonic granite (Pgt2) is pinkish to pinkish gray, medium to coarse grained rock that shows the variation in composition. The average composition of this basalt is 45 % k-feldspar, 37 % quartz, 14 % plagioclase, 3 % better and subordinate and accessory minerals, including Muscovite, Epidote, calcite, rarely zircon, apatite and garnet and Opaques. Agglomerate (Tag) is found in Kola Aklat, Geregera Mariam, Mutera and Debtera Berkenay hills forming sharp cliffs. Its thickness at the Kola Aklat hill is about 135 m. The agglomerate (Tag) is pink, red, greenish gray and yellow in color. Pyroclasts (Qv1) are commonly outcrop as pyroclasts of scoraceous basalt forming cones and crater rims. The cones have moderate to steep slopes with a half-breached morphology, and most are quarried that are used for road and other construction use. It commonly has rock fragments of pebble to cobble size which are scoraceous olivine and olivine-pyroxenephyric basalts. Thin Scoraceous basalt (Qv2) rock covers 4.59% of the watershed and these basalts are filled by calcite and zeolite minerals. Yejube (Tv2) basalt covers about 1.93% and is found in the eastern part of the study area. The topmost part of this unit is at places overlain by sandstone and ignimbrite or sandstone and pyroclastic Tuff or sandstone and anhydrite-gypsum rock. Debre Markos basalt (Tv3) covers about 2.53% of the catchment and forms escarpment, ridges, hills, moderate slope, gentle slope, and flat-lying topography. From the petrographic study, the Tv3 basalt is olivine-plagioclase phyric basalt, plagioclase-olivine phyric basalt, and olivine phyric basalt one grade into another.

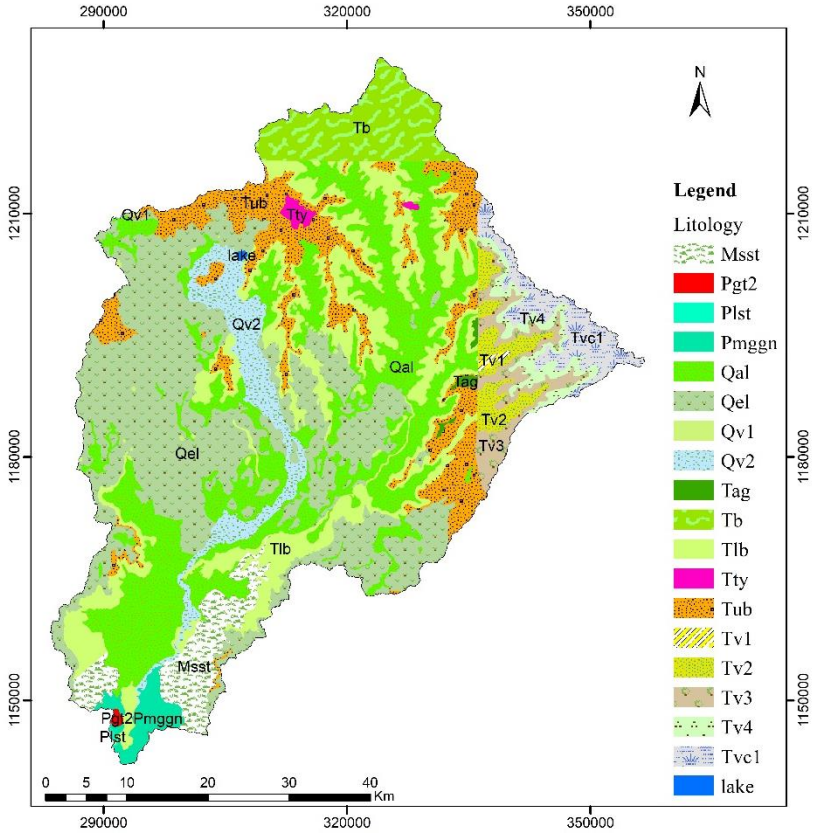

Figure 3. 4 Lithology map of the study area

Table 3. 1 Description of the lithology of study area

Lithologic Units	**Area (km^2)**	**Area%**
Mesozoic sediments (Msst)	122.08	3.86
Paleozoic (glacial) sediments (Plst)	1.16	0.04
Migmatitic gneiss (Pmggn)	44.04	1.39
Late to post tectonic granite (Pgt2)	2.37	0.07
Alluvial soil (Qal)	716.74	22.66
Elluvial soil (Qel)	838.74	26.51
Pyroclasts (Qv1)	5.06	0.16
Thin Scoraceous basalt flows (Qv2)	145.23	4.59
Agglomerate (Tag)	7.15	0.23
Tarmaber Gussa formation (Tb)	172.81	5.46
Lower basalt (Tlb)	482.17	15.24
Trachytic flows and plugs (Tty)	11.22	0.35
Upper basalt (Tub)	323.79	10.24
Arero Gidabo basalt (Tv1)	4.43	0.14
Yejube basalt (Tv2)	60.92	1.93
Debre Markos basalt (Tv3)	80.11	2.53
Lumame basalt (Tv4)	51.54	1.63
Rob Gebeya basalt (Tvc1)	92.68	2.93
Water Bodies	1.23	0.04

3.1.4 Hydrology

According to the geological survey of Ethiopia (GSE, 2012) the hydrologic units and the groundwater potential of the study area are highly controlled by the varying of geology, physiography, and lithologic structures. The different rock groups can be classified into different aquifers. The Aquifers in the Abbay basin are basaltic aquifers with less than 4L/s yield and the discharge to streams has been declining for over 30 years. Quaternary sediments have high productivity and are the major source of groundwater for private and communal use in the study area developed by hand-dug wells. The lithological units of the study area are classified into six aquifer groups (GSE, 2012) (Figure 3.5). The area coverage of the study area aquafers is described in Table 3.2.

The aquifer classification of Birr watershed;

- Extensive, locally developed and moderately productive porous aquifer, this aquifer unit include the quaternary rocks of the alluvial (Qal) and elluvial (Qel) sediments. (> 100 km², T=10-100m ²/d, q= 0.1 - 1 l/s.m and Q=1-5 l/s)
- Extensive and highly productive fissured aquifers, consists of the quaternary scoraceous basalts (Qv2), the Cenozoic Upper and Lower basalt (Tub and Tlb), Arero Gidabo basalt (Tv1) and Mesozoic sandstone (Msst). (> 100 km², T > 100 m ²/d, q>1 l/s.m and well Q> 5 l/s)
- Extensive and low productive fissured aquifers consist of the rock type Migmatitic gneiss (pmggn), Late to post tectonic granite (Pgt2), and glacial sediment (plst). (> 100 km², T =1-10 m^2/d, q = 0.01 - 0.1 l/s.m and well Q = 0.5 -1 l/s)
- The Aquitards and/or Minor fissured aquifers that have local and limited groundwater resources makes up some of the metamorphic rocks and volcanism, such as Agglomerate (Tag), Trachytic flow and plugs (Tty) and Pyroclasts (Qv1). (< 100 km², T = 0.1-1 m²/d, q = 0.001 - 0.01 l/s.m and well Q = 0.05-0.5l/s).
- Moderate Productive aquifer consists of Tarmaber-Gussa Formation (Tb), Lumame basalt (Tv4) with transmissivity value ranging 50-100m^2 per day and yield 2-5 l/s.
- Very low productivity consists of basalts like Debre Markos basalt (Tv3), Rob Gebeya basalt (Tcv1) that have transmissivity value between 1-10m^2 per day and yield 0.05-0.5L/s.

Table 3. 2 Hydrology description of the watershed

Hydrology	Area(km^2)	Area%
Lake	1.247103	0.039
Aquitards and minor fissured aquifer with local and limited ground water resource	23.435636	0.741
Extensive and low productive fissured aquifer	47.570525	1.504
Moderately productive fracture aquifer	83.026592	2.625
Extremely low productive fracture aquifer	318.544495	10.069
Extensive and highly productive fissured aquifer	1134.195838	35.853
Extensive locally developed and moderately productive porous aquifer	1555.477743	49.17

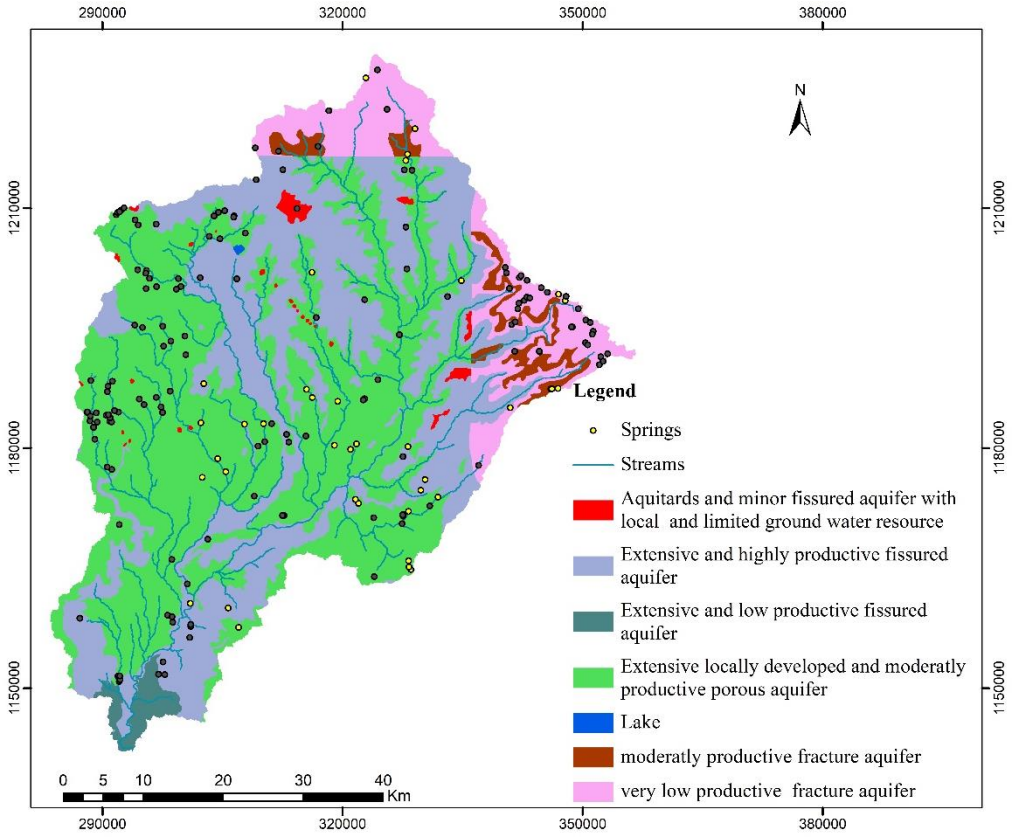

Figure 3. 5 Hydrology map of Birr watershed

3.2 Methodology

To assess the effect of LULC change and climate variability on ground recharge, the WetSpass model was employed. Primely, the necessary spatiotemporal data of the study area were gathered. Then the raw data was processed, manipulated, analyzed using different software packages and then the data were prepared in proper file formats for the model simulation. The input data for this model includes LULC maps, soil texture, slope, elevation map, and rainfall, temperature, wind speed and groundwater depth maps. In addition, the model needs LULC and soil parameters tables. The general work flows of the study is shown in Figure 3.6. The model uses two types of input data file formats. These are the database file format (.dbf) of land use and soil texture parameter tables and ASCII file format of the grid maps of climatological variables, classified images, the soil texture map, slope and elevation maps of the input data. Arc GIS 10.8, Quantum GIS (QGIS 3.16) and ERDAS imagen 2015 are used to prepare the WetSpass input parameters. Arc GIS 10.8 was used to prepare elevation map, the slope map, potential evapotranspiration map, the LULC map, the soil map, and groundwater level map of the watershed. In addition, it was used to convert grid maps to ASCII file formats and to convert network common data form (NetCDF) climate data to separate raster files. ERDAS imagine was used for classification purpose and to mosaic different scene of Landsat imageries to cover the whole study area. The study area covers part three scene of Landsat imageries that has a path of 169, 170 and 170 with raw of 53, 52 and 53 respectively (Table 3.9). QGIS also used for image preprocessing and satellite scanline error removal using gap mask fill data.

The topography and the slope grid maps were derived from high resolution ALOSPLASAR radiometric terrain corrected DEM free of charge in https://asf.alaska.edu/data-sets/. LULC map was classified from Landsat imageries of Landsat 5, Landsat 7 and Landsat 8 for 1990, 2005 and 2020 years, respectively. The climate hazard group infrared precipitation with station data (CHIRPS) data set was used as a source of precipitation data for this study which was downloaded from https://data.chc.ucsb.edu/products/CHIRPS-2.0/.

The monthly high resolution Terraclimate data is used to prepare temperature and wind speed data of the study which is downloaded from the terrestrial climate data set free of charge (http://thredds.northwestknowledge.net:8080/thredds/terraclimate_catalog.html). Moreover, the groundwater level map was prepared from the elevation of static water level measurements in boreholes (Figure 3.19).

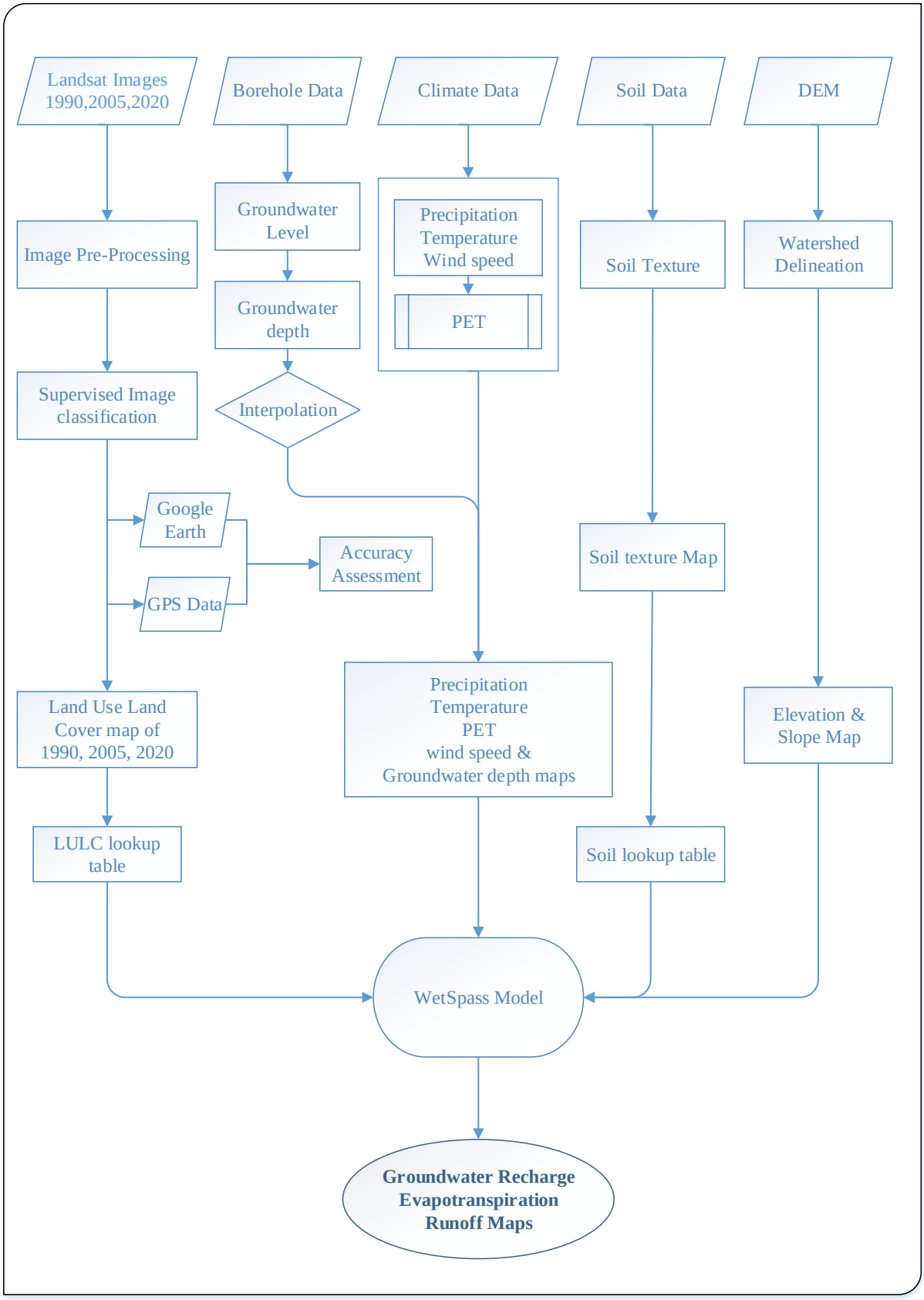

Figure 3. 6 Flow chart of the research process

3.3 Data Sources and Materials

To compile this paper, both spatial and non-spatial data were collected from various sources. The major data elements to WetSpass model were climatological variables, including monthly rainfall, monthly minimum and maximum temperature, monthly wind speed and potential evapotranspiration data. In addition, the model uses the soil data, topographic data (slope, elevation) and LULC data (Table 3.4). In this study different software packages and materials were used for data preparation, manipulation, analysis, and management tasks (Table 3. 3).

Table 3. 3 Software's used in the study

Software Used	Purpose
Arc GIS 10.8	For spatial data analysis, data visualization, managing, interpolation, displaying, and mapping
ERDAS 2015	For image preprocessing, land use classification, change detection analysis, and accuracy assessment activities
QGIS (Quantum GIS)	Preprocessing of Landsat TM and scan line error removal
R software	To generate PET using Thornthwaite method
WETSPASS	To generate recharge, ET and surface runoff
Handheld GPS	Ground data collection for accuracy assessment
Microsoft Office Package	For data preparation and analysis
Google earth	For accuracy assessment

3.4 WetSpass Model Input Data Elements

To estimate the hydrologic units of the study area, precipitation which is the primary hydrometeorological element, temperature, potential evapotranspiration, and wind speed data has been collected. These are the basic necessary input variables collected in high-resolution reanalysis of satellite products and meteorological stations. The WetSpass simulation model was used to determine the trend hydrologic balances of the watershed. For the model simulation, the variables were prepared in 30m*30m resolution. All the grid maps were prepared with the same column and row size, which is 2445 and 2906, respectively. Finally, the long-term annual and seasonal groundwater recharge, surface runoff, and actual evaporation hydrological components have been estimated using this model. The study evaluates the groundwater recharge of the study area using 30 years of time-serious climate data by dividing it into three phases. The first phase covers 1990-1999, the second from 2000-2009, and the third from 2010-2020.

Table 3. 4 Description of WetSpass model input parameters and data sources

Input Data	Year	Spatial Resolution	Measurement units	Data Source
DEM	Constant	12.5m*12.5m	Meter(m)	https://asf.alaska.edu/data-sets/
Slope	Constant	12.5m*12.5m	Degree(^{o})	https://asf.alaska.edu/data-sets/
Precipitation	1990-2020	0.05^o*0.05^o	Millimeter(mm)	https://data.chc.ucsb.edu/products/CHIRPS-2.0/
Temperature	1990-2020	0.04°C*0.04°C	Degree centigrade (°C)	http://thredds.northwestknowledge.net:8080/thredds/terraclimate_catalog.html
Wind speed	1990-2020	0.04°C*0.04°C	Meter per second(m/s)	
PET	1990-2020	30m*30m	Millimeter(mm)	calculated from R software using the Thornthwaite method
LULC	2020, 2005, 1990	30m*30m	–	https://earthexplorer.usgs.gov/
Soil type	Constant	30m*30m	–	Ministry of Agriculture

3.3.1 Climate Data

Precipitation

Precipitation is the primary factor that affects the spatial and temporal distribution of water resources. The rainfall distribution in the watershed increases from the south (Abbay Gorge) towards the north (mount Adama) and northeastern part of the watershed. In the watershed, there is a mono-modal type of rainfall system with two distinct seasons (four months of summer from June to September and eight months of winter from October to May), with rainfall peaks occurring in July.

In the Birr watershed, rain gauge stations are scarce, and not evenly distributed, most of the gauges have short-length recorded data, and only a few have temperature and wind speed data. As a result, reanalysis satellite data products were used in this study. Nowadays, to overcome station data limitations, high-resolution gridded satellite climatological products were produced as an alternative observed data set (Paredes-Trejo et al., 2021). Studies show that limitations of weather stations such as limited spatial coverage, irregular distribution of stations (Nsengiyumva et al., 2021), a short length of a record period (Derin & Yilmaz, 2014), and availability of high missing data were not sufficient to produce reliable rainfall analysis. In high-elevation areas absence of gauge stations underestimates the rainfall analysis at highlands (Bhattacharya et al., 2020).

In this study 30 years monthly precipitation data of the watershed which was downloaded from https://data.chc.ucsb.edu/products/CHIRPS-2.0/ to quantify groundwater recharge.

CHIRPS (https://www.chc.ucsb.edu/data/chirps) is a quasi-global satellite estimate precipitation data developed by USGS and Earth Resources Observation and Science (EROS) Center. It spans from 50°S-50°N and has 0.05°*0.05° resolution. CHIRPS rainfall product is a reanalysis result of real-time observing meteorological stations with infrared data, ranging from 1981 to the near present. The rationale that CHIRPS was selected in this study was its long-term temporal coverage, and relatively high spatial resolution and scholars noted that the CHIRPS data set is good at the regional and global scales as compared to other reanalysis products in terms of bias and person's correlation coefficient (Beck et al., 2020; Paredes Trejo et al., 2016; Dinku et al., 2018).

The rainfall in the watershed is mainly caused by orographic effects. Thus, precipitation in the watershed varies with altitude. The altitude and rainfall distribution in the study area are strongly correlated (Table3.5, Figure3.7). Therefore, using lower elevation gauge station data for analysis in the study area under estimates the rainfall in higher elevation areas. As a result, satellite products of CHIRPS data are more appropriate in the study area. The historical rainfall distribution in the Birr watershed is analyzed by dividing it into three phases.

Table 3. 5 Correlation of elevation and rainfall distribution in the study area

	DEM	Precipitation 1990	Precipitation 2005	Precipitation 2020
DEM	1			
Precipitation 1990	0.88	1		
Precipitation 2005	0.93	0.99	1	
Precipitation 2020	0.92	0.99	1.00	1

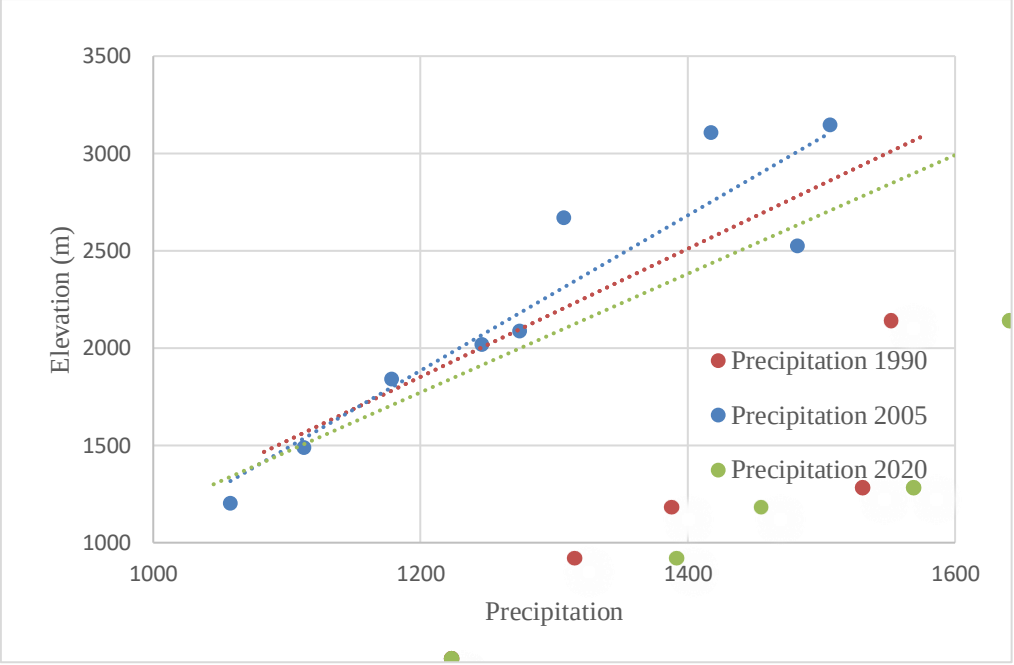

Figure 3. 7 Scatter plot of elevation and precipitation in the study area

The long-term average monthly rainfall distribution map in some stations in and around of the watershed (Figure 3.8).

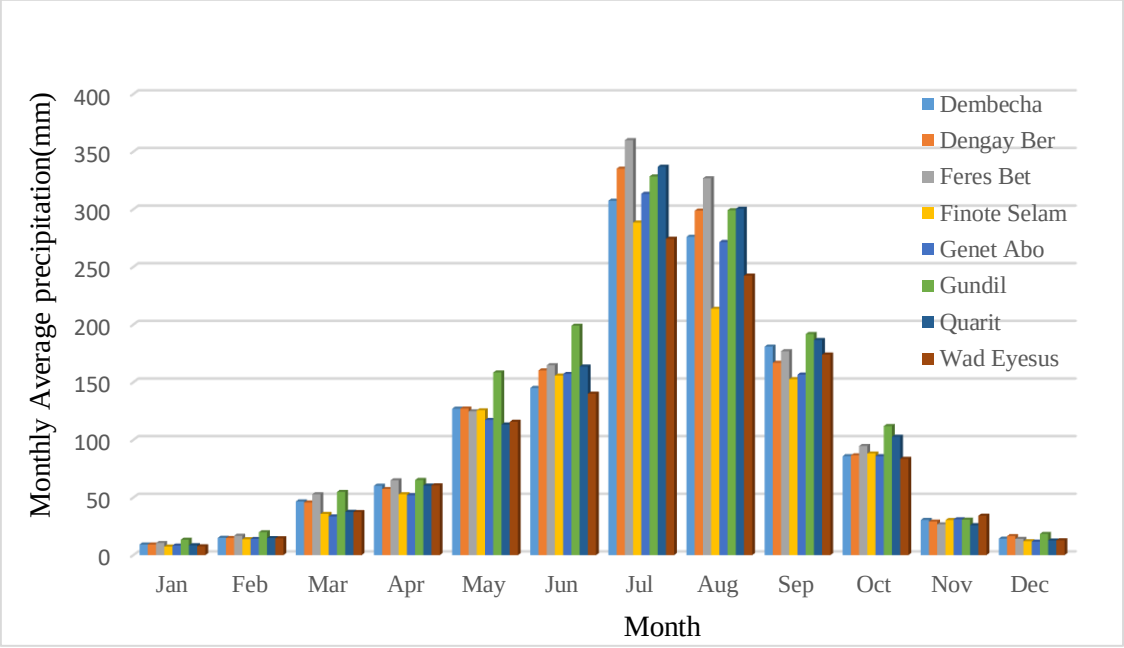

Figure 3. 8 The mean monthly precipitation of the study area (1990-2020)

The long-term average precipitation in the study area is 1501.03mm for 1990, 1269.24mm for 2005, and 1322.80mm for 2020. The annual precipitation in 1990 ranges 1312 to 1863mm, in 2005, it ranges 1030mm to 1604mm and in 2020 it ranges from 1020mm to 1746mm (Figure 3.9).

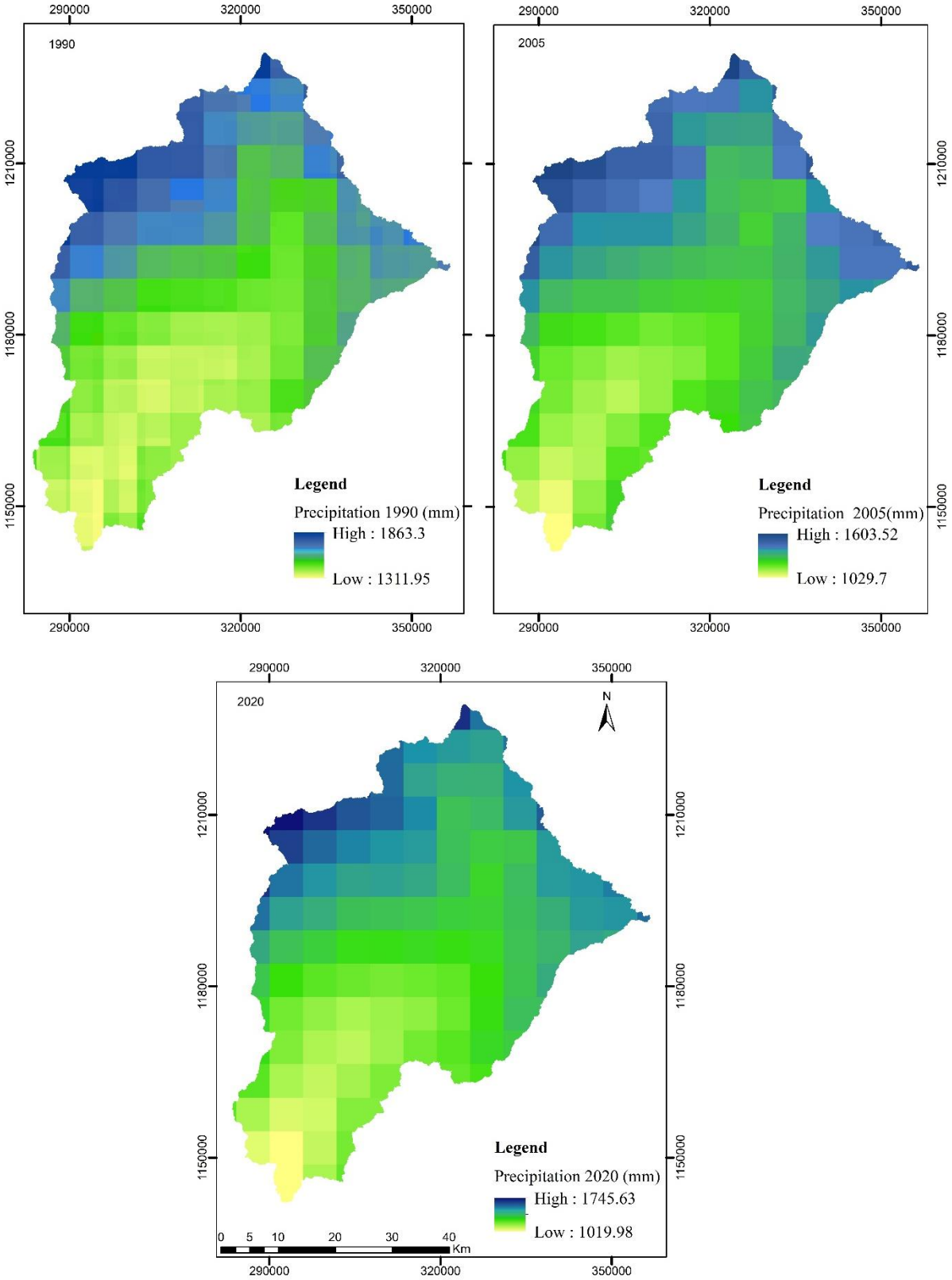

Figure 3. 9 The mean annual precipitation maps of the study area in 1990, 2005 and 2020

Temperature

To use reanalysis products as a substitute observation, Bhattacharya et al., (2020) evaluates four reanalysis products with global meteorological data in the Beas River basin and confirmed that there is no high variation between the observed temperature and reanalysis temperature. Reanalysis temperature has good agreement with observation, this is because radiosondes and satellite-derived atmospheric temperature products have regularly assimilated with the reanalysis system (Essou et al., 2016). Climate reanalysis data combines climate model products with observation at the regular grid and is not limited to topography. Thus, it is helpful to use climate reanalysis products in gauge station data-limited areas.

In this study, the minimum and maximum monthly temperature data were downloaded from terraclimate (http://thredds.northwestknowledge.net:8080/thredds/terraclimate_catalog.html) Catalog. It has a spatial resolution of 1/24°C. Terraclimate is a data set of monthly climate and climatic water balance of the global terrestrial surface from 1958 to the present. It was created by using climatically aided interpolation, combining high-spatial resolution climatological normals from the WorldClim dataset, with coarser spatial resolution, but time-varying data from CRU Ts4.0 and the Japanese 55-year Reanalysis (JRA55) (Abatzoglou et al., 2018). TerraClimate was selected for this study because of its resolution, and a lengthy period of recorded data to extract time serious temperature and windspeed data. The temperature data was analyzed in three phases in ten-year intervals. The mean monthly temperature is used to run the model. Thirty years of time-serious data in the watershed show an increasing temperature trend. The average temperature ranges between 12.1-23.8^{o}c, 12.5-24.2^{o}c, and 13.3-25^{o}c for the first, second, and third phases, respectively, in Figure 3.10.

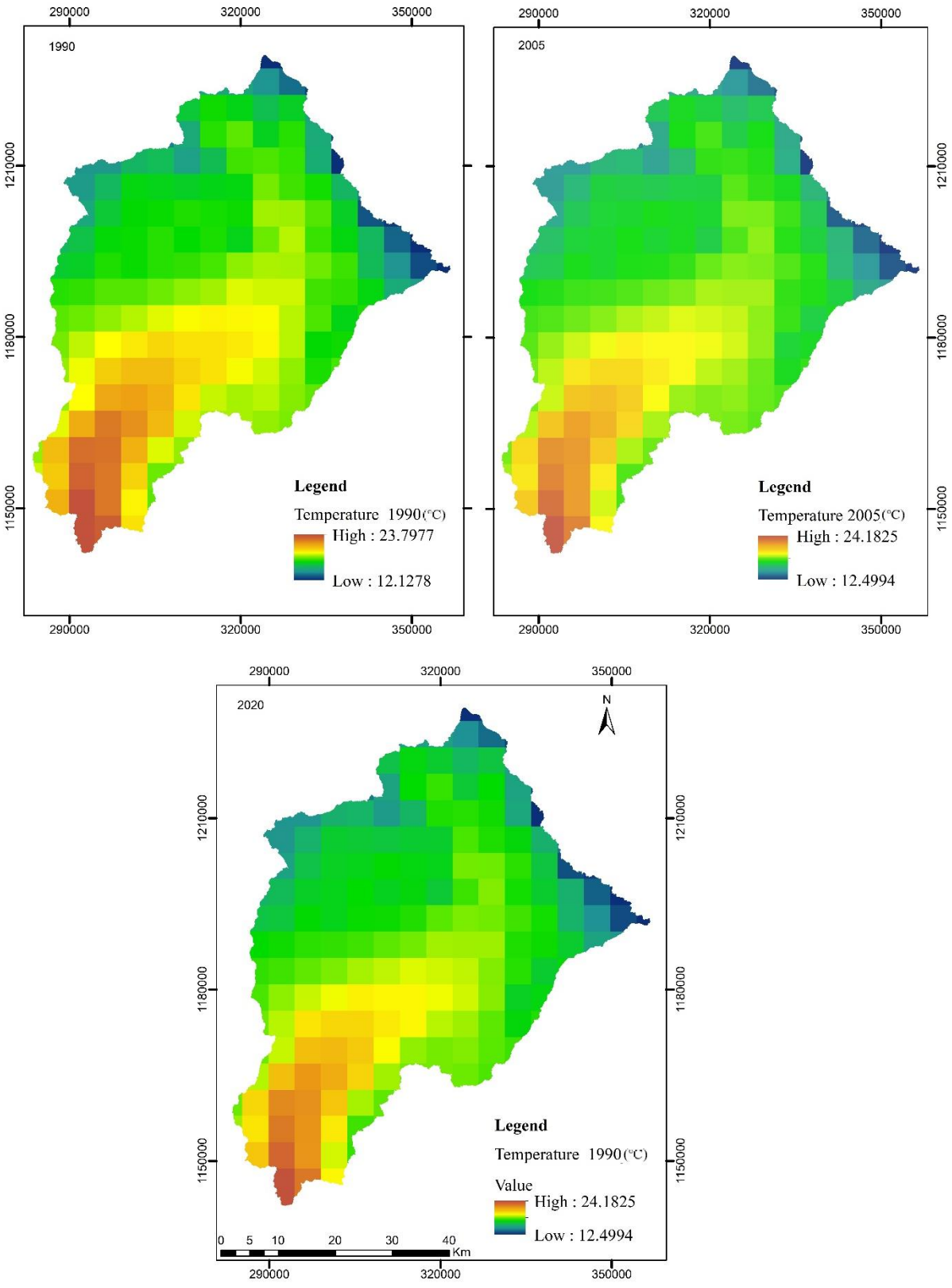

Figure 3. 10 The mean annual temperature maps of the study area in 1990, 2005 and 2020

Wind Speed

The wind speed data were downloaded from a high-resolution global data set of monthly climates, and climatic water balance, Terraclimate website, and analyzed in three phases. Each phase has a 10-year interval. Like other input data, the long-term mean annual wind speed grid map was also prepared in the same time intervals for each phase. For the first phase, the wind

speed value ranges from 0.98-1.86m/s, for the second phase 1.09-1.95m/s, and 1.05-1.93m/s for the third phase (Figure 3.11).

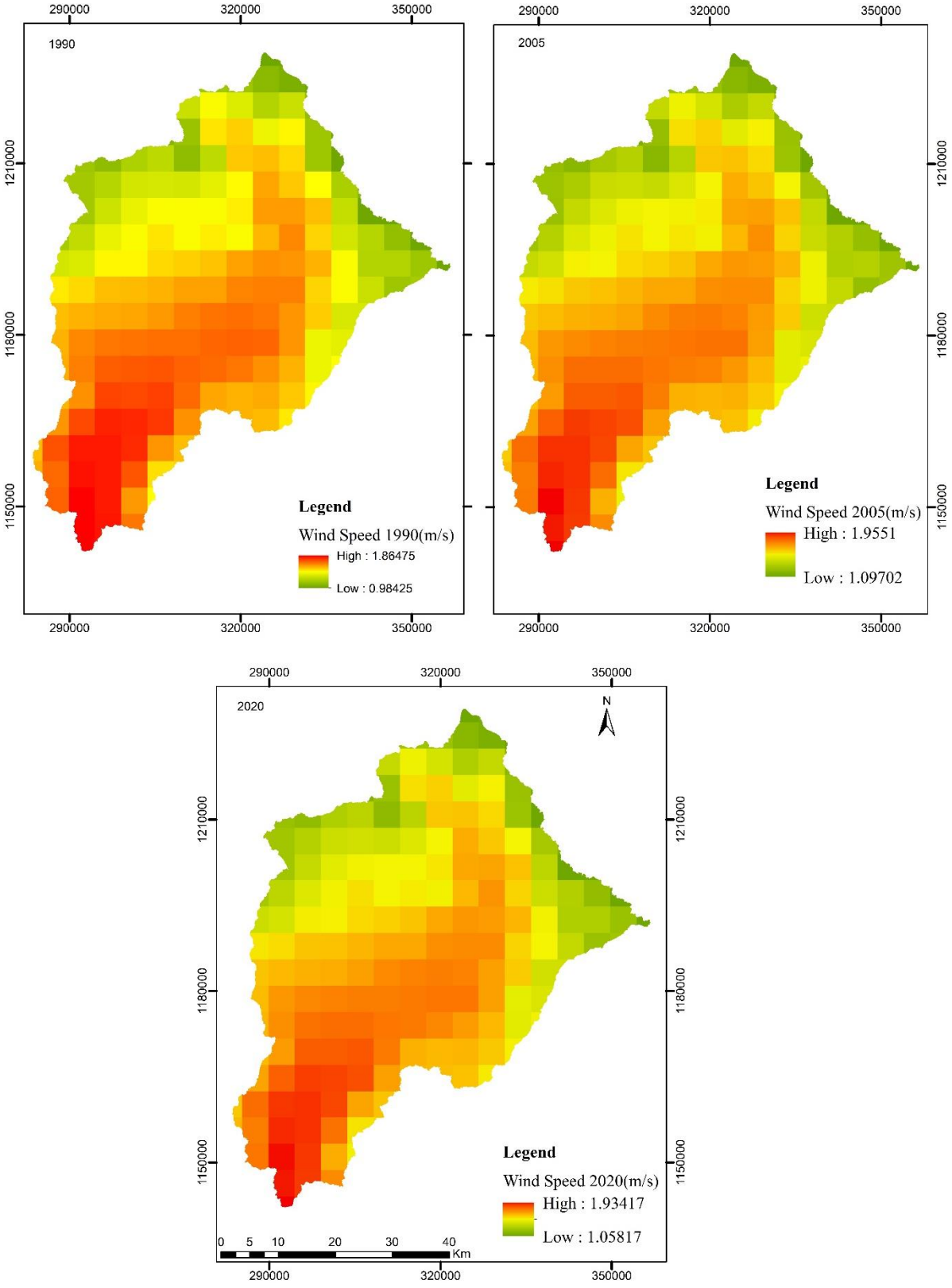

Figure 3. 11 The mean annual wind speed maps of the study area in 1990, 2005 and 2020

3.3.2 Satellite Climatological Variables Validation

The validity of satellite estimations can be evaluated using a categorical index and various statistical elements like Pearson correlation, root mean square error, and bias (Ayehu et al., 2018). The Pearson correlation coefficient is among the techniques used to evaluate the strength of relationships between variables. It is a number between -1 and 1 that shows the strength of variables in linear relationships. In this study the Pearson correlation coefficient is used to show the agreement of gauge observation with CHIRPS data (Table 3.6; Figure 3.12) and Terraclimate estimates (Table 3.7; Figure 3.13) in a 95% level of confidence. Both the

Table 3. 6 Correlation of station observations and CHIRPS rainfall

	Correlations	Gauge Rainfall Observation	Correlations Rainfall
Gauge Rainfall Observation	Pearson Correlation	1	.876**
	Sig. (2-tailed)		.000
	N	1711	1711
CHIRPS Satellite Rainfall	Pearson Correlation	.876**	1
	Sig. (2-tailed)	.000	
	N	1711	1711

**. Correlation is significant at the 0.01 level (2-tailed).

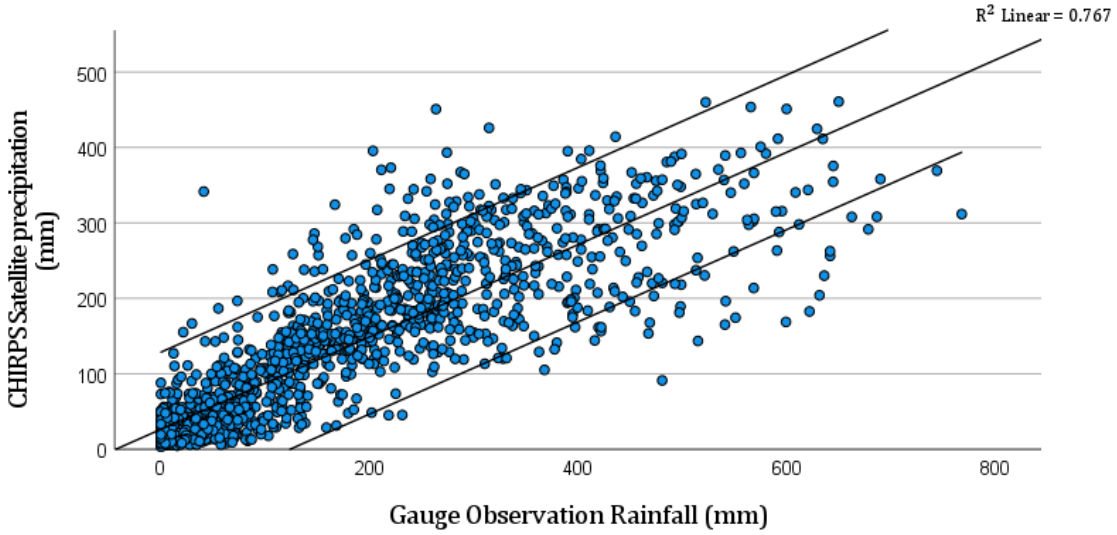

Figure 3. 12 The correlation plot of CHIRPS Vs station observation

Table 3. 7 Correlation of Gauge temprature and Satellite observation

Correlations		Gauge Average T°	Terraclimate Average T°
Gauge Average T°	Pearson Correlation	1	.823**
	Sig. (2-tailed)		.000
	N	993	993
Terraclimate Average T°	Pearson Correlation	.823**	1
	Sig. (2-tailed)	.000	
	N	993	993

**. Correlation is significant at the 0.01 level (2-tailed).

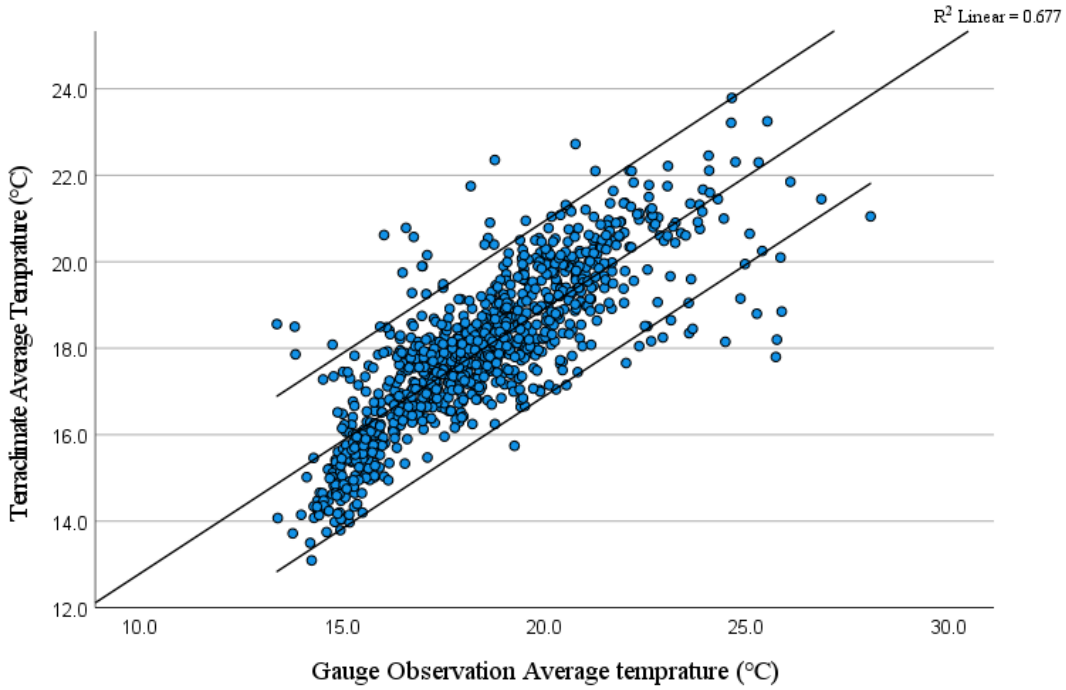

Figure 3. 13 The correlation plot of Terraclimate Vs station observation

Potential Evapotranspiration

Evapotranspiration refers to the total amount of water lost due to the combined effect of evaporation from the ocean surface, the soil, and transpiration through the plant leaves (Poeter et al., 2020b). It could be explained as potential and actual evapotranspiration. Potential evapotranspiration is described as the quantity of water evaporated per unit area and time from an idealized, extensive free water surface under existing atmospheric conditions. The rate of evapotranspiration could be affected by factors such as the amount of solar radiation, atmospheric vapor pressure, temperature, wind, and soil moisture.

Potential evapotranspiration (PET) is one of the input data elements to the WetSpass model in the groundwater recharge quantification process. It can be measured directly on the field or calculated using physical or empirical equations. There are several approaches to estimate evaporation and evapotranspiration. The commonly known approaches include temperature-based, radiation-based, and mass-transfer methods. Some researchers show that radiation-based approaches are better than other approaches and others show that temperature-based empirical techniques are more acceptable while others recommend that either using the combined methods of energy balance and mass transfer or using parametric methods are the right methods. For instance, Jakimavičius et al., (2013) compares the above techniques and confirmed that the Thornthwaite, Schendel, and Vikulina (temperature-based) techniques were the most exact estimates with the lowest uncertainties. But, Tegos et al., (2013) show that the empirical methods are limited in the prediction of the entire locations because such models are functional only in a specific condition for the area they are modeled. Though, the choice of the best method depends on data availability, location conditions, needed accuracy, cost, and

complexity of the input data parameters. In this study, the Thornthwaite technique is selected due to data limitation and its simplicity to calculate PET in R software using the standard precipitation index (SPEI) package.

In this method PET is calculated in the following formulas (Hafeez et al., 2020).

$$PET = 16(\left(\frac{10T_i}{I}\right)^a$$

Where, T_i is the mean monthly air temperature and I is the heat index

$$I = \sum_{i=1}^{12} \left(\frac{T_i}{5}\right)^{1.534}$$

$$a = 675 * 10^{-9}I^3 - 771 * 10^{-7}I^2 + 1792 * 10^{-5}I + 0.49239$$

In the study area PET is calculated for all phases for the same time interval like temperature and precipitation. The mean annual PET of the Birr watershed is 978.58 to 1352.26 for the first phase, 1201.19 to 1650.27 for the second phase, and 1208.71 to 1670.26mm per year for the third phase (Figure 3.14).

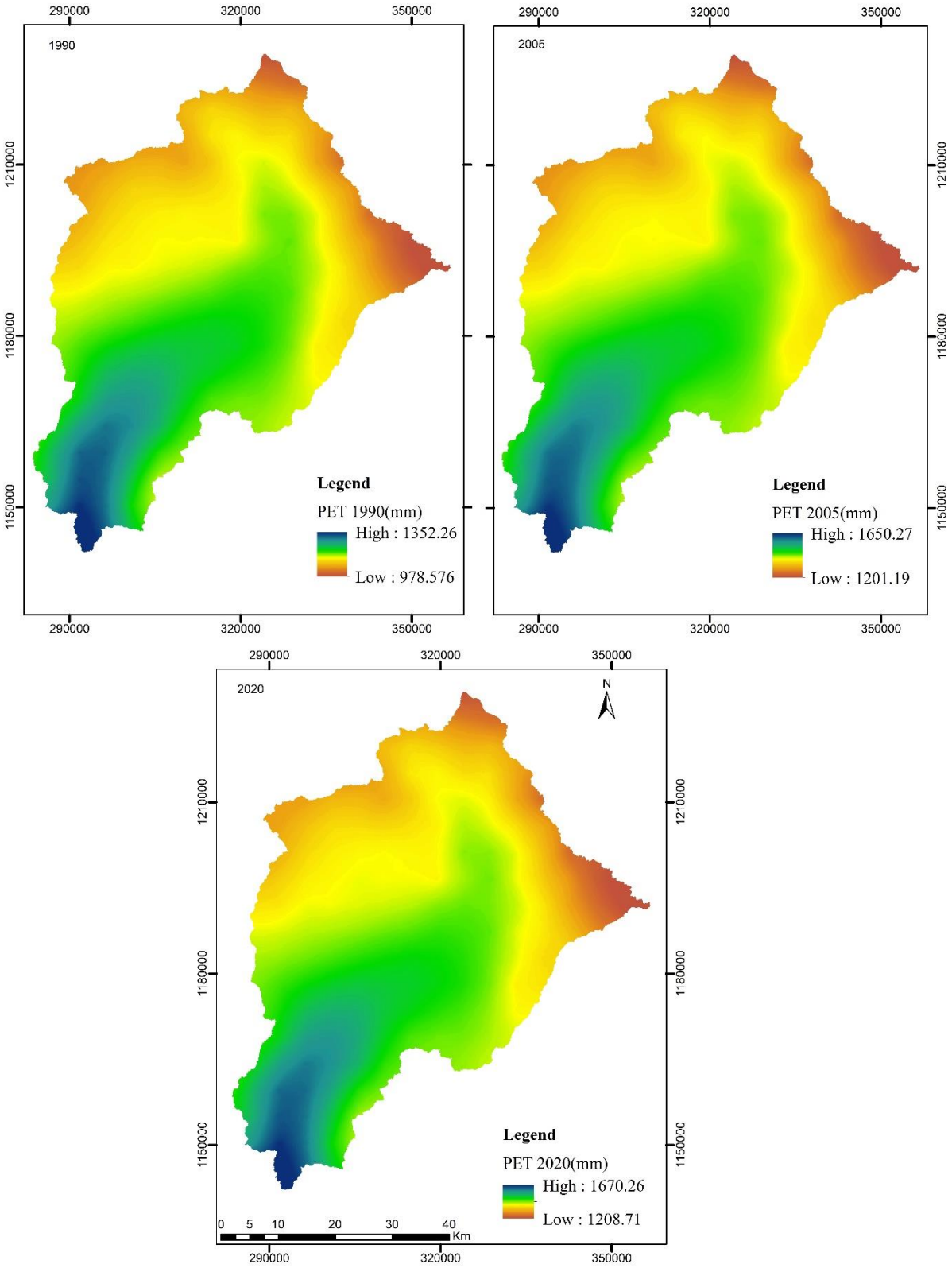

Figure 3. 14 The mean annual PET map of the study area

3.3.2 Elevation and Slope

ALOSPLASAR radiometric terrain corrected DEM were used to delineate the watershed boundary, to produce slope and elevation map of the study area. ALOS is one of earth observation satellites whose purpose is global monitoring, disaster monitoring, cartography, regional observation and technology development by collecting high resolution land observation data. It has a spatial resolution of 12.5 m*12.5m. But, for the model simulation of the study area the slope and elevation map were resampled to 30m*30m spatial resolution (Figure 3.15) to make it similar resolution with other WetSpass input elements. The model needs same resolution, equal raw and column size for all input grid maps.

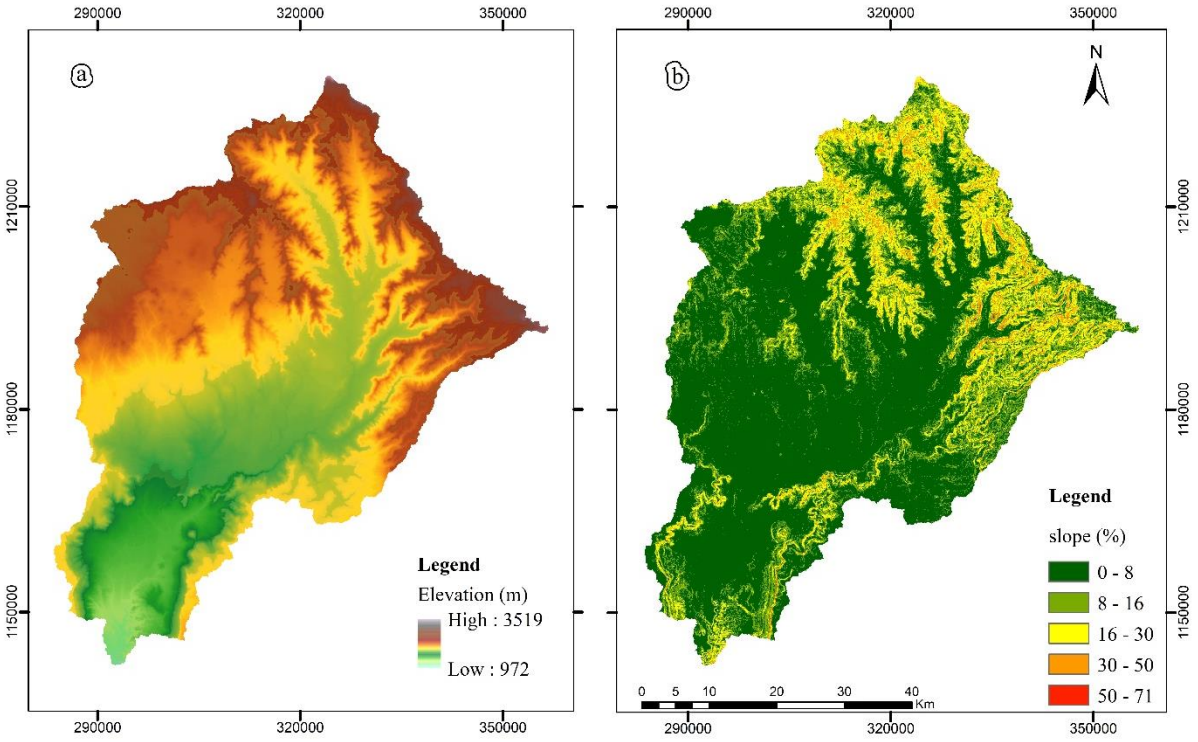

Figure 3. 15 Elevation(a), and slope(b) map of the watershed

3.3.3 Soil Texture

In groundwater recharging, soil texture has a paramount effect on recharging. The proportion of clay, silt, and sand components decides the level of infiltration. During infiltration, coarse-grained soils have a higher recharge rate than fine-grained soils (Cook et al., 1992). The study area soil data is obtained from the ministry of agriculture and has two soil texture class (Table 3.8; Figure 3.16) namely the clay and loam textural class.

Table 3. 8 Soil texture description of the watershed

Soil Texture	Area (m^2)	Area %
Clay	752.212696	23.77959
Loam	2411.057599	76.22041

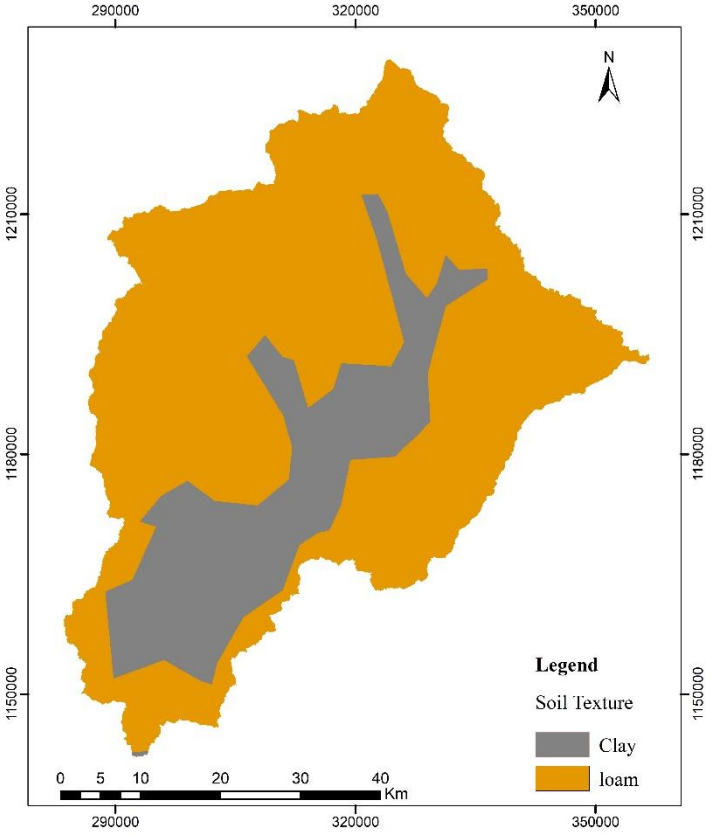

Figure 3. 16 Soil texture map of the study area

3.3.4 Landsat imageries

In this study, Landsat 5(TM), Landsat 7 (ETM+), and Landsat 8 (OLI) multi-temporal satellite Landsat imageries were downloaded from USGS free of charge (https://earthexplorer.usgs.gov/). It is used to produce the time serious land use land cover map of the study area (Figure 4.1). The study area consists of three scene of Landsat imageries. The study area lays in the Landsat WRS_Path of 169, 170 and 170 with WRS_Row of 53, 52 and 53 respectively (Table 3.9). To examine the land use land cover change of the study area fifteen-year interval was selected and, the imageries in 1990, 2005 and 2020 were classified by supervised classification technique to prepare a LULC map of the watershed for the respective years.

Table 3. 9 Description of satellite data

Satellite data	Acquisition date	WRS_Path	WRS_Row	Resolution
Landsat 5	01/07/90	169	53	30m*30m
	05/22/90	170	52	30m*30m
	05/22/90	170	53	30m*30m
Landsat 7	03/29/05	169	53	30m*30m
	04/05/05	170	52	30m*30m
	04/05/05	170	53	30m*30m
Landsat 8	02/27/20	169	53	30m*30m
	02/11/20	170	52	30m*30m
	02/11/20	170	53	30m*30m

3.3.4.1 Image Preprocessing

The role of image preprocessing is to remove undesired distortions and improve the quality of an image to interpret it in a better way. In different image processing applications, the preprocessing operation is a crucial step that should be done before the main data analysis and data extraction performed. Remote sensing image pre-processing activities are grouped under geometric and radiometric correction (Ravi & Ashokkumar, 2017).

Geometric correction is adjusting the geometric distortions occurred due to sensor-earth variations. Geometric distortions mainly occurred because of the relative motion of the platform, its scanner and the earth (Sowmya et al., 2017). Landsat imageries were geometrically corrected (Mohajane et al., 2018) and for this study level 1 Landsat images were used.

Radiometric correction is the process of removing distortions in the degree of electromagnetic energy registered by each detector (sensor irregularities). It includes atmospheric correction, sun angle and topographic correction as well as detector response calibration tasks like de-striping, missing scan line removal, and random noise removal. In this study, to increase the visual interpretation of imageries, radiometric corrections were performed using Quantum GIS (QGIS) software. The Semi-Automatic Classification Plugin tool of QGIS was used to apply atmospheric corrections (Mohajane et al., 2018) based on Dark Object Subtraction (DOS) algorithm (Chavez, 1988) for the Landsat images of 2020 (Landsat 8 OLI), 2005 (Landsat 7 ETM+), and 1990 (Landsat 5 TM). Additionally, for the Landsat image of 2005, satellite scanline error correction (Destrippng) was performed using QGIS by gap mask fill data. Satellite images consist of digital numbers (DN) arranged in rows and columns that stand for the color, brightness, and wavelength values of an image element. Thus, image calibration is done by converting DN values into reflectance units at-sensor spectral

radiance (Chander et al., 2007; Chander et al., 2009; Vicente-Serrano et al., 2008) through Equation (1).

$$L_\lambda = \left(\frac{LMAX_\lambda}{Q_{calmax}} - \frac{LMIN_\lambda}{Q_{calmin}}\right)(Q_{cal} - Q_{calmin}) + LMIN_\lambda \ldots\ldots\ldots\ldots\ldots\ldots\ldots\ldots\ldots\ldots (1)$$

Where; L_λ is the spectral radiance at the sensor's aperture, DN is the digital number of the quantized calibrated pixel value, $LMAX_\lambda$ is the maximum spectral radiance that is scaled to Q_{calmax}, $LMIN_\lambda$ is the minimum spectral radiance that is scaled to Q_{calmin}, Q_{calmax} is the maximum quantized calibrated pixel value in DN (corresponding to Llmax) and Q_{calmin} is the minimum quantized calibrated pixel value in DN (corresponding to $LMIN_\lambda$. Then, the radiance is converted into top-of-atmosphere (TOA) reflectance using Equation (2) (Chander et al., 2007).

$$P = \frac{\pi L d^2}{ESun_{\lambda}\cos\theta} \ldots\ldots\ldots\ldots\ldots\ldots\ldots\ldots\ldots\ldots\ldots\ldots\ldots\ldots\ldots\ldots\ldots\ldots\ldots\ldots\ldots\ldots\ldots\ldots\ldots (2)$$

Where; ρ is unit less planetary reflectance, L is spectral radiance at sensor aperture, d is the Earth-Sun distance, which is on the date of imaging, Esun is mean solar exoatmospheric irradiance for band λ, π is unitless mathematical constant value ~3.14159, and θ is solar zenith angle in degree.

3.3.4.2 Land Use Land Cover Classification

Image classification is the process of categorizing all pixels in an image or remotely sensed imagery to obtain a given set of land cover themes (Sowmya; Deepa & Venugopal K., 2017). Digital image classification is mostly classified as supervised and unsupervised classification. Unsupervised classification is a process of clustering pixels based on the reflectance properties of pixels.

In supervised classification, the analyst identifies homogeneous training samples of different cover types. The quality of classification depends on the accuracy of training samples. The most used supervised classification is maximum likelihood classification (MLC) (Sowmya; Deepa & Venugopal K., 2017). MLC has high probability and uses variance and co-variance to classify an unknown pixel of spectral response pattern. Thus, it is the best algorithm as compared to others in overall accuracy and kappa coefficient (Agenagnew et al, 2021). In this study, the MLC technique was employed using ERDAS imagine 2015. The land use map of Birr watershed was derived by ERDAS imagine 2015 from Landsat 8 operational land imager multispectral image of 2020, Landsat 7 enhanced thematic mapper of 2005, and Landsat 5 thematic mapper of 1990 using supervised classification method and MLC algorithm. The LULC of the watershed was classified into eight classes (Figure 4.1) according to Table 3.10 classification scheme. It includes agriculture, forest, grassland, built-up, shrub, water body, bare land, and wetland land use class.

Table 3. 10 Land cover classification scheme

Land cover	Description
Water body	Lakes, reservoirs, stream, rivers
Built up areas	The Land that covered by buildings and other manufactured structures like roads, residential, commercial services, and industrial areas.
Bare land	Lands with exposed soil, sand or rocks, bare exposed rocks, and quarries.
Shrubs	Lands with small woody vegetation.
Forest	Lands dominated by trees
Agriculture	Lands covered with temporary crops followed by harvest period
grass land	pastoral or grazing lands, with sparse trees
wet land	saturated lands and swamps

3.3.4.3 Accuracy Assessment

Accuracy assessment is the technique used to quantify the reliability of classified images. Scholars show that there is no single universally accepted measure of accuracy assessments. The most applied accuracy assessment technique is an error matrix (Deng et al., 2008). In assessment, the sampling strategy used to gather ground truth points and the sample size determination are especially important aspects. Thus, selecting a sufficient and representative sample size enables minimizing biases (Hay, 1979) and using two or more accuracy assessment measures were perceived as a workable, and reasonable way to provide good accuracy assessment measures. During accuracy assessment, using only ground training points is not recommended because training sits are not random (biased) and are subjected to analysts' prior knowledge (Jensen & Lulla, 1987) and applying a purely random sampling technique is not also practical because it ignore small land use categories. Thus, stratified random sampling is recommended (Congalton, 1991).

For this study, both user-defined ground training points and stratified random sampling methods were used. The accuracy of image classification is often measured by percentages and expressed consumer (CA) and producer accuracy (PA). PA measures error of omission, which refers to how well real-world land cover types can be classified. User accuracy (UA) measures commission errors, which is the likelihood of a classified pixel matching the land cover type of its corresponding real-world location. And the overall accuracy shows the comparison of each of the classified pixels versus the definite land cover conditions obtained from their corresponding ground truth data.

In this study the accuracy assessment of classified images was tested using the confusion matrix and kappa coefficient using sample ground control points collected in the field using Garmin72 handheld GPS, google earth image and google earth history images. The accuracy assessment

was examined by a confusion matrix which helps to obtain the user accuracy, the producer accuracy, the overall accuracy and the kappa coefficient for all the three classified satellite images. These parameters are calculated by the following equation from error matrix (Anand, 2012).

$$\text{User accuracy} = \frac{\text{No. of correctly classified pixels}}{\text{total classified pixels}} * 100 \ldots\ldots\ldots\ldots\ldots\ldots\ldots\ldots\ldots \text{eq1}$$

$$\text{Producer accuracy} = \frac{\text{No. of correctly classified pixels}}{\text{total reference pixels}} * 100 \ldots\ldots\ldots\ldots\ldots\ldots\ldots\ldots \text{eq2}$$

$$\text{Overall accuracy} = \frac{\text{sum of correctly classified pixels}}{\text{total number of reference pixels}} * 100 \ldots\ldots\ldots\ldots\ldots\ldots\ldots\ldots \text{eq3}$$

A kappa analysis another method of accuracy assessment which is applied in KHAT statistic according to the following equation (Congalton, 1991).

$$\text{kappa coefficient} = \frac{N\sum_{i=1}^{r} X_{ii} - \sum_{i=1}^{r}(X_{ri} * X_{ci})}{N^2 - \sum_{i=1}^{r}(X_{ri} * X_{ci})} \ldots\ldots\ldots\ldots\ldots\ldots\ldots\ldots\ldots\ldots\ldots\ldots \text{eq4}$$

Where, r is the number of rows in the error matrix, X_{ii} is the number of observations of pixels in row i and column i, $X_{ri}$is the total number of observations in row i $X_{ci}$is total number of observations in column i and N is the total number of observations in matrix.

For accuracy assessment of this study, 440 points were used for each classified images. For LULC map of 2020, 200 ground truth points, gathered around towns and the main roads of the watershed, and 240 points that generated using stratified random sampling technique in ERDAS software are used for accuracy assessment. Based on land use category, for agriculture 70 point, for grassland 60 points, for forest 60 points and for the rest land uses 50 points used for each land uses to test the accuracy of LULC map of 2020 (Annex V). Both google earth and ground truth points used as a reference. For the rest classified images of 1990 and 2005 all points were generated by software and the image accuracy is checked with reference to google earth history images. For LULC map of 2005, for agriculture 66, forest and gras 60 point for each, bare land and shrub 54 points for each and for the rest land use 50 points for each is used to test the accuracy of the classified images (Annex IV). Similarly, for LULC of 1990, 70 points for agriculture, 56 points for forest, 60 points for grass, 54 points for shrub and for built-up, water, bare land and wetland 50 points was used for each land uses (Annex III). The overall accuracy for 1990 is 0.85% with kappa coefficient of 0.83%, and for 2005 and 2020 the overall accuracy is 0.87% and 0.89% with kappa coefficient of 0.85% and 0.87%, respectively.

3.3.5 Groundwater Depth

Groundwater depth data was produced from the elevation of static water level measurements in boreholes. The overall static water level measurements were used for interpolation to produce the groundwater depth grid map of the study area (Figure 3.17). The groundwater depth was found by subtracting the static water level of boreholes from elevation. The annual grid map of the study area is then interpolated using the available groundwater depth data by ordinary kriging interpolation technique in a GIS environment. Ordinary kriging interpolation technique has minimized error variance and gives a consistent result with known values (Yamamoto, 2005). Thus, ordinary kriging selected since it is the better measurement of the accuracy. Due to lack of well-organized long term yearly groundwater depth data, similar groundwater level input data were used for all years.

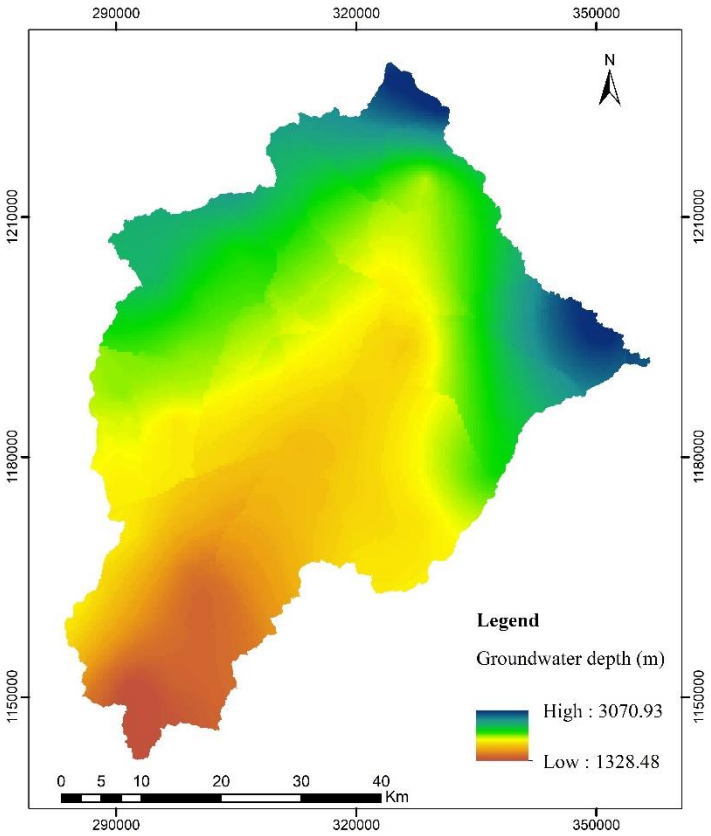

Figure 3. 17 Groundwater depth map of the watershed

3.3.6 Lookup Tables

For this study, two parameter tables were prepared in database file format, the LULC and soil texture, parameter tables. These different biophysical data are obtained and reviewed from scholarly published literature. The developed grid maps and the parameter data together make the required interaction with each other to produce average values during the simulation processes. In addition, the model can run when all input grid maps have similar cell size (same column and same row of all raster input data of the model). For this study it has 2445 and 2906 column and row size, respectively.

3.4 Water Balance Components Computation

WetSpass model is a quasi-steady state spatially distributed water balance model that describes the water and energy transfer between soils, plants and the atmosphere (Batelaan & De Smedt, 2001). The model has the capability to simulate interception from vegetated surface, runoff, evapotranspiration, soil water balance and recharge at monthly and yearly time scale. In this model the water balance calculations are done at a raster cell level. The water balance in every single raster cell is obtained by summing the independent water balance components of a given raster cell. The total water balance in an area is calculated by the sum of the water balance of each raster cell (Batelaan & De Smedt, 2007).

In this study, WetSpass model was used to estimate the annual groundwater recharge based on the water balance equation. The model uses long term average climate data, elevation, slope, groundwater depth, LULC, and soil data, simulate average spatial patterns of surface runoff, evapotranspiration, and groundwater recharge as shown in Figure 3.18 in the watershed. The total water balance of a raster cell is split into independent water balances for the vegetated, bare land, open water and impervious surface of each raster cell (Batelaan & De Smedt, 2001). It is calculated using equations 3.1-3.8 (Batelaan & De Smedt, 2001; Gebreyohannes et al, 2013; Batelaan & De Smedt, 2007).

$$\text{Etraster} = \text{avETv} + \text{asEs} + \text{aoEo} + \text{aiEi}, \quad (3.1)$$

$$\text{Sraster} = \text{avSv} + \text{asSs} + \text{aoSo} + \text{aiSi}, \quad (3.2)$$

$$\text{Rraster} = \text{avRv} + \text{asRs} + \text{aoRo} + \text{aiRi}, \quad (3.3)$$

$$P = I + S_v + T_v + R_v \quad (3.4)$$

Where, ET_{raster}, S_{raster} and R_{raster} are total evapotranspiration, surface runoff, and groundwater recharge of a raster cell of vegetation (v), bare soil (s), open water (o) and impervious area (i) respectively. The coefficient, a, expresses the fraction area of each land use.

P, I, S_v, T_v and R_v represent the total seasonal precipitation, the interception by vegetation, surface runoff over the land surface beneath the vegetation, the actual transpiration of the vegetated surface and groundwater recharge expressed in [LT^{-1}] units, respectively.

$$ET_{tot} = I + T_v + E_s \quad (3.5)$$

ET_{tot} is the total actual evapotranspiration, I stand for evaporation of water intercepted by vegetation, T_v transpiration of vegetation cover and E_s is evaporation from the bare soil between the vegetation.

$$R_v = P - S_v - ET_v - I \quad (3.6)$$

Etv is the actual evapotranspiration [LT^{-1}] given as the sum of transpiration, T_v, and the evaporation from bare soil in between the vegetative E_s [LT^{-1}].

The spatially distributed recharge is therefore estimated from the vegetation type, soil type, slope, groundwater depth, climatic variability of precipitation, potential evapotranspiration, temperature, and wind-speed values. Precipitation is the starting point for water balance calculations. The interception fraction is considered a constant percentage of the annual precipitation value. Thus, the interception fraction decreases with an increase in the annual total rainfall.

Surface runoff is computed in relation to precipitation amount, precipitation intensity, interception, and soil infiltration capacity. Initially the potential surface runoff (Sv-pot) is calculated as

$$Sv - pot = Csv\,(P - I) \qquad 3.7$$

Where, C_{sv} is a surface runoff coefficient for vegetated infiltration areas, and is a function of vegetation, soil type and slope. Saturated surface runoff occurs in groundwater discharge areas giving rise to a remarkably high surface runoff coefficient. This is due to the reduced dependency on soil, vegetation type and the vicinity of the area to the river, the coefficient is here usually assumed to be constant. Secondly, actual surface runoff is calculated from the S_{v-pot} by considering the differences in precipitation intensities in relation to soil infiltration abilities.

$$S_v = C_{Hor} * S_{v-pot} \qquad 3.8$$

Where C_{Hor} is a coefficient for parameterizing that part of a seasonal precipitation contributing to the Hortonian overland flow. C_{Hor} for groundwater discharge areas is equal to 1.0 since all intensities of precipitation contribute to surface runoff. Only high intensity storms can generate surface runoff in infiltration areas.

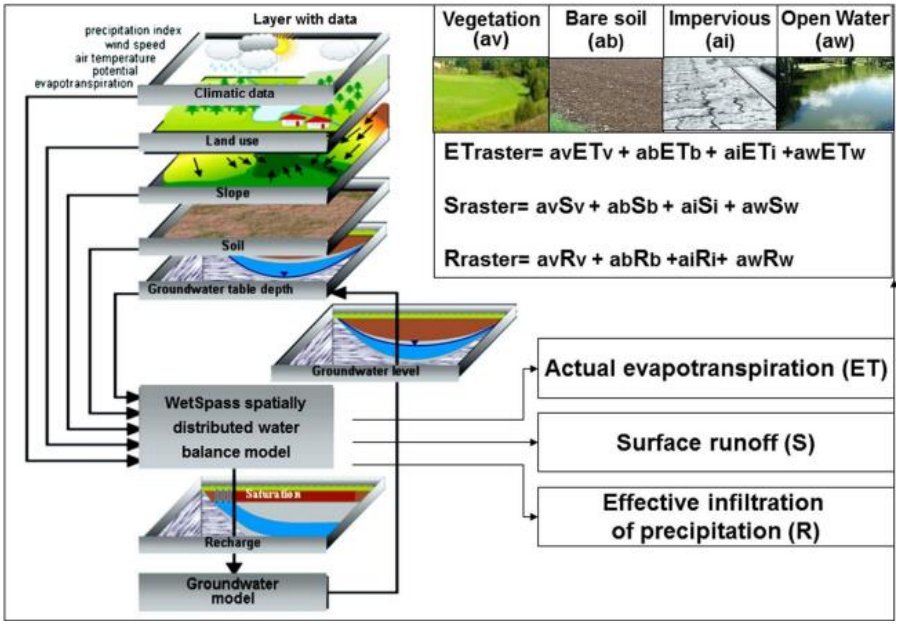

Source: (Graf & Przybyłek, 2018)

Figure 3. 18 Conceptual diagram of WetSpass model

Chapter Four

Results and Discussion

4.1 Results

4.1.1 Land Use Land Cover Dynamics

Land use change is one of the major anthropogenic factors that affect groundwater resources by changing patterns of water balance components such as infiltration, base flow, and surface runoff. To understand the future effect of LULC change on groundwater resources, it is important to understand the effect of historic LULC changes on the hydrological components. The LULC of the watershed were classified into eight land use classes (Figure 4.1) using the supervised maximum likelihood classification algorithms. It is based on identifying training samples for each land use class with the help of Google Earth and ground control points. To investigate the long-term variation of land cover changes, this study was conducted from 1990 to 2020 by dividing it into three phases with a nearly 15-year interval.

For the model simulation, LULC maps of 1990, 2005, and 2020 were prepared using Landsat 5, Landsat 7, and Landsat 8 satellite imageries, respectively. The land use classification of the study area shows that agricultural land, built-up, and bare land increases. For example, agricultural land use increased from 56.52% to 65.34% from 1990 to 2005 and increased to 73.88% in 2020, while other land uses such as forest, shrub, wetland, and grassland areas decreased (Table 4.1). The forest decreases from 44183.65 hectares to 20548.98 hectares, and the grassland decreases by half between 1990 and 2020. The area change of each land uses in the year 1990, 2005 and 2020 are described in Figure 4.2. moreover, the detailed over all change of the land uses in the watershed between 1990 and 2020 is described in Tables 4.2 and Figure 4.3.

Table 4. 1 Area coverage of each LULC classes in1990, 2005, and 2020

LULC Class	1990		2005		2020	
	Area (ha)	Area (%)	Area (ha)	Area (%)	Area (ha)	Area (%)
Agriculture	178791.28	56.52	206690.72	65.34	233702.33	73.88
Grassland	52068.37	16.46	36651.29	11.59	25093.88	7.93
Forest	44183.65	13.97	32329.77	10.22	20548.98	6.50
Shrub	27619.46	8.73	24997.12	7.90	16151.32	5.11
Built-up	1562.85	0.49	3500.68	1.11	10276.22	3.25
Water	580.32	0.18	550.53	0.17	541.44	0.17
Wetland	11262.97	3.56	8274.81	2.62	4993.96	1.58
Bare Land	278.1	0.09	3352.08	1.06	5038.87	1.59
Total	316347	100	316347	100	316347	100

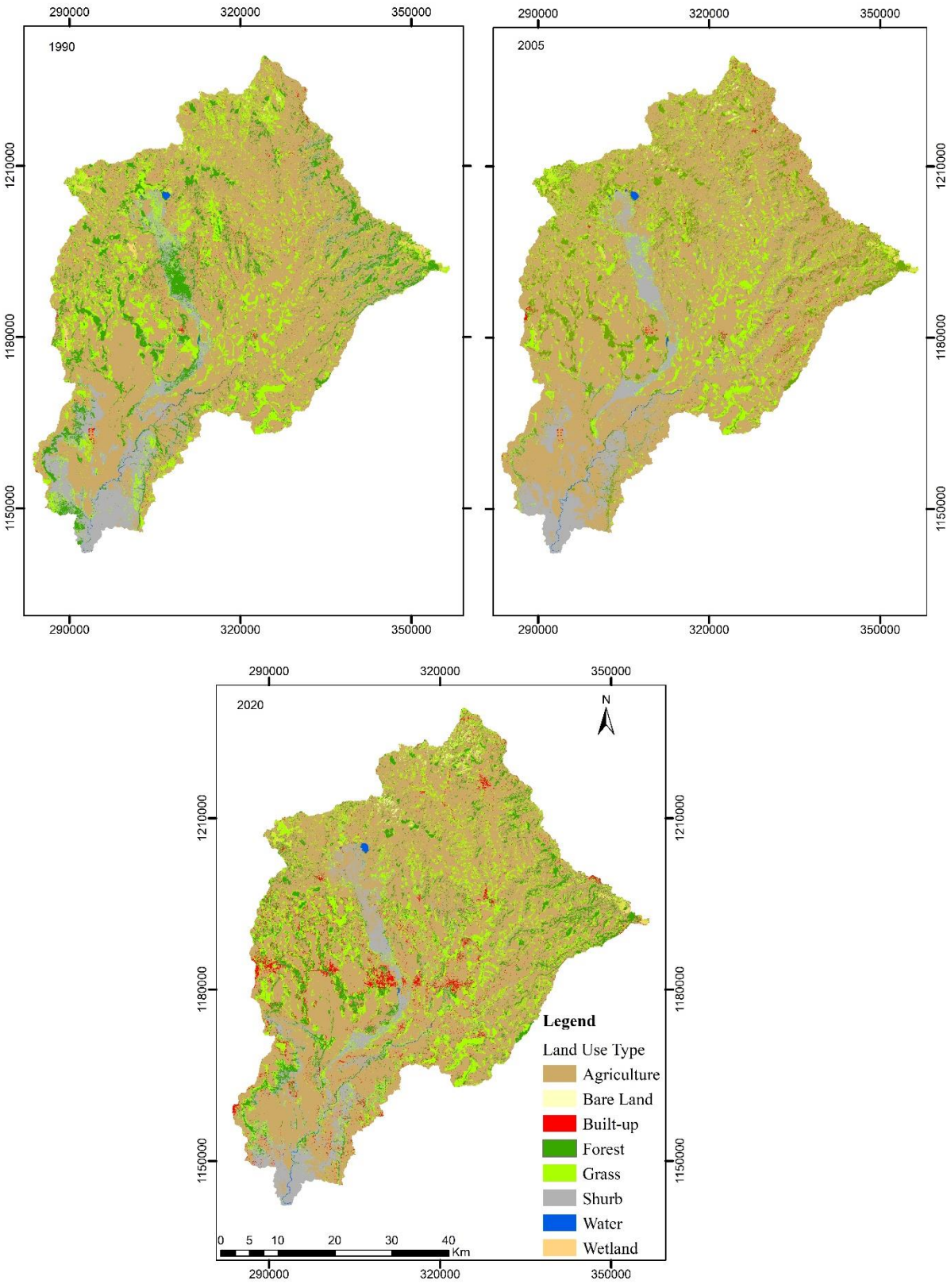

Figure 4. 1 LULC maps of the study area for 1990, 2005, and 2020

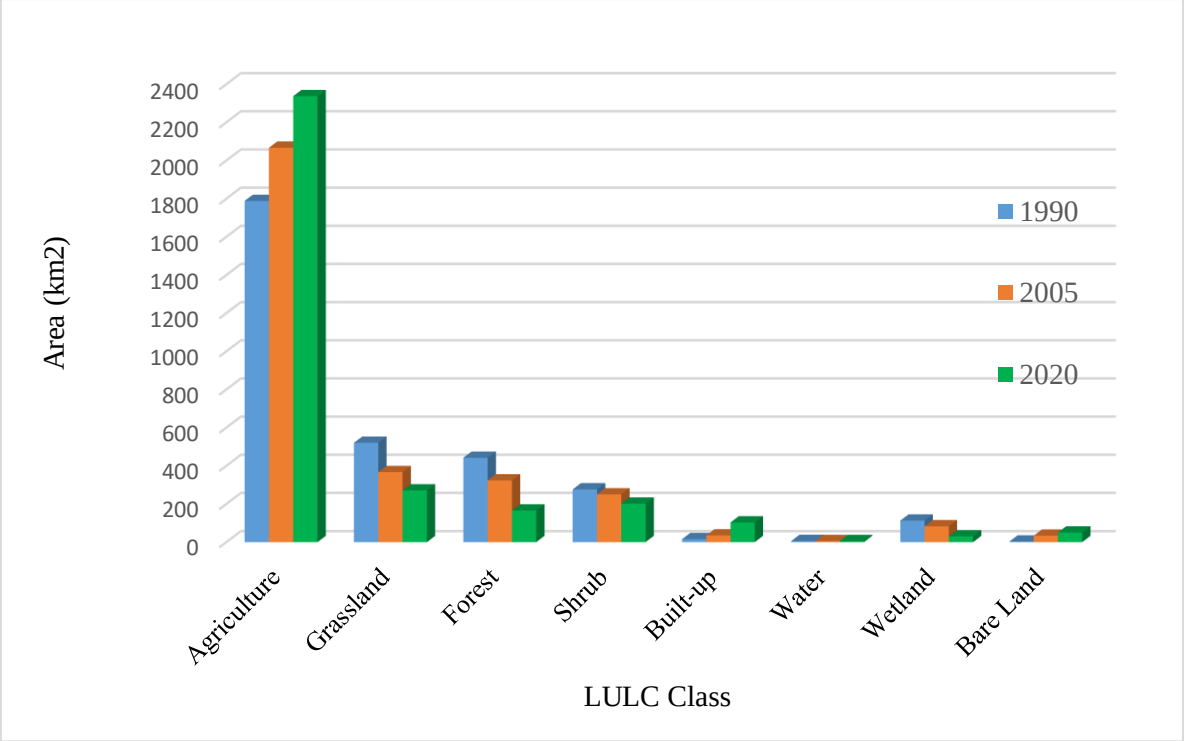

Figure 4. 2 Graphical representation of LULC changes of the study area

Table 4. 2 Overall LULC change of the study area from 1990 – 2020

LULC class	1990 Area (ha)	2020 Area (ha)	overall change Area (ha)	percentage change Area (%)
Agriculture	178791.28	233702.33	54911.05	17.36
Grassland	52068.37	25093.88	-26974.49	-8.53
Forest	44183.65	20548.98	-23634.67	-7.47
Shrub	27619.46	16151.32	-11468.14	-3.63
Built-up	1562.85	10276.22	8713.37	2.75
Water	580.32	541.44	-38.88	-0.01
Wetland	11262.97	4993.96	-6269.01	-1.98
Bare Land	278.1	5038.87	4760.77	1.50

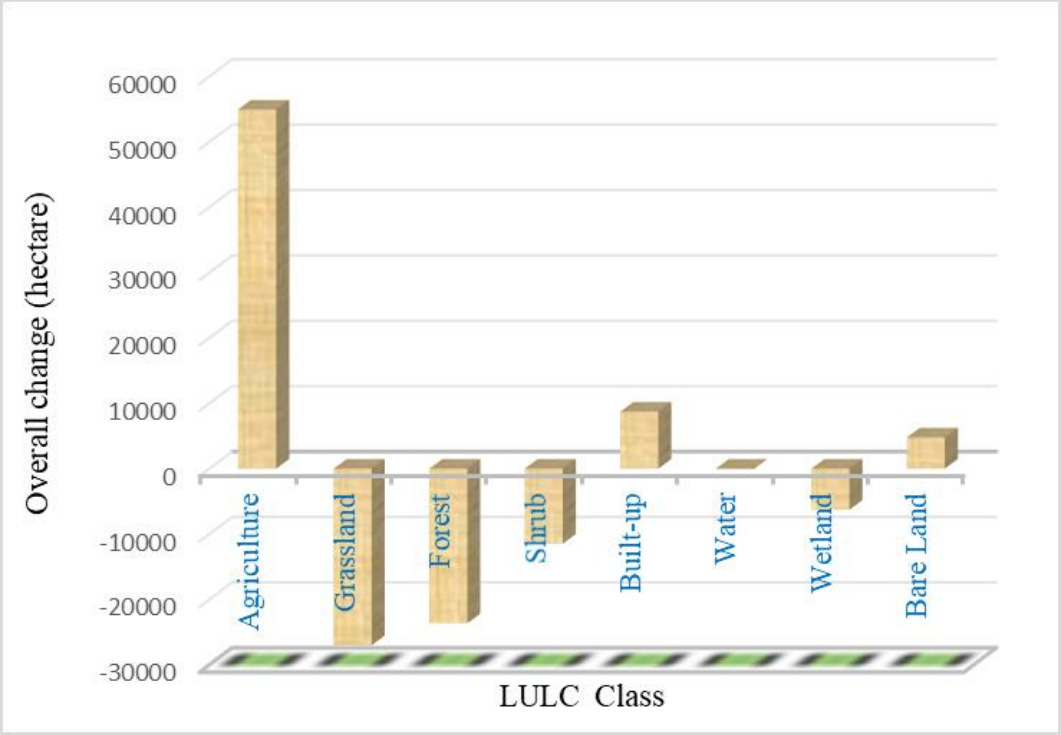

Figure 4. 3 Overall LULC change in the study area from 1990 – 2020

The overall LULC change of the Birr watershed shows that agricultural land increases by 17.36%, built-up increases by 2.75% and bare land increased by 1.5%. While forest, grassland, shrub and wetland decreased by 8.53%, 7.47%, 3.63% and 1.89%, respectively (Table 4.2). The LULC change is a continuous process (Mondal et al., 2016) that can occur in response to both human and climatic drivers. Recently, LULC change is one of the major global issues of environmental change. The change in land use components can be diagnosed using a change detection method. In this study, the change detection matrix was computed for 1990-2005 and 2005-2020 to analyze the 30 years of overall land use change of the Birr watershed (Table 4.3 and 4.4). Agriculture is the dominant land cover in the study area which constitutes 56.52%, 65.34% and 73.88% of the total area of the watershed respectively for 1990, 2005 and 2020 respectively. Next to agriculture, grass land and forest are the dominant land cover types respectively with 16.46%, 11.59%, 7.93% and 13.97%, 10.22 %, 6.50% for the same respective years.

Table 4. 3 Change detection matrix of Birr watershed from 1990 – 2005

LULC category	Agriculture	Grass	Forest	Shrub	Built-up	Water	Wetland	Bare Land	Total in 1990
Agriculture	163794.86	6739.42	4799.67	1060.75	681.41	0	0	1715.17	178791.28
Grass	19857.02	26255.58	1203.02	1637.01	786	0	992	1337.74	52068.37
Forest	16478.83	1277.55	23807.49	2618.03	1.75	0	0	0	44183.65
Shrub	3422.26	1388.96	2354.78	19678.53	774.93	0	0	0	27619.46
Built-up	149.58	101.7	0.65	0	1242.85	0	0	68.07	1562.85
Water	0	0	0	0	0	542.53	37.79	0	580.32
Wetland	2988.17	857.62	164.16	0	0	8	7245.02	0	11262.97
Bare Land	0	30.46	0	2.8	13.74	0	0	231.1	278.1
Total in 2005	206690.72	36651.29	32329.77	24997.12	3500.68	550.53	8274.81	3352.08	316347

Table 4. 4 Change detection matrix of Birr watershed from 2005 – 2020

LULC category	Agriculture	Grass	Forest	Shrub	Built-up	Water	Wetland	Bare Land	Total in 2005
Agriculture	196163.17	1380.11	2700.94	2119.37	3474.58	0	0	852.55	206690.72
Grass	11008.64	20413.94	1262.77	1904.29	1097.95	0	353.2	610.5	36651.29
Forest	11889.93	862.73	14526.42	2840.18	2210.51	0	0	0	32329.77
Shrub	11564.14	1442.56	2014.99	9283.72	379.82	0	85.12	226.77	24997.12
Built-up	2.37	118.2	0	0	3081.57	0	0	298.54	3500.68
Water	0	0	0	0	0	539.44	11.09	0	550.53
Wetland	3071.03	583.35	43.21	0	30.67	2	4544.55	0	8274.81
Bare Land	3.05	292.99	0.65	3.76	1.12	0	0	3050.51	3352.08
Total in 2020	233702.33	25093.88	20548.98	16151.32	10276.22	541.44	4993.96	5038.87	316347

4.1.2 Climate Trend of the Watershed

For this study, high-resolution monthly reanalysis climatological data were used to prepare precipitation, temperature, and wind speed maps. The long-term meteorological variables of the Birr watershed have many missing data, many rain gauges have short period recorded data, and the available gauge stations are not evenly distributed in the watershed. Most of the rain gauge stations are available around the central part of the watershed along the major roads. There are no stations found around the Abbay Gorge in the kola region of the study area and around the mountains or the highland part of the watershed that has relatively high rainfall in

the watershed. Thus, the rain gauge station products were not sufficient to produce reliable temperature, precipitation, and wind speed analysis for WetSpass model simulation. Using only available stations by interpolation has a bias by minimizing rainfall amount and temperature in highland areas and kola regions of the watershed, respectively. As a result, in this study, high-resolution gridded reanalysis modeled climate data, which is the combined result of rain gauge stations and satellite products were used to determine the groundwater recharge of the study area.

Temperature Trend

The monthly maximum and minimum gridded temperature data of the watershed were downloaded from Terraclimate dataset, and the long-term mean monthly temperature was prepared with the help of GIS. The long-term mean annual temperature was analyzed in three phases, from 1990-1999, 2000-2009, and 2010-2020 for the first, second, and third phases, respectively. The long-term mean annual temperature of the Birr watershed shows 12.13^{o}c to 23.80^{o}c for the first phase, 12.50^{o}c to 24.18^{o}c for the second phase, and 13.35^{o}c to 25.07^{o}c for the third phase (Figure 3.10). This figure shows that the decadal mean annual temperature of the study area has an increasing trend. The decadal average temperature in the study area shows that there were 0.37^{o}c and 0.87^{o}c increase in the mean temperature from the first to second and, second to third phases, respectively. The temperature trend of the watershed was analyzed and tested in R programing software by using modified Mann-Kendall test for serially correlated data using the Yue and Wang variance correction approach (Yue & Wang, 2004). The result of the trend analysis shows that the temperature of the study area has significant increase in all months and years with p value less than 0.05 in two-sided test at 95% confidence level. The Sen's slope magnitude of the annual temperature increase is about 0.033℃ per year in nine tested gauge observation points (Table 4.5; Figure 4.4).

Table 4. 5 Temperature trend test

Station	Corrected Zc	Original Z	new P-value	old P.value	Tau	Sen’ s slope	old.variance	new.variance
Burie	18.415	4.997	9.89486E-76	5.8245E-07	0.634	0.034	3461.667	254.879
Feres Bet	17.439	4.827	4.16304E-68	1.3862E-06	0.613	0.032	3461.667	265.208
Finote Selam	18.509	4.997	1.73684E-76	5.8245E-07	0.634	0.034	3461.667	252.298
Genet Abo	17.562	4.827	4.77536E-69	1.3862E-06	0.613	0.033	3461.667	261.496
Quarit	17.529	4.861	8.53528E-69	1.1681E-06	0.617	0.033	3461.667	266.192
Wad	18.337	4.963	4.21536E-75	6.9429E-07	0.630	0.033	3461.667	253.585
Yechereka	18.109	4.895	2.68273E-73	9.8322E-07	0.622	0.033	3461.667	252.914

Where, Corrected Zc is Z statistic after variance Correction, new P.value is P-value after variance correction, N/N* is Effective sample size, Original Z – Original Mann-Kendall Z statistic, Old P-value is Original Mann-Kendall p-value, Tau is Mann-Kendall’s Tau, Sen's Slope - Sen's slope, old. Variance - Old variance before variance Correction, and new. Variance - Variance after correction.

0

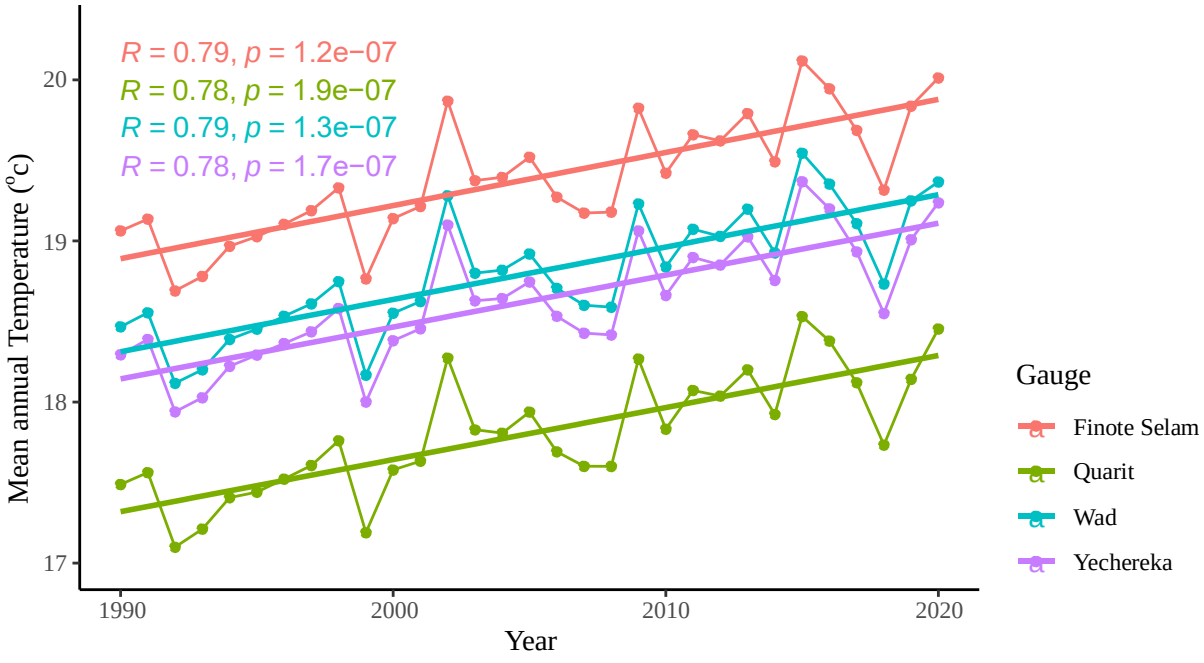

Figure 4. 4 Temperature trend plot

Precipitation Trend

The long-term annual mean rainfall of the study area ranged from 1311.95mm to 1863.30mm for the first phase, 1029.70mm to 1603.52mm, and 1019.98mm to 1745.63mm for the second and third phases, respectively (Figure 3.9). The long-term annual average rainfall is 1501.03mm, 1269.24mm, and 1322.80mm for each phase, respectively. Rainfall is the key climatologic variable that affects both the temporal and spatial distribution of water resources of an area. The analysis of annual and seasonal distribution of rainfall in the study area varies in elevation and time. The simple mean estimate of the long-term analysis shows, there was a decreasing trend of annual precipitation from first to the second phase, but there was relatively slight increase in the second phase. In the Birr watershed there is a 232mm decrease in the decadal mean annual rainfall from 1990 to 2005 and 54mm increase from 2005 to 2020. However, the analysis of rainfall pattern in the study area in R software through man Kendall non parametric test shows the rainfall pattern of the three decades in the study area has no significant increase or decreasing trend in 95% level of confidence (Figure 4.5). In all stations the p value is more than 0.05 which implies that the null hypothesis or the study area has no trend is accepted. The trend analysis has increasing precipitation of a minimum Sen's slope magnitude of 2.8mm/yr in Finote Selam station and maximum of 5mm/yr increase in Feresbet station.

Figure 4. 5 Precipitation trend plot

Wind Speed Trend

Like other WetSpass input climatological variables, the trend of wind speed was analyzed in R software. The wind speed of the watershed has no either increasing or decreasing trend. Wind speed is one of the fundamental atmospheric quantities that can occur due to atmospheric circulation changes and ground surface variations. The mean annual wind speed value is ranging from 0.98 to 1.86ms^{-1}, 1.09 to 1.95ms^{-1}, and 1.06 to 1.93ms^{-1} for the first, second, and third phases respectively (Figure 3.11). Aerosol emissions, sea surface temperature, and greenhouse gas concentration are the major causes affecting atmospheric circulation and wind speed variability (Ramanathan et al., 2001). The Sen's slope magnitude of wind speed increase is 0.002m/s per year with insignificant p value that indicate there is no trend in the study area (Figure 4.6).

Figure 4. 6 Wind speed trend plot

4.4 WetSpass Model Outputs

The WetSpass model simulation gives various hydrological results on a seasonal and yearly basis (Batelaan & De Smedt, 2001). The model's major outputs include various water balance components such as surface runoff, actual evapotranspiration (AET), interception, and recharge. The spatial variability of groundwater recharge, actual evapotranspiration, and surface runoff can be calculated as a function of the LULC type, soil type, and climate variability of the watershed. Therefore, it is possible to visualize the impact of LULC change and climate variability on various hydrological components and their spatial distribution. The result of the model simulation consists of the long-term mean annual, and seasonal values of the spatial distribution of water balance components such as groundwater recharge, actual evaporation, and surface runoff. In this study, the long-term mean monthly grid maps of input

variables were prepared using Arc GIS10.8 and converted into ASCII file formats for WetSpass-M model simulation, and the long-term water balance variables were quantified. The model outputs are in ASCII file format, which can be opened in a GIS environment in raster format. Every pixel of the output raster map represents the magnitudes of the respective water balance components. The model runs 36 times for each phase. The quantified mean annual result of the recharge and other water balance components were discussed below.

4.4.1 Actual Evapotranspiration (AET)

Actual evapotranspiration refers to the quantity of water removed from a surface through evaporation and transpiration. It explains the exchange of water and energy between soil, land surface, and the atmosphere. Usually, AET is estimated from PET. The WetSpass model computes actual evapotranspiration by adding up the water that is intercepted by vegetation, the transpiration of vegetative cover, and evaporation from the bare soil and open water bodies (Batelaan & De Smedt, 2001).

The WetSpass model simulation result of AET in Birr watershed gives that for the first phase, the long-term minimum, mean, and maximum annual evapotranspiration is 372.45mm, 739.27mm and 3275.81mm, respectively. The second phase, long-term annual evapotranspiration is 302.18mm, 533.52mm, and 3385.76mm minimum, mean and maximum values, respectively. The third phase also has a 287.54mm minimum, and 3385.71mm maximum annual evapotranspiration with 562.63mm mean values. It accounts for 49.25%, 42.03% and 42.53% of the total mean annual rainfall of the catchment for the first, second, and third phases, respectively. Interception loss is one of the important processes in the hydrological cycle where rainfall is abstracted by plants before reaching the ground. The whole rainfall could not reach the earth's surface directly. Because a part of precipitation may be in contact with vegetation surfaces and a certain percentage of it is kept on or intercepted by the vegetation. Even some amounts can also evaporate before it reaches the surface of the Earth. The rainfall rate depends on the level of precipitation, its intensity, duration, vegetation type, age, density, the season of the year, the area's climate, and wind velocity. Interception loss can be estimated by subtracting the gross rainfall from the sum of through fall and stem flow. Kołodziej, (2011) noted that during the vegetative season, interception can be in the range of 30-40%. Grasslands can intercept 10-20% and forests account for more than 20-40 and above (Brye et al., 2000).

The simulation result of the model shows that the annual cell interception has a minimum value of zero for all phases with 180.58mm, 145.18mm, and 145.95mm mean values and 383.77mm, 312.45mm, and 321.63mm maximum values for the first, second and third phases, respectively. It accounts for 12%, 11.44%, and 11% of the average long-term annual precipitation. In the

study area interception is high in shrub and forest areas while low in grass and wetlands compared to agricultural land. The model result agrees with the literature, interception in forest areas accounts for 24.5%, shrub accounts for 38.3%, agriculture 18.6% and grassland 11.4%, and wetland 6.6%.

Transpiration is the evaporation of water from the vascular system of vegetation. The soil water is absorbed through the plant root and translated into the vascular system of roots, and then the water molecules diffuse from the stomata cavity to the leaf surface and finally into the atmosphere. The soil texture and the level of groundwater saturation affect how quickly the land surface evaporates. The soil hydraulic conductivity, permeability, and water-conserving capability of a given area can be influenced by different variables such as rainfall conditions, topography, vegetation cover, and soil texture characteristics. Wet and dry soil has no equal influence on evaporation. Coarse-textured soils such as sandy and sandy loam soils are expected to have higher infiltration while clay and silt soils have lower infiltration rates and leading to increased runoff. Evaporation from saturated clay soil is slower than from saturated sandy soil. The model gives 663.56mm, 523.3mm, and 556.33mm maximum values with 436.18mm, 340mm, and 366.78mm mean value transpiration for the first, second, and third phases, respectively. The mean value accounts for 29%, 26.79%, and 27.73% of the mean rainfall, respectively. The sum of interception and transpiration in the model result gives 41%, 38.43%, and 38.76% for each phase, respectively. The spatial distribution of WetSpass-M simulation result of AET in Birr watershed is shown in Figure 4.7.

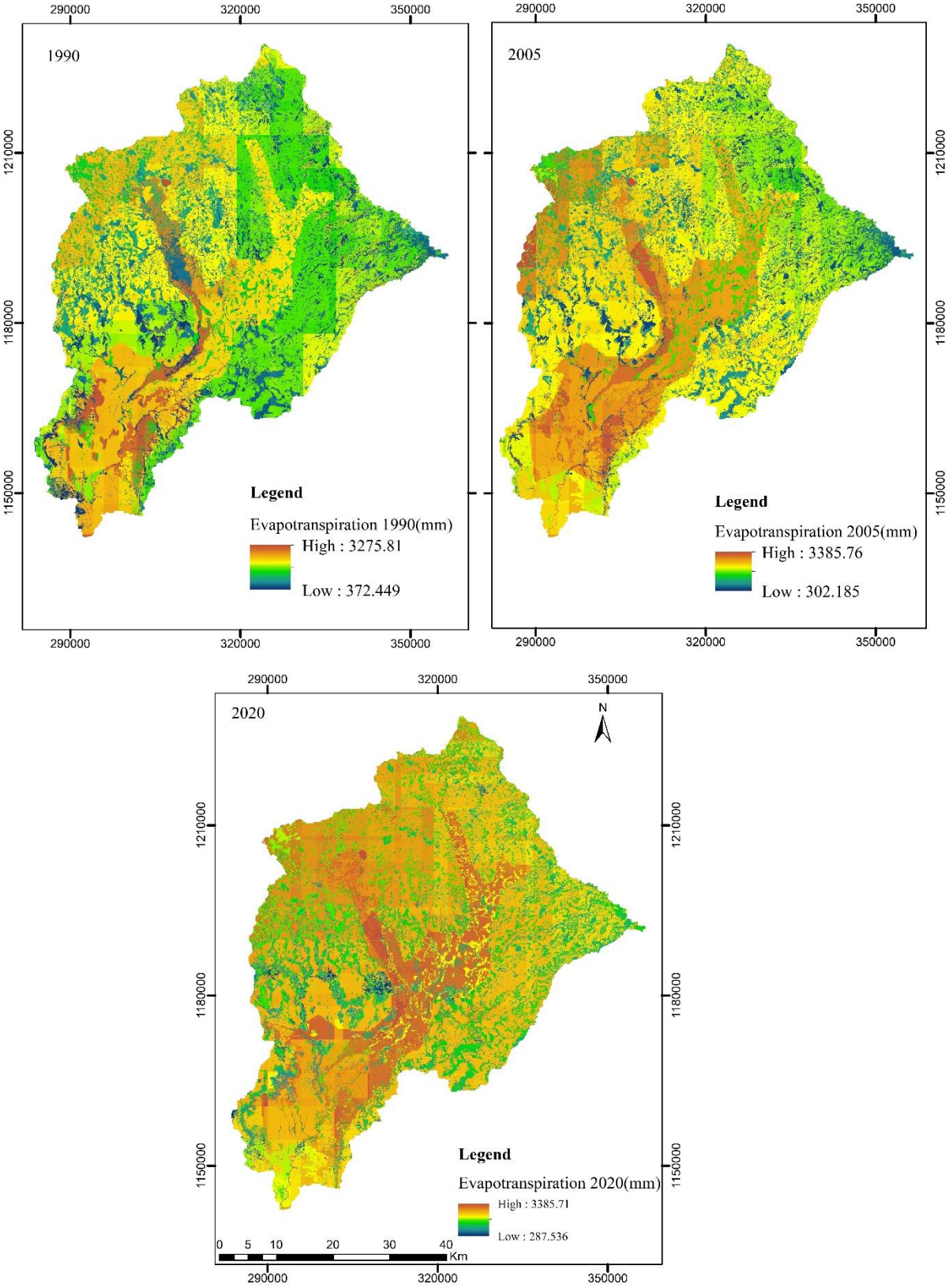

Figure 4. 7 The mean annual actual evapotranspiration map

4.4.2 Surface Runoff

Runoff is an intricate part of a natural water cycle. As soon as rain falls, the water does not sit there, it starts moving according to the law of gravity. Some portions of it seep into the ground and replenish the groundwater, while the remaining either evaporated or flow as runoff. The surface runoff depends on several climatological and topographical variables such as the soil type and texture, land cover condition, slope, rainfall intensity, amount, and duration of the watershed. The WetSpass model estimates runoff using a runoff coefficient method, a function of soil texture, vegetation type, and slope.

According to the simulation result of the WetSpass model in the watershed, the surface runoff varies spatially in the watershed because of the topography and other consequences of the watershed characteristics. The simulated annual surface runoff in the Birr watershed ranges from 275.77mm/yr. to 1789.84mm/yr. with a mean value of 599.76mm/yr. for the first phase. For the second and third phases, the simulated surface runoff varies from a minimum of 249.45mm/yr. to 1442.61mm/yr. and from 213.29mm/yr. to 1550.65mm/yr. with a mean value of 607.22mm/yr. and 639.58mm/yr. respectively (Figure 4.8). The mean value accounts for 39.96%, 47.84%, and 48.35% of the total mean long-term annual rainfall for the first, second, and third phases, respectively. In the study area, runoff is highly influenced by the topography's slope. The higher elevation areas have a higher runoff. The topography which is above 2100m has a slope range of 30% to 71% and these areas have the highest runoff in the study area for all phases. In the study area, the lower runoff occurs in clay soil textural class that have below 1800m elevation with lower than 12% slop range. By considering the total area of the watershed the average total surface runoff is 1897 million m^3, 1920.64 million m^3, and 2022.99 million m^3 for the first, second, and third phases, respectively. The simulation result of the model shows that runoff is high in built-up and bare land areas. For instance, in the first phase surface runoff in built-up is 17.23%, bare land is 16.45% and the waterbody is 21.79%. The lowest runoff is shown in shrub and forest land uses with 6% and 8.18% values. In the second phase and third phases, built up constitutes 17.16% and 15.93%, bare land 15.92% and 17.09%, agriculture 9.82% and 9.99%, forest 8.99% and 8.8% and shrub 6.33% and 5.79%, respectively (Table 4.6).

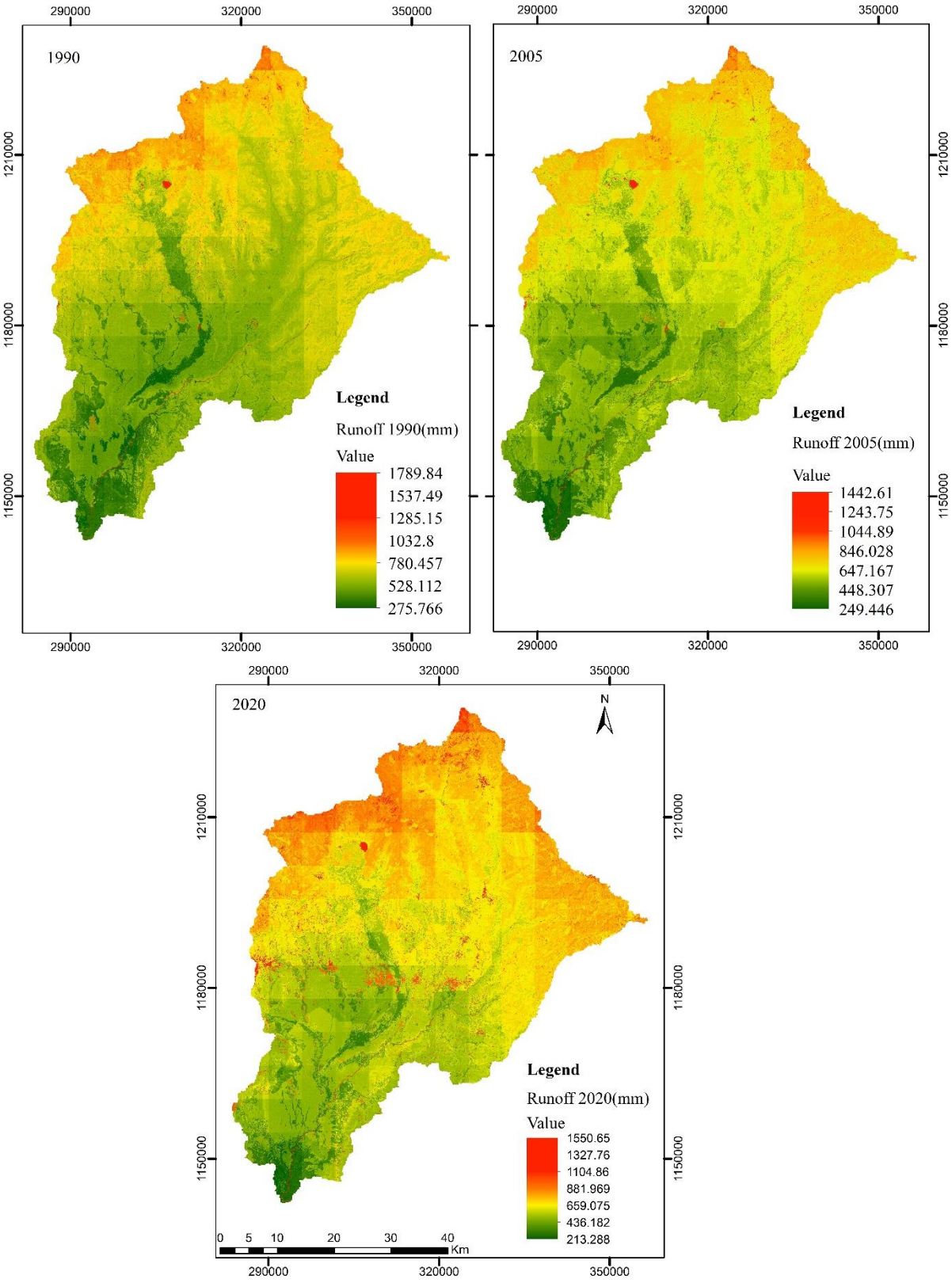

Figure 4. 8 The mean annual Runoff map

Table 4. 6 The mean annual runoff in different land uses category

Land Use Category		Area km^2	Area %	Min	Max	Mean	% Mean Runoff
Runoff in 1990	grass land	520.6837	16.46	372.58	1068.30	657.77	9.88
	built up	15.6285	0.49	958.83	1476.03	1147.28	17.23
	forest	441.8365	13.97	263.39	901.01	544.96	8.18
	wetland	112.6297	3.56	456.74	1051.74	723.32	10.86
	water	5.8032	0.18	1284.14	1765.34	1451.52	21.79
	bare land	2.781	0.09	698.48	1328.98	1095.82	16.45
	agriculture	1787.913	56.52	400.70	1009.84	638.87	9.59
	shrub	276.1946	8.73	251.27	844.36	400.77	6.02
Runoff in 2005	grass land	366.5129	11.59	349.54	975.14	609.73	10.22
	built up	35.0068	1.11	752.90	1273.93	1023.29	17.16
	forest	323.2977	10.22	247.22	834.53	536.14	8.99
	wetland	82.7481	2.62	386.21	976.76	689.46	11.56
	water	5.5053	0.17	1003.59	1419.11	1193.84	20.01
	bare land	33.5208	1.06	490.08	1166.74	949.49	15.92
	agriculture	2066.907	65.34	345.22	923.76	585.69	9.82
	shrub	249.9712	7.9	225.95	789.61	377.28	6.33
Runoff in 2020	grass land	250.9388	7.93	287.86	1038.46	622.70	10.23
	built up	102.7622	3.25	720.10	1378.79	969.59	15.93
	forest	205.4898	6.5	195.09	873.39	535.60	8.80
	wetland	49.9396	1.58	364.79	1044.71	740.36	12.16
	water	5.4144	0.17	989.81	1523.15	1218.04	20.01
	bare land	50.3887	1.59	696.57	1265.28	1040.43	17.09
	agriculture	2337.023	73.88	298.39	975.38	608.00	9.99
	shrub	161.5132	5.11	185.79	803.74	352.60	5.79

4.3.3 Groundwater Recharge

Generally, recharge and infiltration are highly correlated with factors such as vegetation cover, soil type and texture, slope, water table depth, and other topographical conditions of the catchment. The WetSpass model determines the spatial distribution of recharge based on land use characteristics, soil texture, slope, and climatological variables including rainfall, temperature, and wind speed conditions. It calculates the annual spatial distribution of groundwater recharge by subtracting the annual evapotranspiration and annual runoff from annual precipitation.

The WetSpass model simulated result of the long-term mean annual groundwater recharge in Birr watershed is 162.28mm/yr. 128.59mm/yr. and 121.15mm/yr. in 1990, 2005, and 2020 respectively (Figure 4.9). These account for 10.81%, 10.13%, and 9.16% of the long-term average precipitation for each respective year.

The estimated long-term average recharge ranges from 0 to 592.5mm/yr. for the first phase, 0 to 490.3mm/yr. for the second phase and 0 to 561.7mm/yr. for the third phase (Figure 4.9). The time-serious recharge simulated result shows that there is a continuous decrease in groundwater recharge in the study area. The trend analysis of groundwater recharge in fifteen selected random points in the watershed shows a minimum of 5.6mm decrease and a maximum of 126.6mm decrease per year (Table 4.7; Figure 4.10). Among the fifteen points at four points the recharge analysis has insignificant p value and from the rest eleven points the recharge analysis has a decreasing trend with significant p values at 95% confidence interval.

Table 4. 7 Recharge trend test

points	x	y	Corrected Zc	new P-value	N/N*	Original Z	old P.value	Tau	Sen's slope	old.variance	new.variance
1	310581	1220075	-2.2	0.0	0.2	-1.0	0.3	-1.0	-5.6	3.7	0.8
2	324401	1220075	-2.2	0.0	0.2	-1.0	0.3	-1.0	-53.6	3.7	0.8
3	315188	1215468	-2.2	0.0	0.2	-1.0	0.3	-1.0	-22.6	3.7	0.8
4	324401	1215468	-2.2	0.0	0.2	-1.0	0.3	-1.0	-16.4	3.7	0.8
5	310581	1210862	-2.2	0.0	0.2	-1.0	0.3	-1.0	-7.5	3.7	0.8
6	338222	1206255	-2.2	0.0	0.2	-1.0	0.3	-1.0	-111.6	3.7	0.8
7	315188	1197041	-2.2	0.0	0.2	-1.0	0.3	-1.0	-71.0	3.7	0.8
8	333615	1187828	-2.2	0.0	0.2	-1.0	0.3	-1.0	-24.1	3.7	0.8
9	338222	1187828	0.0	1.0	0.2	0.0	1.0	-0.3	-25.1	3.7	0.8
10	310581	1174008	-2.2	0.0	0.2	-1.0	0.3	-1.0	-54.2	3.7	0.8
11	310581	1164794	-2.2	0.0	0.2	-1.0	0.3	-1.0	-126.6	3.7	0.8
12	296761	1206255	0.0	1.0	0.2	0.0	1.0	-0.3	-7.8	3.7	0.8
13	301368	1174008	-2.2	0.0	0.2	-1.0	0.3	-1.0	-35.8	3.7	0.8
14	296761	1150974	0.0	1.0	0.2	0.0	1.0	-0.3	-14.9	3.7	0.8
15	301368	1164794	0.0	1.0	0.2	0.0	1.0	-0.3	-14.6	3.7	0.8

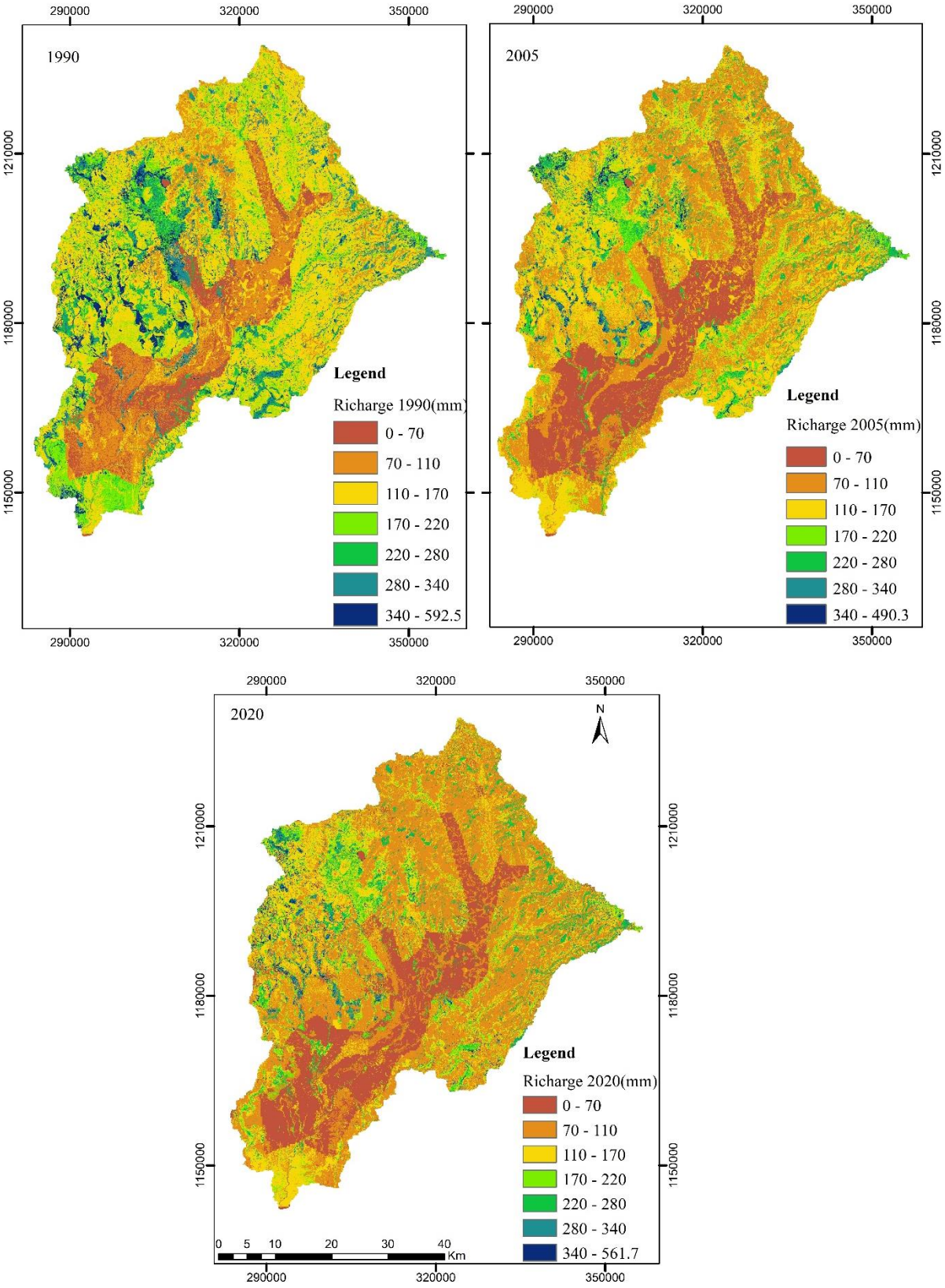

Figure 4. 9 The mean annual groundwater recharge map

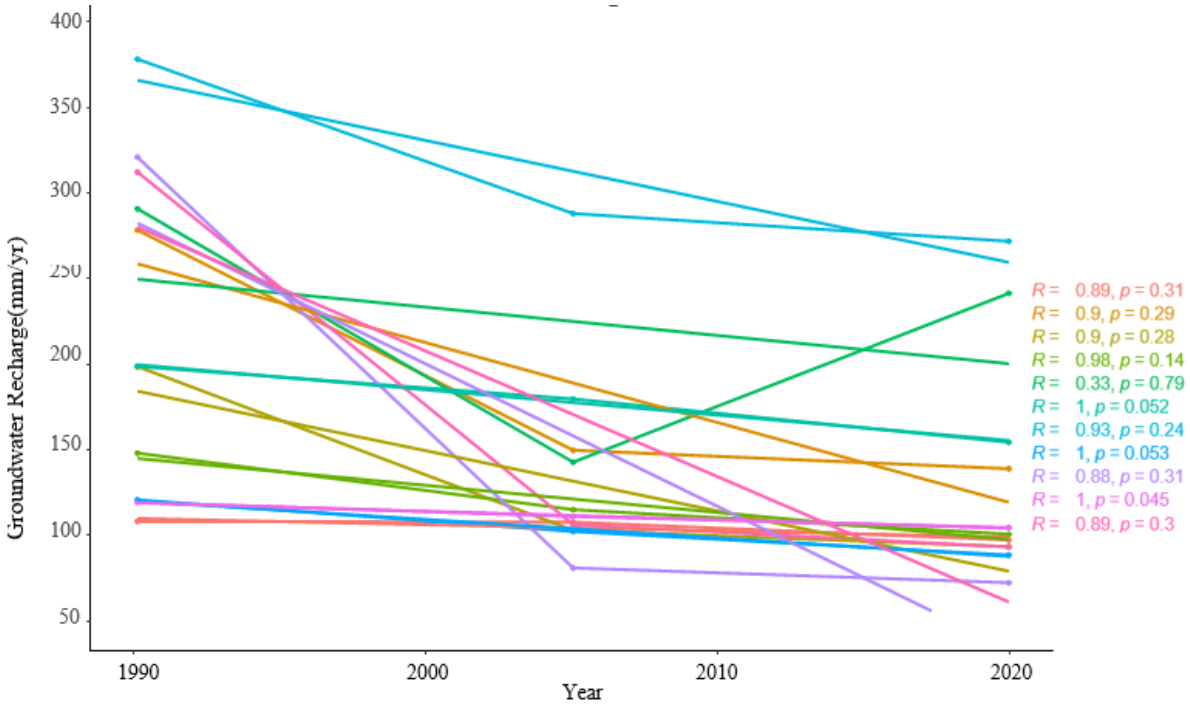

Figure 4. 10 Groundwater Recharge plot

The relationship between land use land cover and recharge in the watershed was computed by GIS zonal statistics tool and shown in Table 4.8 below.

Table 4. 8 Pattern of mean annual groundwater recharge in different land uses category

Land Use Category		Area km^2	Area %	Min	Max	Mean	% Mean Recharge
Recharge in 1990	grass land	520.6837	16.46	130.48	396.65	239.35	19.45
	built up	15.6285	0.49	26.92	73.51	45.17	3.67
	forest	441.8365	13.97	214.97	592.47	364.18	29.59
	wetland	112.6297	3.56	126.77	370.56	256.93	20.88
	water	5.8032	0.18	0.00	0.00	0.00	0.00
	bare land	2.781	0.09	0.00	91.76	0.63	0.05
	agriculture	1787.9128	56.52	76.02	266.44	139.92	11.37
	shrub	276.1946	8.73	115.91	301.43	184.60	15.00
Recharge in 2005	grass land	366.5129	11.59	111.49	356.01	193.60	18.53
	built up	35.0068	1.11	41.37	80.79	60.61	5.80
	forest	323.2977	10.22	194.04	490.27	296.22	28.35
	wetland	82.7481	2.62	113.75	326.68	222.44	21.29
	water	5.5053	0.17	0.00	0.00	0.00	0.00
	bare land	33.5208	1.06	0.00	53.02	0.75	0.07
	agriculture	2066.9072	65.34	70.24	224.02	110.75	10.60

	shrub	249.9712	7.9	90.60	283.01	160.32	15.35
Recharge in 2020	grass land	250.9388	7.93	105.12	380.40	174.13	17.49
	built up	102.7622	3.25	40.63	79.36	64.01	6.43
	forest	205.4898	6.5	185.73	561.67	289.76	29.11
	wetland	49.9396	1.58	104.94	341.09	201.82	20.27
	water	5.4144	0.17	0.00	0.00	0.00	0.00
	bare land	50.3887	1.59	0.00	104.57	0.81	0.08
	agriculture	2337.0233	73.88	63.17	244.01	101.93	10.24
	shrub	161.5132	5.11	94.66	311.15	163.06	16.38

The maximum recharge is occurred in forest lands with 592.47mm, 490.27mm and 561.67mm respectively in 1990, 2005 and 2020. Next to forests grass lands have higher recharge rate than other land uses. The lowest recharge occurred in the study area in bare land. Most probably it is possible to say there is no recharge in bare lands in the study area. Next to bare land built-up areas has low recharge with minimum values of 26.92mm, 41.37mm and 40.63mm recharge per year for a raster cell for the same periods respectively. Similarly, for the rest land uses the detailed recharge of the raster cell per year is described in Table 4.9.

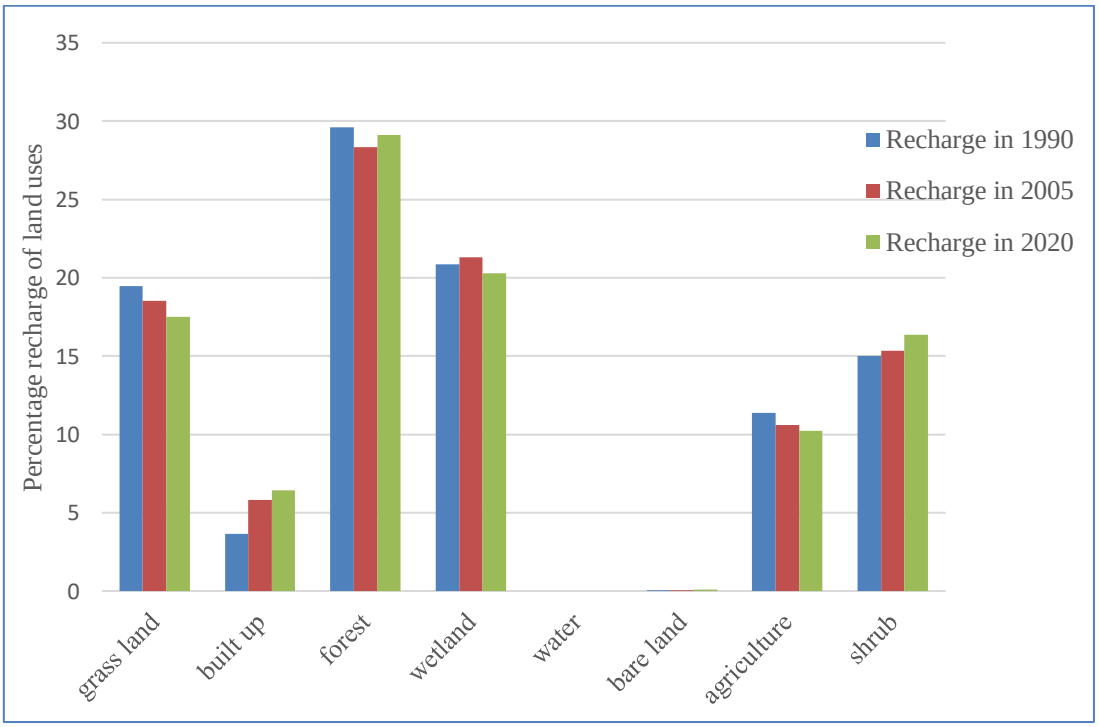

Figure 4. 11 Groundwater recharge of different land uses

The correlation plot of water balance components in the Birr watershed (Figure 4.12).

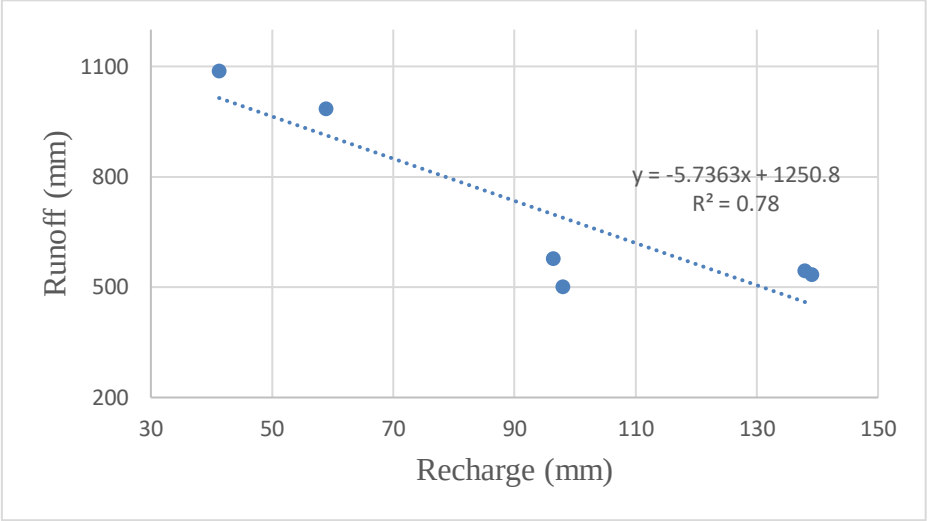

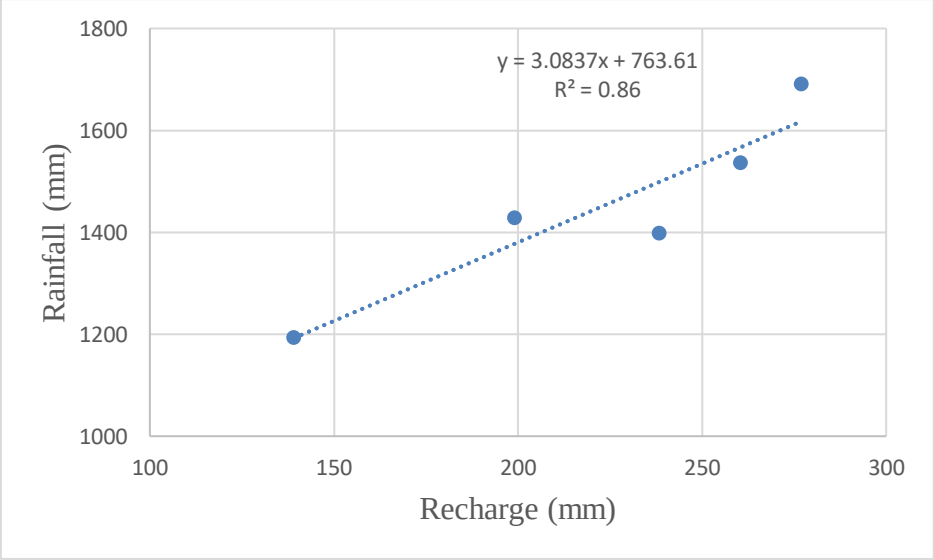

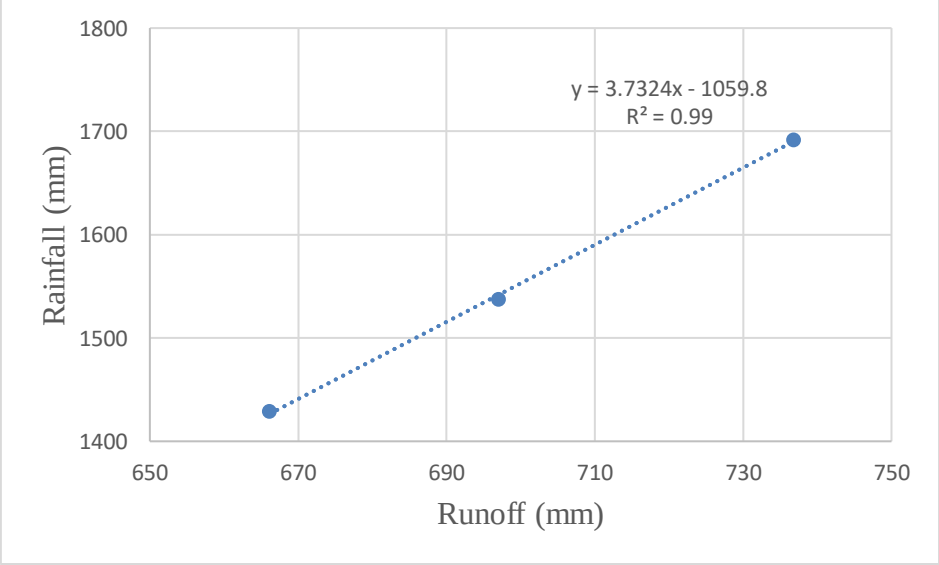

Figure 4. 12 The correlation plot of water balance components

4.2 Discussion

In the study area, agriculture has been rapidly expanding and dominating other land cover types which is followed by grass and shrub land covers respectively. The change detection shows that there has been LULC change over the 30 years. The classification result indicates that agricultural land use increases by 17.36% between 1990 and 2020 due to population growth. The severity of LULC change aggravates worldwide, mainly because of rapid population growth and intense agricultural development (Tolessa et al., 2020). In the Gilgel Abay, the neighborhood watershed of the study area, agricultural land increases by 24.12% from 1986 to 2000 and increased again with 9.67% from 2000 to 2011 while grass land, shrub, water and forest land uses decreased (Gebrie & Gebremariam, 2015).Similarly, in the study area, rapid population growth, agriculture expansion, overgrazing, and massive fuel wood and charcoal production accelerates LULC dynamics. The watershed has about 284,000 peoples who led their lives through rainfed agriculture and about 5000 ha area is cropped under small scale irrigation (MoWR, 1995) cross reference Bahir Dar University community service report in 2014. On the other hand, forest, shrub, grassland, and wetland land uses decreased by 6.5%, 5.11%, 7.935 and 1.58% respectively because of farmland intensification and urban expansion. The altitude, latitude, the interaction and response of climate variables such as the atmosphere, land surface, and ocean, and the region's physiography decide the region's warming rate. In Ethiopia, the mean annual temperature is below 15^{o}c in highland areas and above 25^{o}c in the lowland regions of the country (Senait et al., 2010). From 1961-2006, the increasing rate of the average annual minimum and maximum temperature in the country was 0.13^{o}c and 0.37^{o}c per decade, respectively (Fazzini et al., 2015). While other sources also show that between 1951 and 2006 the annual minimum temperature increased by 0.37^{o}c in every decade and from 1960-2006 the mean annual temperature increased by 1.3^{o}c at an average rate of 0.28^{o}c per decade (Senait et al., 2010). The study area also has an increasing trend like the literature. it has 0.03^{o}c increase per.

Regasa et al., (2021) state that the rapid LULC change in Ethiopia causes a loss of biodiversity in the entire Blue Nile basin and affects the hydrological balance of the basin by changing the rainfall, evaporation, runoff, and infiltration elements in the area. In Ethiopia, the rainfall distribution is highly inconsistent among seasons (Philip et al., 2018), and geographically both the annual and seasonal precipitation show high variability (Senait et al., 2010). The summer and spring rain in Ethiopia decreases by 15-20% since the mid-1970s (USGS & USAID, 2012). The trend of the Upper Blue Nile River basin (Conway, 2000), the trend of northern highland Ethiopia (Mekonen & Berlie, 2020), and the trend of the Amhara region specifically Adet station, which is found around the near distance of the study area shows a decreasing trend of precipitation (Gedefaw et al., 2018). Mekonen & Berlie, (2020) also noted there was a

6.537mm decrease in a decade in the Northern highlands of Ethiopia. However, the decadal trend analysis of precipitation has no trend. It nearly similar rainfall pattern in the three decades. The result of groundwater recharge in the study area agrees with the results of other similar studies undertaken in Ethiopia. For instance, the WetSpass model simulation of groundwater recharge in Modjo watershed accounts 8.9% (Bedaso et al., 2019), of the annual precipitation and upper Bilate catchment is 9.4% (Dereje & Nedaw, 2018) with a mean recharge of 83mm/yr and 116mm/yr, respectively. Similarly, Warku et al., (2022) show that groundwater recharge in upper Gibe watershed decreases from 17% to 14% and declined to 10% in three consecutive decades from 1985-2018. Likewise in the study area has average recharge 162.28mm/yr. 128.59mm/yr. and 121.15mm/yr which covers 10.81%, 10.13%, and 9.16% of the mean precipitations of the first, second and third decades from 1990 to 2020.

Chapter Five

Conclusion and Recommendation

5.1 Conclusion

Evaluating the effect of LULC and climate change on groundwater at the watershed level enables to plan immediate conservation measures, and proper use of the resource. Groundwater recharge in the Birr watershed is quantified by using the physical based quasi steady state WetSpass model. The WetSpass model quantifies the annual recharge by subtracting the sum of evapotranspiration and surface runoff from annual precipitation. However, the spatial distribution of recharge is dependent on different variables that govern groundwater infiltration. The land cover change, the rainfall distribution, temperature and soil texture, the topographical conditions are the main factors that decide the recharge in the study area.

In the study area, there is a continuous expansion of the built-up area, and agricultural activities while forest areas, grasslands, wetlands, and shrubs are decreasing. Forest, wetland, and grassland land uses has higher groundwater recharge rate than agriculture and built-up land covers, the continuous expansion of agriculture and built-up area affects the ground water by minimizing the infiltration condition. Moreover, such land use conversions increase runoff and minimizes recharge rate in the study area. As a result, groundwater recharge decrease overtime. In addition, the increasing trend of temperature affects the water balance components by changing interception, transpiration, evaporation, and infiltration.

The analysis of the 30-year LULC change of the study area shows continuous spatial land use variation through time within the watershed. Because of rapid population growth and the increasing demand of farmland, agricultural land use increases over time in the study area. On the other hand, forest, shrub, grassland, wetland and water body decreased. Therefore, the depletion of forest areas, expansion of agricultural land and built-up has a negative impact on groundwater recharge. The expansion of agriculture and built-ups phenomenon increases paved and the volume of surface runoff, which so minimizes the percolation rate or groundwater recharge of the catchment. Therefore, the conversion of forests, shrubs and wetlands to agricultural land has a negative impact on groundwater recharge in the Birr watershed. Milkias & Toru, (2018b) note that forest degradation and deforestation are serious environmental challenges in Ethiopia that not only result in the destruction of plant and animal species but also decrease water quality, aggravate soil erosion, and reduce agricultural productivity. In the study area, groundwater recharge in forests, wetlands and grasslands were higher than other land uses (Table 4.8). The conversion of these land uses to other land uses reduces the recharge rate. Literature shows that LULC changes greatly affect the watershed environment by altering the hydrological components of the watershed such as groundwater recharge, infiltration, base

flow, and Runoff (Bronstert et al., 2002). According to the simulation result the decreasing phenomena of groundwater recharge is mainly occurred due to LULC change.

The long-term meteorological and climatological variable analysis of the study area also has varied both spatially and temporally. The 30-year temperature trend shows that the minimum, maximum and mean temperature in the study area increases over time. The long-term annual precipitation and wind speed has increasing trend, but it is insignificant. As the temperature increases, evapotranspiration also increases which so declines groundwater recharge. Similarly, the clearance of forests and an increase in built-up areas causes fast runoff which minimizes infiltration and causes a decrease in groundwater recharge which consequently affects the ground water resource.

Climate variability, such as increasing temperature, and LULC change are highly interlinked. Both can affect each other. LULC change contributes to climate change by changing the atmospheric flux of CO2 and energy (Virginia, 1997). The alteration of energy, carbon or water fluxes depends on the spatial distribution of vegetation cover of the given area. In the study area, the volume of runoff increases while evapotranspiration and recharge decrease over time. The annual evapotranspiration value is about 49.25%, 42.03%, and 42.53% and groundwater recharge is 10.81%, 10.13%, and 9.16% of the annual mean precipitation of the first, second, and third phases, respectively. Similarly, the surface runoff result of the model simulation is 39.96%, 47.84% and 48.35% of the annual mean precipitation, respectively. The overall water balance component analysis of the Birr watershed shows that evapotranspiration and runoff constitute the major water loss process while groundwater recharge has the lowest proportion. The mean annual water balance difference is -0.29, -0.08, and -0.52 for the first, second, and third phases, respectively Table 4.9. This result shows that the simulated result of the model is good in the estimation of recharge in the watershed. According to the model result, the total recharge in the study area was 513.31 million m^3, in 1990, and 406.7 million m^3 in 2005 and 383.2 million m^3 in 2020.

Table 4. 9 Water Balance Component

Water Balance Components		Precipitation (P)	Evapotranspiration (ET)	Runoff (S)	Recharge ®	Difference (P -ET - S - R)
First Phase (1990-2000)	min	1311.95	372.45	275.77	0	
	max	1863.3	3275.81	1789.84	592.47	
	mean	1501.03	739.28	599.76	162.29	-0.29
Perecentage of water balance components from preciptarion (%)			**49.25**	**39.96**	**10.81**	
Second Phase (2001-2010)	min	1029.7	302.19	249.45	0	
	max	1603.52	3385.76	1442.61	490.27	
	mean	1269.24	533.52	607.22	128.59	-0.09
Perecentage of water balance components from preciptarion (%)			**42.03**	**47.84**	**10.13**	
Third Phase (2011-2020)	min	1019.98	287.54	213.29	0	
	max	1745.63	3385.71	1550.65	561.67	
	mean	1322.8	562.63	639.58	121.15	-0.6
Perecentage of water balance components from preciptarion (%)			**42.53**	**48.35**	**9.16**	

5.2 Recommendation

The study examines the trend of land use, land cover change and climate variability experiences in the Birr watershed. In addition, the long-term annual average groundwater recharge of the study area is quantified by using the WetSpass water balance model integrated with a geographic information system (GIS) to figure out the long-term effects of land cover change and climate variability.

- According to the model's result, groundwater recharge is decreases overtime; this implies that there should be a wise use and proper management of groundwater resources in the study area.
- The regional government should take effective mitigation and adaptation measures on climatic and LULC changes in the environment to minimize their negative impacts on hydrological components.
- The study uses low-resolution satellite images for land use classification and preexisted temperate regions' land use and soil parameter tables, thus a further study using high-resolution satellite images and modified parameter tables of the study area will improve the result of this study.

Reference

Abatzoglou, J. T., Dobrowski, S. Z., Parks, S. A., & Hegewisch, K. C. (2018). TerraClimate, a high-resolution global dataset of monthly climate and climatic water balance from 1958–2015. *Scientific Data*, *5*(1), 170191. https://doi.org/10.1038/sdata.2017.191

Abdo, K. S., Fiseha, B. M., Rientjes, T. H. M., Gieske, A. S. M., & Haile, A. T. (2009). Assessment of climate change impacts on the hydrology of Gilgel Abay catchment in Lake Tana Basin, Ethiopia. *Hydrological Processes*, *2274*(November 2008), n/a-n/a. https://doi.org/10.1002/hyp.7363

Addisie, M. B. (2022). *Groundwater recharge estimation using water table fl uctuation and empirical methods*. *5*(3), 457–468. https://doi.org/10.2166/h2oj.2022.026

Agarwal, C., Green, G. M., Grove, J. M., Evans, T. P., & Schweik, C. M. (2002). A review and assessment of land-use change models: dynamics of space, time, and human choice. In *Apollo The International Magazine Of Art And Antiques*. https://doi.org/10.2737/NE-GTR-297

Aish, A. M., Batelaan, O., & De Smedt, F. (2010). Distributed recharge estimation for groundwater modeling using wetspass model, case study - gaza strip, palestine. *Arabian Journal for Science and Engineering*, *35*(1), 155–163.

Aklilu, A., & Alebachew, A. (2012). Assessment of climate change-induced hazards, impacts and responses in the southern lowlands of Ethiopia, FSS Research Report No. 4. In *Addis Ababa, Ethiopia* (Vol. 34, Issue 1). Cordaid and Forum for Social Studies (FSS).

Alemayehu, F., Taha, N., Nyssen, J., Girma, A., Zenebe, A., Behailu, M., Deckers, S., & Poesen, J. (2009). The impacts of watershed management on land use and land cover dynamics in Eastern Tigray (Ethiopia). *Resources, Conservation and Recycling*, *53*(4), 192–198. https://doi.org/10.1016/j.resconrec.2008.11.007

Ali, M., & Mubarak, S. (2017). Approaches and Methods of Quantifying Natural Groundwater Recharge – A Review. *Asian Journal of Environment & Ecology*, *5*(1), 1–27. https://doi.org/10.9734/AJEE/2017/36987

Alley, W. M., Healy, R. W., LaBaugh, J. W., & Reilly, T. E. (2002). Flow and Storage in Groundwater Systems. *Science*, *296*(5575), 1985–1990. https://doi.org/10.1126/science.1067123

Anand, A. (2012). Unit 14 Accuracy Assessment. In *Processing and Classification of Remotely Sensed Images* (Issue January 2017, pp. 59–77). https://www.researchgate.net/publication/319963167

Armanuos, A. M., & Negm, A. (2016). Assessment of the Variations of Local Parameters of Wetspass Model: Case Study Nile Delta Aquifer. *Procedia Engineering*, *154*, 276–283. https://doi.org/10.1016/j.proeng.2016.07.475

Arnell, N. W. (2003). Relative effects of multi-decadal climatic variability and changes in the mean and variability of climate due to global warming: future streamflows in Britain. *Journal of Hydrology*, *270*(3–4), 195–213. https://doi.org/10.1016/S0022-1694(02)00288-3

Asefa, M., Cao, M., He, Y., Mekonnen, E., Song, X., & Yang, J. (2020). Ethiopian vegetation types, climate and topography. *Plant Diversity*, *42*(4), 302–311. https://doi.org/10.1016/j.pld.2020.04.004

Awulachew, S. B., Yilma, A. D., Loulseged, M., Loiskandl, W., Ayana, M., & Alamirew, T. (2007). *Water Resources and Irrigation Development in Ethiopia.* (Working Paper 123). International Water Management Institute.

Ayehu, G. T., Tadesse, T., Gessesse, B., & Dinku, T. (2018). Validation of new satellite rainfall products over the Upper Blue Nile Basin, Ethiopia. *Atmospheric Measurement Techniques*, *11*(4), 1921–1936. https://doi.org/10.5194/amt-11-1921-2018

Batelaan, O., & De Smedt, F. (2001). WetSpass: A flexible, GIS based, distributed recharge methodology for regional groundwater modelling. *IAHS-AISH Publication*, *269*, 11–18.

Batelaan, O., & De Smedt, F. (2007). GIS-based recharge estimation by coupling surface–subsurface water balances. *Journal of Hydrology*, *337*(3–4), 337–355. https://doi.org/10.1016/j.jhydrol.2007.02.001

Beck, H. E., Vergopolan, N., Pan, M., Levizzani, V., van Dijk, A. I. J. M., Weedon, G. P., Brocca, L., Pappenberger, F., Huffman, G. J., & Wood, E. F. (2020). Global-Scale Evaluation of 22 Precipitation Datasets Using Gauge Observations and Hydrological Modeling. In *Advances in Global Change Research* (Vol. 69, pp. 625–653). https://doi.org/10.1007/978-3-030-35798-6_9

Bedaso, N., Kebede, A., & Birihanu, S. (2019). *Estimation of Spatially Distributed Groundwater Recharge in Modjo River Catchment, Awash Basin, Central Ethiopia*. *5*(1).

Bhattacharya, T., Khare, D., & Arora, M. (2020). Evaluation of reanalysis and global meteorological products in Beas river basin of North-Western Himalaya. *Environmental Systems Research*, *9*(1), 24. https://doi.org/10.1186/s40068-020-00186-1

Bronstert, A., Niehoff, D., & Bürger, G. (2002). Effects of climate and land-use change on storm runoff generation: present knowledge and modelling capabilities. *Hydrological Processes*, *16*(2), 509–529. https://doi.org/10.1002/hyp.326

Brye, K. R., Norman, J. M., Bundy, L. G., & Gower, S. T. (2000). Water-Budget Evaluation of Prairie and Maize Ecosystems. *Soil Science Society of America Journal*, *64*(2), 715–724. https://doi.org/10.2136/sssaj2000.642715x

Chander, G., Markham, B. L., & Barsi, J. A. (2007). Revised Landsat-5 Thematic Mapper Radiometric Calibration. *IEEE Geoscience and Remote Sensing Letters*, *4*(3), 490–494. https://doi.org/10.1109/LGRS.2007.898285

Chander, G., Markham, B. L., & Helder, D. L. (2009). Summary of current radiometric calibration coefficients for Landsat MSS, TM, ETM+, and EO-1 ALI sensors. *Remote Sensing of Environment*, *113*(5), 893–903. https://doi.org/10.1016/j.rse.2009.01.007

Chavez, P. S. (1988). An improved dark-object subtraction technique for atmospheric scattering correction of multispectral data. *Remote Sensing of Environment*, *24*(3), 459–479. https://doi.org/10.1016/0034-4257(88)90019-3

Chen, H., Xu, C. Y., & Guo, S. (2012). Comparison and evaluation of multiple GCMs, statistical downscaling and hydrological models in the study of climate change impacts on runoff. *Journal of Hydrology*, *434–435*, 36–45. https://doi.org/10.1016/j.jhydrol.2012.02.040

Clements, R. (2009). *The Economic Cost of Climate Change in Africa* (P. A. and P. W. Rachel Berger (ed.); Issue November). The Pan African Climate Justice Alliance (PACJA).

Coltorti, M. (2014). Geomorphology. In *ResearchGate* (Issue January 2005, pp. 759–763). Harrassowitz Verlag, Wiesbaden.

Congalton, R. G. (1991). A review of assessing the accuracy of classifications of remotely sensed data. *Remote Sensing of Environment*, *37*(1), 35–46. https://doi.org/10.1016/0034-4257(91)90048-B

Conway, D. (2005). From headwater tributaries to international river: Observing and adapting to climate variability and change in the Nile basin. *Global Environmental Change*, *15*(2), 99–114. https://doi.org/10.1016/j.gloenvcha.2005.01.003

CONWAY, D. (2000). The Climate and Hydrology of the Upper Blue Nile River. *The Geographical Journal*, *166*(1), 49–62. https://doi.org/10.1111/j.1475-4959.2000.tb00006.x

Cook, P. G., Walker, G. R., Buselli, G., Potts, I., & Dodds, A. R. (1992). The application of electromagnetic techniques to groundwater recharge investigations. *Journal of Hydrology*, *130*(1–4), 201–229. https://doi.org/10.1016/0022-1694(92)90111-8

Delleur, J. W. (1999). *The Handbook of Groundwater Engineering* (second edi). School of Civil Engineering Purdue University West Lafayette, Indiana.

Deng, J. S., Wang, K., Deng, Y. H., & Qi, G. J. (2008). PCA-based land-use change detection and analysis using multitemporal and multisensor satellite data. *International Journal of Remote Sensing*, *29*(16), 4823–4838. https://doi.org/10.1080/01431160801950162

Dereje, B., & Nedaw, D. (2018). Groundwater Recharge Estimation Using WetSpass Modeling in Upper Bilate. *Momona Ethiopian Journal of Science (MEJS)*, *11*(1), 37–51. https://doi.org/doi.org/10.4314/mejs.v11i1.

Derin, Y., & Yilmaz, K. K. (2014). Evaluation of Multiple Satellite-Based Precipitation Products over Complex Topography. *Journal of Hydrometeorology*, *15*(4), 1498–1516. https://doi.org/10.1175/JHM-D-13-0191.1

Dessalegn, O. G., & Akalu, D. S. (2015). The impacts of climate change on African continent and the way forward. *Journal of Ecology and The Natural Environment*, *7*(10), 256–262. https://doi.org/10.5897/JENE2015.0533

Dinku, T., Funk, C., Peterson, P., Maidment, R., Tadesse, T., Gadain, H., & Ceccato, P. (2018). Validation of the CHIRPS satellite rainfall estimates over eastern Africa. *Quarterly Journal of the Royal Meteorological Society*, *144*(S1), 292–312. https://doi.org/10.1002/qj.3244

Dragoni, W., & Sukhija, B. S. (2008). Climate change and groundwater: a short review. *Geological Society, London, Special Publications*, *288*(1), 1–12. https://doi.org/10.1144/SP288.1

Essou, G. R. C., Arsenault, R., & Brissette, F. P. (2016). Comparison of climate datasets for lumped hydrological modeling over the continental United States. *Journal of Hydrology*, *537*, 334–345. https://doi.org/10.1016/j.jhydrol.2016.03.063

Fazzini, M., Bisci, C., & Billi, P. (2015). *The Climate of Ethiopia* (Issue October, pp. 65–87). https://doi.org/10.1007/978-94-017-8026-1_3

Funk, C., Nicholson, S. E., Landsfeld, M., Klotter, D., Peterson, P., & Harrison, L. (2015). The Centennial Trends Greater Horn of Africa precipitation dataset. *Scientific Data*, *2*(1), 150050. https://doi.org/10.1038/sdata.2015.50

Gebreyohannes, T., De Smedt, F., Walraevens, K., Gebresilassie, S., Hussien, A., Hagos, M., Amare, K., Deckers, J., & Gebrehiwot, K. (2013). Application of a spatially distributed water balance model for assessing surface water and groundwater resources in the Geba basin, Tigray, Ethiopia. *Journal of Hydrology*, *499*, 110–123. https://doi.org/10.1016/j.jhydrol.2013.06.026

Gebrie, T., & Gebremariam, B. (2015). *Impact of Land Use Land Cover Change on Stream Flow and Sediment Yield Approval Page*. *3*(11), 28–42.

Gedefaw, M., Yan, D., Wang, H., Qin, T., Girma, A., Abiyu, A., & Batsuren, D. (2018). Innovative Trend Analysis of Annual and Seasonal Rainfall Variability in Amhara Regional State, Ethiopia. *Atmosphere*, *9*(9), 326. https://doi.org/10.3390/atmos9090326

Gessesse, A. A., Melesse, A. M., & Abiy, A. Z. (2021). Land use dynamics and base and peak flow responses in the Choke mountain range, Upper Blue Nile Basin, Ethiopia. *International Journal of River Basin Management*, *19*(1), 109–121. https://doi.org/10.1080/15715124.2019.1672700

Gizaw, M. S., Biftu, G. F., Gan, T. Y., Moges, S. A., & Koivusalo, H. (2017). Potential impact of climate change on streamflow of major Ethiopian rivers. *Climatic Change*, *143*(3–4), 371–383. https://doi.org/10.1007/s10584-017-2021-1

Graf, R., & Przybyłek, J. (2018). Application of the WetSpass simulation model for determining conditions governing the recharge of shallow groundwater in the Poznań Upland, Poland. *Geologos*, *24*(3), 189–205. https://doi.org/10.2478/logos-2018-0020

GSE. (2008). *Geologoical Survey of Ethiopia. Geology of Bure map sheet (NC-37 / 5) Compiled by Lulu Tsige; Memoir No. 18*.

GSE. (2012). *Ministry of Mines Geological Survey of Ethiopia. Integrated hydrological and hydrochemical mapping of Burie map sheet (NC 37-5). Compiled by Yonas Mulugeta and Meklit Yadeta. December*.

GSE. (2015). *Geologoical Survey of Ethiopia Geology. Geology of Debremarkos Map Sheet (Nc 37-6) Compiled by: Ferede Chumburo; Memoir No. 27*.

Hafeez, M., Bakhsh Gulshan, A., Basit, A., Ahmad Chattha, Z., Akhtar Khan, A., Adnan Majeed, M., & Tahira, F. (2020). Penman and Thornthwaite Equations for Estimating Reference Evapotranspiration Under Semi-Arid Environment. *Journal of Plant Sciences*, *8*(5), 146. https://doi.org/10.11648/j.jps.20200805.16

Hagos, E. Y. (2005). *Development and management of irrigated lands in Tigray, Ethiopia*. A.A. Balkema Publishers, a member of Taylor & Francis Group plc.

Hay, A. M. (1979). Sampling designs to test land-use map accuracy. *Photogrammetric Engineering and Remote Sensing*, *45*(4), 529–533.

Healy, R. W., & Scanlon, B. R. (2010a). Groundwater recharge. In *Estimating Groundwater Recharge* (pp. 1–14). Cambridge University Press. https://doi.org/10.1017/CBO9780511780745.002

Healy, R. W., & Scanlon, B. R. (2010b). Modeling methods. In *Estimating Groundwater Recharge* (pp. 43–73). Cambridge University Press. https://doi.org/10.1017/CBO9780511780745.004

Herrera-Pantoja, M., & Hiscock, K. M. (2008). The effects of climate change on potential groundwater recharge in Great Britain. *Hydrological Processes*, *22*(1), 73–86. https://doi.org/10.1002/hyp.6620

Huntington, T. G. (2006). Evidence for intensification of the global water cycle: Review and synthesis. *Journal of Hydrology*, *319*(1–4), 83–95. https://doi.org/10.1016/j.jhydrol.2005.07.003

IPCC. (2007). *Climate Change 2007;The Physical Science Basis;Contribution of Working Group I to the Fourth Assessment Report of the Intergovernmental Panel on Climate Change [Solomon, S., D. Qin, M. Manning, Z. Chen, M. Marquis, K.B. Averyt, M. Tignor and H.L. Miller(e*. Cambridge University Press, Cambridge, United Kingdom and New York, NY, USA.

IPCC. (2014). *Climate Change 2014 Synthesis Report. Contribution of Working Groups I, II and III to the Fifth Assessment Report of the Intergovernmental Panel on Climate Change(Core Writing Team, R.K. Pachauri and L.A. Meye (eds))*. IPCC, Geneva, Switzerland, 151 pp.

Islam, S., Singh, R. K., & Khan, R. A. (2016). Methods of Estimating Ground water Recharge Methods of Estimating Ground water Recharge. *Jornal of Researchgate*. https://www.researchgate.net/publication/303435940

Jacobs, K., Adams, D. B., & Gleick, P. H. (2000). *Potential Consequences of Climate Variability and Change for Water Resource of the United States. pacific Institute for Studies in Development, Environment, and Security.*

Jakimavičius, D., Kriaučiūnienė, J., Gailiušis, B., & Šarauskienė, D. (2013). Assessment of uncertainty in estimating the evaporation from the Curonian Lagoon. *Baltica*, *26*(2), 177–186. https://doi.org/10.5200/baltica.2013.26.18

Jensen, J. R., & Lulla, K. (1987). Introductory digital image processing: A remote sensing perspective. *Geocarto International*, *2*(1), 65–65. https://doi.org/10.1080/10106048709354084

Jyrkama, M. I., & Sykes, J. F. (2007). The impact of climate change on spatially varying groundwater recharge in the grand river watershed (Ontario). *Journal of Hydrology*, *338*(3–4), 237–250. https://doi.org/10.1016/j.jhydrol.2007.02.036

Kalhor, K., Ghasemizadeh, R., Rajic, L., & Alshawabkeh, A. (2019). Assessment of groundwater quality and remediation in karst aquifers: A review. *Groundwater for Sustainable Development*, *8*, 104–121. https://doi.org/10.1016/j.gsd.2018.10.004

Karunakalage, A., Sharma, R., & Daqiq, M. T. (2023). Assessment of Climatic and Vegetation Influence on Spatial Distribution of Groundwater Recharge in Humid Subtropical Central Gangetic Plain Assessment of Climatic and Vegetation Influence on Spatial Distribution of Groundwater Recharge in Humid Subtropica. *Manuscript Submitted to Water Resources Research, May 05 2023*. https://doi.org/10.22541/essoar.168332180.04445793/v1

Kebede, S. (2013). Groundwater in Ethiopia. In *Groundwater in Ethiopia: Features, Numbers and Opportunities*. Springer Berlin Heidelberg. https://doi.org/10.1007/978-3-642-30391-3

Kołodziej, J. (2011). *Encyclopedia of Agrophysics* (J. Gliński, J. Horabik, & J. Lipiec (eds.)). Springer Netherlands. https://doi.org/10.1007/978-90-481-3585-1

Kurwadkar, S., Kanel, S. R., & Nakarmi, A. (2020). Groundwater pollution: Occurrence, detection, and remediation of organic and inorganic pollutants. *Water Environment Research*, *92*(10), 1659–1668. https://doi.org/10.1002/wer.1415

Lambin, E. F., Geist, H. J., & Lepers, E. (2003). Dynamics of Land-Use and Land-Cover Change in Tropical Regions. *Annual Review of Environment and Resources*, *28*(1), 205–241. https://doi.org/10.1146/annurev.energy.28.050302.105459

Legesse, D., Vallet-Coulomb, C., & Gasse, F. (2003). Hydrological response of a catchment to climate and land use changes in Tropical Africa: case study South Central Ethiopia. *Journal of Hydrology*, *275*(1–2), 67–85. https://doi.org/10.1016/S0022-1694(03)00019-2

Leh, M., Bajwa, S., & Chaubey, I. (2013). Impact Of Land Use Change on Erosion Risk: An Integrated Remote Sensing, Geographic Information System and Modeling Methodology. *Land Degradation & Development*, *24*(5). https://doi.org/10.1002/ldr.1137

Lupo, F., Reginster, I., & Lambin, E. F. (2001). Monitoring land-cover changes in West Africa with SPOT Vegetation: Impact of natural disasters in 1998-1999. *International Journal of Remote Sensing*, *22*(13), 2633–2639. https://doi.org/10.1080/01431160117700

Margat, J., & Gun, J. van der. (2013). *Groundwater around the World. A Geographic Synopsis*. CRC Press Taylor & Francis Group.

Mekonen, A. A., & Berlie, A. B. (2020). Spatiotemporal variability and trends of rainfall and temperature in the Northeastern Highlands of Ethiopia. *Modeling Earth Systems and Environment*, *6*(1), 285–300. https://doi.org/10.1007/s40808-019-00678-9

Melesse, A. M., Loukas, A. G., Senay, G., & Yitayew, M. (2009). Climate change, land-cover dynamics and ecohydrology of the Nile River Basin. *Hydrological Processes*, *23*(26), 3651–3652. https://doi.org/10.1002/hyp.7522

Meresa, E., & Taye, G. (2019). Estimation of groundwater recharge using GIS-based WetSpass model for Birki watershed, the eastern zone of Tigray, Northern Ethiopia. *Sustainable Water Resources Management*, *5*(4), 1555–1566. https://doi.org/10.1007/s40899-018-0282-0

Mertz, O., Halsnæs, K., Olesen, J. E., & Rasmussen, K. (2009). Adaptation to Climate Change in Developing Countries. *Environmental Management*, *43*(5), 743–752. https://doi.org/10.1007/s00267-008-9259-3

Milkias, A., & Toru, T. (2018a). Assessment of Land Use Land Cover Change Drivers and Its Impacts on above Ground Biomass and Regenerations of Woody Plants: A Case Study at Dire Dawa Administration, Ethiopia. *Atmospheric and Climate Sciences*, *08*(01), 111–120. https://doi.org/10.4236/acs.2018.81008

Milkias, A., & Toru, T. (2018b). Assessment of Land Use Land Cover Change Drivers and Its Impacts on above Ground Biomass and Regenerations of Woody Plants: A Case Study at Dire

Dawa Administration, Ethiopia. *Atmospheric and Climate Sciences*, *08*(01), 111–120. https://doi.org/10.4236/acs.2018.81008

Ministry of Water Resource. (2002). *Water Sector Development Program; Main Report Volume II.* (Issue October 2002).

Misstear, B. D. R. (2000). *GROUNDWATER RECHARGE ASSESSMENT: A KEY COMPONENT OF RIVER BASIN MANAGEMENT Bruce D.R. Misstear Department of Civil, Structural & Environmental Engineering, Trinity College Dublin*. 51–58.

Mohajane, M., Essahlaoui, A., Oudija, F., El Hafyani, M., Hmaidi, A. El, El Ouali, A., Randazzo, G., & Teodoro, A. C. (2018). Land Use/Land Cover (LULC) Using Landsat Data Series (MSS, TM, ETM+ and OLI) in Azrou Forest, in the Central Middle Atlas of Morocco. *Environments*, *5*(12), 131. https://doi.org/10.3390/environments5120131

Mondal, M. S., Sharma, N., Garg, P. K., & Kappas, M. (2016). Statistical independence test and validation of CA Markov land use land cover (LULC) prediction results. *The Egyptian Journal of Remote Sensing and Space Science*, *19*(2), 259–272. https://doi.org/10.1016/j.ejrs.2016.08.001

NASEM. (2018). *National Academies of Sciences, Engineering, and Medicine.Thriving on Our Changing Planet: A Decadal Strategy for Earth Observation from Space.* National Academies Press. https://doi.org/10.17226/24938

Niang, I., O. C., Ruppel, M. A., Abdrabo, A., Essel, C., Lennard, J., & Padgham, and P. U. (2014). Africa. in: In V. R. Barros, C. B. Field, D. J. Dokken, M. D. Mastrandrea, & K. J. Mach (Eds.), *Climate Change 2014: Impacts, Adaptation and Vulnerability* (pp. 1199–1266). Cambridge University Press. https://doi.org/10.1017/CBO9781107415386.002

Nicholson, S. E. (2016). An analysis of recent rainfall conditions in eastern Africa. *International Journal of Climatology*, *36*(1), 526–532. https://doi.org/10.1002/joc.4358

Niraula, R., Meixner, T., & Norman, L. M. (2015). Determining the importance of model calibration for forecasting absolute/relative changes in streamflow from LULC and climate changes. *Journal of Hydrology*, *522*, 439–451. https://doi.org/10.1016/j.jhydrol.2015.01.007

Nsengiyumva, G., Dinku, T., Cousin, R., Khomyakov, I., Vadillo, A., Faniriantsoa, R., & Grossi, A. (2021). Transforming Access to and Use of Climate Information Products Derived from Remote Sensing and In Situ Observations. *Remote Sensing*, *13*(22), 4721. https://doi.org/10.3390/rs13224721

Obiefuna, G. I., & Orazulike, D. M. (2011). Application and comparison of groundwater recharge estimation methods for the semiarid Yola area, northeast, Nigeria. *Global Journal of Geological Sciences*, *9*(2), 177-204–204.

Obuobie, E. (2008). Estimation of groundwater recharge in the context of future climate change in the White Volta River Basin , West Africa. Bonn. *Ecology and Development Series. No. 62*, 168. https://hdl.handle.net/20.500.11811/3712

Oki, T., & Kanae, S. (2006). Global Hydrological Cycles and World Water Resources. *Science*, *313*(5790), 1068–1072. https://doi.org/10.1126/science.1128845

Paredes-Trejo, F., Alves Barbosa, H., Venkata Lakshmi Kumar, T., Kumar Thakur, M., & de Oliveira Buriti, C. (2021). Assessment of the CHIRPS-Based Satellite Precipitation Estimates. In *Inland Waters - Dynamics and Ecology* (p. 13). IntechOpen. https://doi.org/10.5772/intechopen.91472

Paredes Trejo, F. J., Álvarez Barbosa, H., Peñaloza-Murillo, M. A., Moreno, M. A., & Farias, A. (2016). Intercomparison of improved satellite rainfall estimation with CHIRPS gridded product and rain gauge data over Venezuela. *Atmósfera*, *29*(4), 323–342. https://doi.org/10.20937/ATM.2016.29.04.04

Philip, S., Kew, S. F., Jan van Oldenborgh, G., Otto, F., O'Keefe, S., Haustein, K., King, A., Zegeye, A., Eshetu, Z., Hailemariam, K., Singh, R., Jjemba, E., Funk, C., & Cullen, H. (2018). Attribution Analysis of the Ethiopian Drought of 2015. *Journal of Climate*, *31*(6), 2465–2486. https://doi.org/10.1175/JCLI-D-17-0274.1

Piao, S., Ciais, P., Huang, Y., Shen, Z., Peng, S., Li, J., Zhou, L., Liu, H., Ma, Y., Ding, Y., Friedlingstein, P., Liu, C., Tan, K., Yu, Y., Zhang, T., & Fang, J. (2010). The impacts of climate change on water resources and agriculture in China. *Nature*, *467*(7311), 43–51. https://doi.org/10.1038/nature09364

Poeter, E., Fan, Y., Cherry, J., Wood, W., & Mackay, D. (2020a). *Groundwater in Our Water Cycle: Getting to Know Earth's Most Important Fresh Water Source*. The Groundwater Project. https://doi.org/10.21083/978-1-7770541-1-3

Poeter, E., Fan, Y., Cherry, J., Wood, W., & Mackay, D. (2020b). *Groundwater in our water cycle –*

getting to know Earth's most important fresh water source. Groundwater Project. https://doi.org/https://doi.org/10.21083/978- 1-7770541-1-3
Qablawi, B. (2016). *A Comparison of Four Methods to Estimate Groundwater Recharge for Northeastern South Dakota. Electronic Theses and Dissertations.* https://openprairie.sdstate.edu/etd/957
Raghunath, H. M. (2006). *Hydrology; Principles,Analysis,Design* (Second). New Age International (P) Ltd., Publishers, New Delhi.
Ramanathan, V., Crutzen, P. J., Kiehl, J. T., & Rosenfeld, D. (2001). Aerosols, Climate, and the Hydrological Cycle. *Science*, *294*(5549), 2119–2124. https://doi.org/10.1126/science.1064034
Ramankutty, N., & Foley, J. A. (1999). Estimating historical changes in global land cover: Croplands from 1700 to 1992. *Global Biogeochemical Cycles*, *13*(4), 997–1027. https://doi.org/10.1029/1999GB900046
Ravi, P., & Ashokkumar, A. (2017). Analysis of Various Image Processing Techniques. *International Journal of Advanced Networking & Applications*, *08*(05), 86–89.
Regasa, M. S., Nones, M., & Adeba, D. (2021). A Review on Land Use and Land Cover Change in Ethiopian Basins. *Land*, *10*(6), 585. https://doi.org/10.3390/land10060585
RRC(Relief and Rehabilitation Commission) of Ethiopia, UNDP, & FAO. (1986). *Assistance to settlement project, Ethiopia land use planning and soil and water conservation development planning of the Harawa, AG:DP/ETH/82/012, field doument 1*.
Scanlon, B. R., Healy, R. W., & Cook, P. G. (2002). Choosing appropriate techniques for quantifying groundwater recharge. *Hydrogeology Journal*, *10*(1), 18–39. https://doi.org/10.1007/s10040-001-0176-2
Seiler, K. P., & Gat, J. R. (2007). *Groundwater Recharge From Run-Off, Infiltration And Percolation.* Springer, Dordrecht, The Netherlands.
Senait Regassa, Christina Givey, and G. E. C. (2010). *The rain doesn ' t come on time anymore poverty, vulnerability, and climate variability in Ethiopia*. Oxfam International.
Shiri, N., Shiri, J., Yaseen, Z. M., Kim, S., Chung, I.-M., Nourani, V., & Zounemat-Kermani, M. (2021). Development of artificial intelligence models for well groundwater quality simulation: Different modeling scenarios. *PLOS ONE*, *16*(5), e0251510. https://doi.org/10.1371/journal.pone.0251510
Simmers. (1988). Estimation of Natural Groundwater Recharge. In I. Simmers (Ed.), *Journal of Chemical Information and Modeling* (1 st editi, Vol. 222, Issue 9). Springer Netherlands. https://doi.org/10.1007/978-94-015-7780-9
Singh, A. (2018a). Managing the salinization and drainage problems of irrigated areas through remote sensing and GIS techniques. *Ecological Indicators*, *89*(December 2017), 584–589. https://doi.org/10.1016/j.ecolind.2018.02.041
Singh, A. (2018b). Managing the environmental problems of irrigated agriculture through the appraisal of groundwater recharge. *Ecological Indicators*, *92*(November), 388–393. https://doi.org/10.1016/j.ecolind.2017.11.065
Singh, A., Panda, S. N., Uzokwe, V. N. E., & Krause, P. (2019). An assessment of groundwater recharge estimation techniques for sustainable resource management. *Groundwater for Sustainable Development*, *9*, 100218. https://doi.org/10.1016/j.gsd.2019.100218
Sophocleous M. (2004). *Groundwater recharge*. http://www.eolss.net/ebooks/Sample Chapters/C07/E2-09-01-05.pdf
Sowmya D. R., Shenoy, P. D., & Venugopal K. R. (2017). Remote Sensing Satellite Image Processing Techniques for Image Classification: A Comprehensive Survey. *International Journal of Computer Applications*, *161*(11), 24–37. https://doi.org/10.5120/ijca2017913306
Sugawara, E., & Nikaido, H. (2014). Properties of AdeABC and AdeIJK Efflux Systems of Acinetobacter baumannii Compared with Those of the AcrAB-TolC System of Escherichia coli. *Antimicrobial Agents and Chemotherapy*, *58*(12), 7250–7257. https://doi.org/10.1128/AAC.03728-14
Tegos, A., Efstratiadis, A., & Koutsoyiannis, D. (2013). A Parametric Model for Potential Evapotranspiration Estimation Based on a Simplified Formulation of the Penman- Monteith Equation. In *Evapotranspiration - An Overview* (Issue August 2015). InTech. https://doi.org/10.5772/52927
Tolessa, T., Dechassa, C., Simane, B., Alamerew, B., & Kidane, M. (2020). Land use/land cover dynamics in response to various driving forces in Didessa sub-basin, Ethiopia. *GeoJournal*, *85*(3), 747–760. https://doi.org/10.1007/s10708-019-09990-4

Turner, B. L., Moss, R. H., & Skole, D. L. (1993). *Relating land use and global land-cover change;a proposal for an IGBP-HDP core project. HDP Report Number 5. International Geosphere-Biosphere Programme, Stockholm, Sweden. 5*.

UNFCC. (2007). *Climate Change: Impacts, Vulnerabilities And Adaptation In Developing Countries*. United Nations Framework Convention on Climate Change.

UNWWAP (United Nations World Water Assessment Programme). (2015). *The United Nations World Water Development Report. Water for a sustainable world.*

USAID. (2020). *Climate Change Information Fact Sheet, Ethiopia*. *2030*(September 2015), 1–7.

USGS & USAID. (2012). A Climate Trend Analysis of Ethiopia. *Famine Early Warning Systems Network—Informing Climate Change Adaptation Series*, *October*, 1–4. http://pubs.usgs.gov/fs/2012/3123/

Vicente-Serrano, S., Perez-Cabello, F., & Lasanta, T. (2008). Assessment of radiometric correction techniques in analyzing vegetation variability and change using time series of Landsat images. *Remote Sensing of Environment*, *112*(10), 3916–3934. https://doi.org/10.1016/j.rse.2008.06.011

Virginia H., D. (1997). The Relationship between Land-Use Change and Climate Change; Environmental Sciences Division, Oak Ridge National Laboratory, Oak Ridge, Tennessee 37831-6038 USA. *Journal of Geophysical Research*, *7*(3), pp. 753–769. https://doi.org/10.1890/1051-0761(1997)007[0753:TRBLUC]2.0.CO;2

Walravens, K., Vandecaseele, I., Martens, K., Nyssen, J., Moeyersons, J., Gebreyohannes, T., De Smedt, F., Poesen, J., Deckers, J., & Van Camp, M. (2009). Groundwater recharge and flow in a small mountain catchment in northern Ethiopia. *Hydrological Sciences Journal*, *54*(4), 739–753. https://doi.org/10.1623/hysj.54.4.739

Warku, F., Korme, T., Wedajo, G. K., & Nedow, D. (2022). Impacts of land use/cover change and climate variability on groundwater recharge for upper Gibe watershed, Ethiopia. *Sustainable Water Resources Management*, *8*(1), 2. https://doi.org/10.1007/s40899-021-00588-8

Woldeamlak Bewket. (2002). Land cover dynamics since the 1950s in Chemoga watershed , Blue Nile basin, Ethiopia. *Mountain Research and Development*, *22*(3), 263–269. https://doi.org/http://dx.doi.org/10.1659/0276-4741(2002)022[0263:LCDSTI]2.0.CO;2

WorldBank. (2008). Managing Water Resources to Maximize Sustainable Growth : A World Bank Water Resources Assistance Strategy for Ethiopia. *World Bank Other Operational Studies*, *13*. https://ideas.repec.org/p/wbk/wboper/11758.html

Yamamoto, J. (2005). Comparing ordinary kriging interpolation variance and indicator kriging conditional variance for assessing uncertainties at unsampled locations. In *Application of Computers and Operations Research in the Mineral Industry* (Issue 2000, pp. 265–269). Taylor & Francis. https://doi.org/10.1201/9781439833407.ch34

Yitebitu, M., Zewdu, E., & Sisay, N. (2010). *Ethiopian Forest Resources: Current status and future management options in view of access to carbon finances; Literature review prepared for the Ethiopian climate research and networking and the united nations development programme (UNDP). Addis Ababa.*

Yue, S., & Wang, C. (2004). The Mann-Kendall Test Modified by Effective Sample Size to Detect Trend in Serially Correlated Hydrological Series. *Water Resources Management*, *18*(3), 201–218. https://doi.org/10.1023/B:WARM.0000043140.61082.60

Zhang, H., Zhang, L. L., Li, J., An, R. D., & Deng, Y. (2018). Climate and Hydrological Change Characteristics and Applicability of GLDAS Data in the Yarlung Zangbo River Basin, China. *Water*, *10*(3), 254. https://doi.org/10.3390/w10030254

Appendices

Annex I land use parameter table of Birr Adama watershed

Code	Luse_Type	Runoff_veg	Veg_area	Bare_area	Imp_area	Openw_area	T_depth	Lai	Min_stom	Veg_height	nManing	LandFactor	AerodynResistance
4	Grassland	grass	1	0	0	0	0.3	2	100	0.2	0.07	0.286	177.468
6	built-up	grass	0.2	0	0.8	0	0.3	2	100	0.12	0.03	0.667	212.014
9	Forest	forest	0.5	0.5	0	0	2	4.5	500	15	0.1	0.2	28.631
12	Wetland	grass	1	0	0	0	0.3	2	100	0.3	0.055	0.364	152.495
13	Water	open water	0	0	0	1	0.05	0	110	0	0.02	1	0.01
20	bare Land	bare soil	0	1	0	0	0.05	0	110	0.001	0.09	0.222	692.160
21	agriculture	crop	0.8	0.2	0	0	0.4	4	180	0.6	0.037	0.541	115.013
23	shrub	grass	1	0	0	0	0.6	6	110	2	0.05	0.4	66.329

Land-use table attributes

Code = land use code; Luse_Type = Land Use Type; Runoff_veg = Runoff Vegetation; Veg_area = Vegetated Area; Bare_area = Bare Area; Imp_area: Impervious Area; Openw_area: Openwater Area; T_depth = Root depth; Lai = Leaf Area Index; Min_stom= Minimum Stomatal Opening; Veg_height = Vegetation Height.

Annex II Soil parameter table of Birr Adama watershed

Soil texture attribute table

Code	SOIL	Fieldcapac	Wiltingpnt	PAW	Residualwc	A1	Evapodepth	Tensionhht	P_frac_sum	P_frac_win	Teta
5	loam	0.25	0.12	0.13	0.027	0.37	0.05	0.11	0.15	0.02	0.333
12	clay	0.46	0.33	0.13	0.09	0.21	0.05	0.37	0.95	0.85	0.852

Code = Soil texture code; Soil = Soil texture class; Fieldcapac = Field capacity; Wiltingpnt = Wilting Point; PAW = Plant available water content; Residualwc = Residual water content; A1 = Calibration parameter dependent on the sand content of the soil; Evapodepth = Bare soil evaporation depth; Tensionhht = Tension saturated height; P_frac_sum = Fraction of summer precipitation contributing to Hortonian runoff; P_frac_win = Fraction of winter precipitation contributing to Hortonian runoff.

Annex III Accuracy assessment of land use classification 1990

Land Use Class in 1990	Agriculture	Grass	Vegetation	Shrub	Built-up	Waterbody	Wetland	Bare land	Total (user)	User accuracy (%)
Agriculture	59	4	5	2	0	0	0	0	70	84.29
Grass	3	50	1	0	2	0	4	0	60	83.33
Vegetation	0	3	44	9	0	0	0	0	56	78.57
Shrub	3	5	2	43	0	0	1	0	54	79.63
Built-up	4	2	0	1	42	0	0	1	50	84.00
Waterbody	1	2	0	0	0	45	2	0	50	90.00
Wetland	1	2	0	0	0	2	45	0	50	90.00
Bare land	2	2	0	0	0	0	0	46	50	92.00
Total (Producer)	73	70	52	55	44	47	52	47	440	
Producers Accuracy (%)	80.82	71.43	84.62	78.18	95.45	95.74	86.54	97.87		

Total number of Correctly classified pixels	374
Total number of reference Pixels	440
overall accuracy	85.00
Kappa Coefficient	82.81

Annex IV Accuracy assessment of land use classification of 2005

Land Use Class in 2005	Agriculture	Grass	Vegetation	Shrub	Built-up	Waterbody	Wetland	Bare land	Total (user)	User accuracy (%)
Agriculture	58	4	0	2	2	0	0	0	66	87.88
Grass	1	48	3	2	2	0	2	0	58	82.76
Vegetation	0	2	47	9	0	0	0	0	58	81.03
Shrub	2	6	2	44	0	0	0	0	54	81.48
Built-up	4	0	0	1	44	0	0	1	50	88.00
Waterbody	0	0	0	0	0	50	0	0	50	100.00
Wetland	0	3	0	0	0	0	46	1	50	92.00
Bare land	3	3	0	0	2	0	0	46	54	10.45
Total (Producer)	68	66	52	58	50	50	48	48	440	
Producers Accuracy (%)	85	73	90	76	88	100	96	96		

Total number of Correctly classified pixels	383
Total number of reference Pixels	440
overall accuracy	87.05
Kappa coefficient	85.17

Annex V Accuracy assessment of land use classification of 2020

Land Use Class in 2020	Agriculture	Grass	Vegetation	Shrub	Built-up	Waterbody	Wetland	Bare land	Total (user)	User accuracy (%)
Agriculture	63	4	0	2	0	0	0	1	70	90.00
Grass	4	52	1	0	1	0	2	0	60	86.67
Vegetation	0	2	49	9	0	0	0	0	60	81.67
Shrub	0	2	2	46	0	0	0	0	50	92.00
Built-up	4	0	0	1	44	0	0	1	50	88.00
Waterbody	0	0	0	0	0	49	1	0	50	98.00
Wetland	0	3	1	0	0	0	46	0	50	92.00
Bare land	2	3	0	0	2	0	0	43	50	86.00
Total (Producer)	73	66	53	58	47	49	49	45	440	
Producers Accuracy (%)	86	79	92	79	94	100	94	96		

Total number of Correctly classified pixels	392
Total number of reference Pixels	440
overall accuracy	89.09
kappa coefficient	87.50

Annex VI Groundwater depth data

No.	Woreda	Town__Kebele	Well, _Id	X	Y	Z	Depth (m)	GWL
1	Dega Damot Finote	Debresia	feresbet#2	348473	1199297	2976	114.65	3.2
2	Selam	Shembekuma	Gocha No.2	312948	1181458	1828	98	14
3	Jabitena	_	F/selam	312926	1181491	1842	82	14.8
4	burie	Boko Tabo	Boko	284109	1142748	1449	46	6.92
5	Bibugn	Woyen wuha	Woyen wuha	359392	1214086	2203	250	3
6	Bure	Burie town # 2	BH9	288531	1183991	2055	59.5	8.94
7	dembecha zuria	gullagodber	dembecha well2	338390	1171713	2095	176	22.45
8	dembecha zuria	Agote	dembecha well1	327460	1170539	1958	200	6.39
9	Jabitena	yedefasguji	finoteselam BH	313296	1180728	1820	120	17.5
10	bure	k03	phibela factory well.2	290217	1183342	2073	220	12.5
11	bure	k03	phibela factory well.1	290489	1184101	2079	153	8
12	shindi	sedabr	shindi	280589	1178683	2019	98	10.08
13	Jabitena	woynama ambaye	woynama	298683	1166071	1595	60	2.8
14	wonberma	marweled	marweled	270000	1161784	1975	150	13.43
15	bure	alefa	bure alefa	282044	1170966	1979	250.6	6
16	dembecha zuria	yechereka	dembecha anjene	337020	1177846	2359	249	8.8
17	Bure	Bure	Baguna	284709	1184202	2021	95	2.56
18	Bure	Bure	Tare mesk	286167	1184258	2042	114	4.7
19	Bure	Guleme	adbaken	292132	1170437	1970	40	11

20	Bure	BIAIPW #1	BH1	292015	1184498	2083	188	12
21	Bure	BIAIPW #4	BH3	291536	1184679	2080	120	31.05
22	Bure	BIAIPW #5	BH4	288910	1182554	2042	150.6	5.8
23	Bure	BIAIPW #6	BH5	290767	1184165	2076	126.8	6.25
24	Bure	BIAIPW #7	BH6	297535	1184451	2001	254	38
25	Bure	BIAIPW #8	BH7	297348	1185133	2014	44	18.85
26	Bure	Burie town # 1	bure, gembo well	290997	1183776	2065	131	5.71
27	Dega Damot	arefa mesikana/debtera	arefa mesikana	357990	1211910	2260	200	21
28	yismala densa	Abune zerabruck	Abune zerabruck Gedam	335341	1241430	2238	175	4.4
29	gozamn	wenka	robgebeya/santera	352304	1144921	2209	204	44.25
30	Bure	Adel Agata	SW12	290633	1177625	2006	52	13
31	machakel	shelel	shelel	348978	1170426	2143	196.1	4.8
32	bure	tengeha	bure	289052	1181106	2043	138	3
33	Dega Damot	wegem	feresbet	350985	1195692	3051	153.3	15
34	basoliben	dgom	Adis Amba	359623	1113500	2317	40	18
35	machakel	kerer	Kerer School	339496	1146715	2171	44	8
36	quarit	genet abo	Genet abo	327115	1194161	1895	159	4
37	Bahir Dar Zuria	Feres Woga	Feres Woga	321423	1255328	2059	181	7
38	yismala densa	goshye	goshye	331800	1237871	2412	61.15	25
39	bure	Denbun	bure coll water factory	280823	1179215	2022	86	3.63
40	yismala densa	debremawe	debremawe	330775	1250594	2180	176	6
41	bure zuria	sentom	fetam sentom	282170	1155390	1962	42.75	7
42	bure zuria	fezel	fezel school	285152	1162119	2013	51	18
43	senan	robgebeya	robgebeya	365872	1164972	2806	150	50
44	yismala densa	ribrib	adet town water supply	332490	1244379	2200	296	40
45	Bure	_	Bure 2 (M.W)	289369	1183244	2100	87.8	6.5
46	Bure	_	Bure 1	287117	1183590	2120	84.8	25.5
47	Burie	_	Zalma	288905	1182608	2047	109	8.55
48	Burie	_	Bure univrsity	286710	1182994	2015	80	10.5
49	Dega Damot	_	Feresbet	350424	1195983	3052	128	16.4
50	Dega Damot	_	Feres Bet	347429	1200407	2990	77	2.2
51	Dembecha	_	Wada Yessus	319923	1163931	1960	80	5.7
52	Dembecha	_	Lejet	336648	1167853	2076	300	62
53	Dembecha	_	Dembecha	335672	1168055	2075	43	36.9
54	Dembecha	_	Yechereka	327536	1171635	2000	42	33
55	Denbecha	_	Denbecha town	336687	1167811	2113	120	50.62
56	Jabi tehinan	_	Frat Adankegn	300627	1163019	1493	202	7.4
57	Jabi tehinan	_	Mircha borabur	322610	1186011	1914	180	3.71
58	Jabitehnan	_	Fenote Selam	310297	1180797	1830	106	6
59	Quarit	_	G/mariam	328711	1214716	2113	250	2
60	Sekela	Gundle Jegrita well-2	Gundle Jegrita well-2	292093	1211083	2563	34	4

61	Sekela	Gundle Jegrita Well	Gundle Jegrita Well	292412	1211764	2588	55	8
62	Sekela	Abay sangeb Well No. 2	Abay sangeb Well No. 2	305186	1213970	2709	37	7
63	Sekela	Abay sangeb Well No. 1	Abay sangeb Well No. 1	304712	1214720	2699	37	6
64	Sekela	Gunbela School Well	Gunbela School Well	307685	1217398	2575	43	5
65	Quarit	Quarit	Endrias	330792	1223962	3064	61.5	3
66	Quarit	Quarit	Chefakit	324369	1227268	3020	64	15
67	Burie	Feten Sentom	Tach Jammo	292110	1150829	1332	43	8
68	Burie	Feten Sentom	Mehal Jammo	291957	1151496	1347	52	4
69	Burie	Fetan Sentome	Gerarma	297021	1151728	1349	61	7
70	Burie	Gebgedel	Teshayta	290615	1187034	2150	45.5	9
71	Burie	Gebgedel	Selala school	290709	1187731	2170	43	10
72	Burie	Wehni	Aguta no.1	298564	1193366	2209	52	28
73	Sekela	Tach Bekello Well	Tach Bekello Well	295507	1202192	2521	63	21
74	Sekela	Lay Bekello	Lay Bekello well	294414	1202284	2548	58	19
75	Sekela	Sekela	Asewa/TH	304688	1206166	2353	50	2
76	Burie Zuriya	arebisie	arebisie	298568	1188321	2103	42.5	6
77	Dembecha	Dembecha	Gedebe	301042	1157716	1483	60	2
78	Sekela	Terefta	Terefta well	299244	1199847	2335	40	8
79	Sekela	Zamayta well	Zamayta well	299820	1200203	2319	46	14